

FIG. 1. Experimental facilities used in the low-energy ion irradiation of naked DNA. (a) The glass sample holder for low-energy ion beam irradiation of naked DNA. (b) The bioengineering ion implanter with a vertical beam line. (c) The stainless steel sample holder for plasma low-energy ion irradiation of naked DNA. (d) The plasma immersion ion irradiation facility.

2.2 Molecular Dynamics Simulation (MDS) of Low-energy Ion Irradiation of DNA

To simulate ion bombardment of DNA in vacuum, DNA in A form that is the DNA form in low humidity or low pressure environment was constructed. For investigating effect on the nitrogenous bases, 20 base pairs of alternating poly-AT and poly-GC double strands were constructed using HyperChem 7.0. The energy minimizations and MDS were performed, AMBER 9 software package [15], in vacuo to imitate the dried and evacuated condition in experimental bombarding chambers. For investigating effect on various bonds, a 30-base-pair-long DNA duplex was constructed in A-form with Discovery Studio 1.7 software package [16]. The selected part was the residues number 760 – 789 of the green fluorescent protein plasmid (pGFP) in the GenBank, sequenced by Chalfie et al. [17]. The CHARMm27 force field [18] was applied on this molecule. To obtain the DNA structure in the equilibrium state in vacuum, the energy minimization, heating, equilibration and production of MDS were performed using Standard Dynamic Cascade protocol. Two sets of ion parameters were used: carbon ion with energy of 2, 20, and 200 eV and nitrogen ion with 0.1, 1, 10 and 100 eV, the former for bombarding the bases and the latter for bombarding the various bonds of DNA. The simulation was performed using combined quantum mechanics and molecular mechanics (QM/MM) coupled potentials. The energy and geometry of the region were calculated by the PM3 semi-empirical Hamiltonians. The long range QM-QM and QM-MM electrostatic interactions were calculated by Ewald sum.

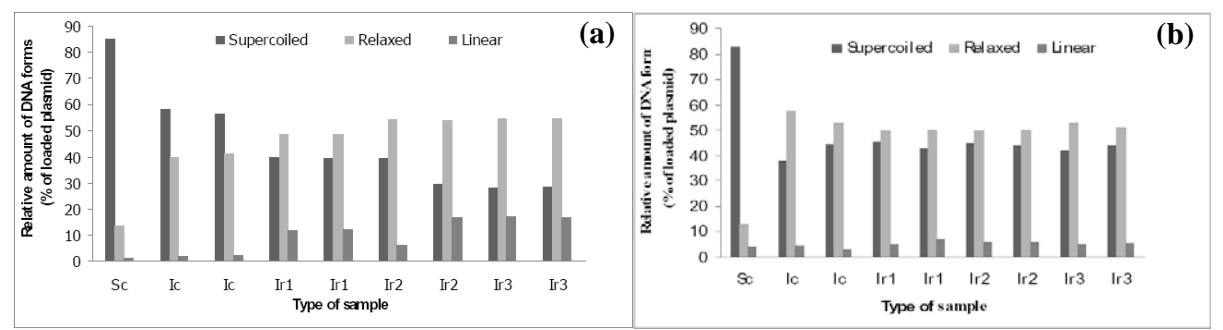


FIG. 2. Examples of electrophoresis results. Sc: solution control, Ic: internal control, Ir: irradiated with fluences of 3×10^{13} (Ir1), 6×10^{13} (Ir2), and 9×10^{13} (Ir3) ions/cm². (b) Quantification of various forms of plasmid DNA after N-ion bombardment. (d) Quantification of various forms of plasmid DNA after Ar-ion bombardment. In each electrophoresis analysis, two samples were used for each ion beam condition.

3. Results and Discussion

3.1 Low-energy and Low-fluence Ion Beam Irradiation of Naked DNA

The results from the electrophoresis analysis are shown in Fig. 2, where Figs. 2(b) and (d) are the normalized relative amounts of the DNA forms obtained from the fluorescence intensities of the electrophoresis bands. It is known that when a single-strand break (SSB) is induced, DNA converts into a relaxed form, and when a double strand break (DSB) or multiple DSBs are produced, DNA converts to a linear full-length form or fragments. From the figures, it is clearly seen that upon the very low-energy low-fluence ion bombardment both relaxed and linear forms are produced and hence SSB and DSB indeed occur. It is noticed that in the vacuum controls, the relaxed form is dominantly produced, indicating vacuum effect on DNA SSB. The changes in the amounts of the DNA forms as increasing the ion fluence are found related to ion species. In Figs. 2(b) and 2(d), the attention should be paid to the relative changes in the DNA forms for each ion species. As the experienced history of each set of samples from initial preparation, ion bombardment to electrophoresis might cause varied amount of the DNA forms, and hence, the amounts of the DNA forms of the vacuum control are considered only as a reference. As increasing the ion fluence, the amount of the original DNA supercoiled form decreases for the N-ion bombardment case but does not much change for the Ar-ion bombardment case; the amount of the relaxed form slightly increases for the N-ion case but does not change noticeably for the Ar-ion bombardment; the amount of the linear form increases for the N-ion case more than for the Ar-ion case. This comparison indicates that nitrogen ions, even with lower energy than that of argon ions, are more effective in producing double strand breaks and thus more capable to induce GFP gene mutation than argon ions. This result seems to be conflict with common knowledge that predicts higherenergy and heavier ions able to produce more damage than lower-energy and lighter ions. Whether more physics and biology are involved is being further investigated. One hypothesis is that because DNA contains much nitrogen at the nitrogenous bases, externally introduced nitrogen will have intimate interaction with the original nitrogen so that more effects can be produced. This implies that the direct interaction of the ions with the DNA is more complex than the indirect process.

AP/P5-08 5



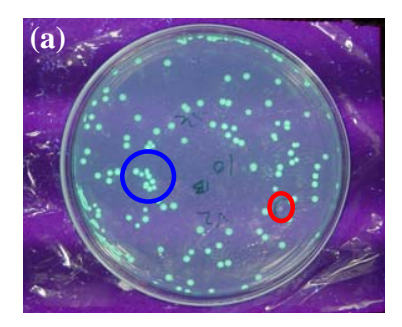
FIG. 3. UV observation of plasmid containing pGFP transferred into E. coli. The white colony indicates pGFP damaged (not functioning) and thus mutated, while the green colonies is non-mutant.

Following the model of the dependence of the change in the DNA forms on the ion fluence proposed in the study on carbon ion bombardment of naked DNA [6], we calculated the cross section of the loss of the supercoiled form of DNA for our N-ion bombardment case to be $(2.35 \pm 0.96) \times 10^{-14}$ cm². This result is very close to but roughly greater than that for the C-ion bombardment case, which gave $(2.2 \pm 0.5) \times 10^{-14}$ cm². For the case of Ar-ion bombardment, obviously the cross section is extremely small as almost no meaningful change is seen. Nitrogen and carbon are neighbors in the periodic table and both abundant in DNA, and thus expected to have similar effect on the molecular structure when they are used as ions to bombard DNA molecules. But, in the chemical structure in living matter, carbon has unique properties compared with all other elements [19]. Carbon is capable to make as many as four highly stable covalent bonds, while nitrogen has five valence electrons to make it less stably bonding or more active. It is then speculated that nitrogen ions may more actively interact with atoms in DNA, especially nitrogen atoms, than carbon ions.

The result of DNA transfer in *E. coli* showed that green (non-mutant) and white (mutant) colonies were produced. The white colonies were picked out and plated on plates again to check for their purity as shown in Fig. 3. The appearance of white colonies that are the evidence of the GFP gene damaged and thus not functioning confirms that low-energy ion beam bombardment indeed induced DNA mutation. Our gene sequencing showed that the sequences of the GFP gene in the mutants induced by both Ar-ion and N-ion bombardments were similar to that of the GFP in the control. This means that the GFP gene is not mutated. Therefore, the mutation can only be attributed to the Lac promoter, because GFP is expressed from the Lac promoter as a fusion with several additional amino acids, including the first five amino acids of the lacZ protein.

3.2 Low-energy Plasma Immersion Ion Irradiation of Naked DNA

Vacuum effect on damage in DNA and subsequently induced mutation of DNA-transferred bacteria *E. coli* was first checked. No mutation was found from the *E. coli* transferred with plasmid DNA pGFP which was exposed to vacuum at a pressure of 10⁻⁵ Torr up to one hour. In fact, under all of the conditions applied (varied low pressures and exposure time lengths), the DNA-transferred *E. coli* all showed green. This result demonstrates that certain long-time exposure of DNA to vacuum basically has no effect on mutation.



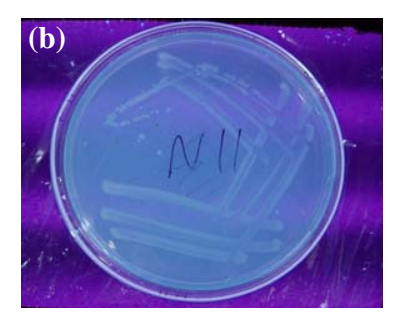


FIG. 4. Demonstration of effect from plasma immersion low-energy-ion bombardment on DNA mutation in DNA transferred E. coli. DNA pGFP was exposed to N-plasma in the conditions of a bias of 2.5 kV and an ion fluence of 10^{13} ions/cm². (a) Mutation selection from the DNAtransferred E. coli. White colonies as indicated by the red circle are the mutant, compared with the un-mutated green colonies as indicated by the blue circle. (b) Purified E. coli mutant from the redcircled mutant in (a) to show all of the bacterial cells white.

Effect from only plasma (without using bias) on DNA mutation was checked by placing the DNA samples in argon or nitrogen plasma generated from RF (radio-frequency) power input but without bias. The sample holder was or not grounded. In the former case, the ions with only the thermal energy were implanted in the DNA, while in the latter case, the ions only "blew" the DNA with the thermal energy. In both conditions, no mutation was found. This means that only with eV ion energy, DNA mutation cannot be induced within the treatment time periods.

At bias of a few kV, DNA mutation in transferred E. coli indicated by the white bacterial colonies was indeed observed, as shown in Fig. 4. Purification of the white colonies with picking up the colonies to grow in culture media LB exhibited all cells in green, demonstrating the white colonies not contaminated but really mutated. However, it was found that the mutation rate was very low as from only one condition of the PIII, i.e. the bias of 2.5 kV (which resulted in the ion energy of 1.25 keV for the majority of N-ions) and the fluence of 10¹³ ions/cm², among a number of conditions, including various fluences, pressures and gases, the mutation was observed. In biased plasma, there are normally not only ions but probably also electrons, X-ray and free radicals, which may also interact with DNA to induce DNA change in structure. But, from the result of the low mutation rate, we may speculate that the mutation source is the bias-accelerated ions which are implanted into DNA but not others, as if it was the latter, there might also be mutation in other conditions where the factors other than ions are also present. Our DNA sequencing analysis (data not shown here) revealed that the GFP fragment of the DNA was not broken but the promoter fragment had suspected breaks. The expression of green color of the plasmid DNA pGFP under UV is controlled by the promoter. If the promoter is damaged, the expression of green fluorescence from the DNA cannot be realized.

3.3 Molecular Dynamics Simulation of Low-energy Ion Irradiation of DNA

In MDS of C-ion irradiation of DNA, the root mean square displacements (RMSD) of the backbone atoms of poly-AT were found remaining in small fluctuation after 1.0 ns of the equilibration, while those of poly-GC were stable after 1.5 ns of the equilibration. The tendency of DNA strand splitting was inspected by measuring the distance between the backbone termini of

two strands, corresponding to A1-T40 and T20-A21 distances for poly-AT and G1-C40 and C20-G21 distances for poly-GC. The results are shown in Table I. It is seen that the poly-AT's T20-A21 backbone termini is the most sensitive to the ion irradiation as it exhibits the largest distance increase subjected to C-ion bombardment. The RMSDs of the base rings were measured to track the flexibility of bases. The behaviors of RMSD of poly-AT and poly-GC are different (Fig. 5). The base rings of poly-GC are quickly stabilized after about only 5 ps of ion bombardment, whereas those of poly-AT take the time more than ten times as poly-GC takes to stabilize. The average RMSD of poly-AT is about one angstrom more than that of poly-CG. All of these results indicate that poly-AT is more unstable and more tend to be broken than poly-GC when subjected to ion attack.

TABLE I: Distance (angstrom, Å) between the backbone termini of two DNA strand after 150 ps MDS. In the case of 200-eV C-ion bombarding poly-GC, the ion passed through DNA after 150 ps simulation. The average distance change is the ratio of the difference between the mean distance of all non-zero energies and the distance of the zero energy over the latter.

Distance between		Average distance			
Distance services	0	2	20	200	change (%)
Poly-AT A1-T40	11.7	12.6	13.0	11.1	4.56
Poly-AT T20-A21	12.0	17.4	17.6	16.3	42.5
Poly-GC G1-C40	16.0	19.1	18.1	1	16.3
Poly-GC C20-G21	15.2	15.2	16.4	-	3.95

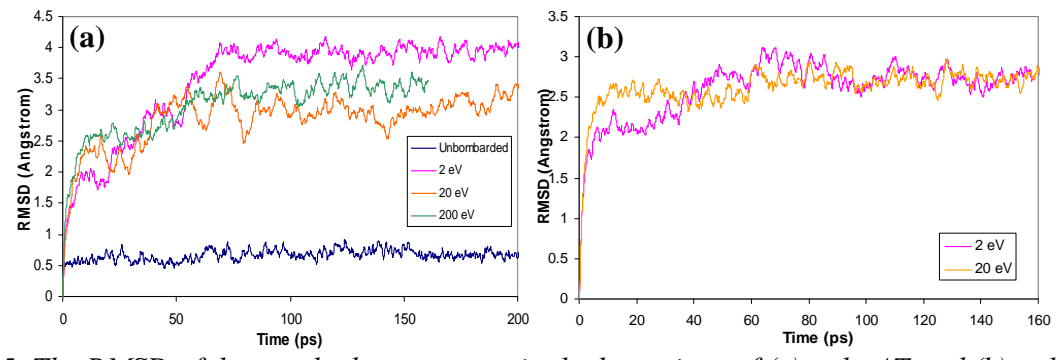


FIG. 5. The RMSD of the non-hydrogen atoms in the base rings of (a) poly-AT and (b) poly-GC.

TABLE II: Summary of the mean values of the distance of maximum radial distribution functions, r_{max} , and the integral of radial distribution functions from 0.0 to 4.0 Å, $I_{4\text{Å}}$, of each atom type.

Atom type	r_{max} (Å)	$I_{4\text{Å}}(\text{Å})$
N	3.85	1.83
0	4.75	2.8
O'	4.45	2.6
OP	3.3	3.25
С	3.9	1.5
C'	4.0	1.43

abbe in. The conditinguis measured after certain time of 17 for inadiation.									
	Average	Modal bond length after ion irradiation (Å)							
Bond type	equilibrium	0.1 eV,	1 eV,	10 eV,	Mean				
	length (Å)	after 10 ps	after 10 ps	after 6 ps	increase (%)				
O-P	1.582	1.618	1.702	1.698	5.73				
O-P (ar)	1.486	1.498	1.498	1.481	0.43				
C-C	1.518	1.560	1.570	1.544	2.64				
C-N	1.490	1.489	1.543	1.515	1.72				
C-O	1.433	1.445	1.432	1.459	0.86				
C-C (ar)	1.387	1.426	1.408	1.399	1.73				
C-N (ar)	1.351	1.388	1.381	1.336	1.28				
C=O	1.230	1.220	1.221	1.218	-0.84				

TABLE III: The bond lengths measured after certain time of N-ion irradiation.

In MDS of N-ion irradiation of DNA, radial distribution functions (RDF), the distances of maximum RDF, r_{max} , and the RDF integrals were studied, as shown in Table II. The results shown in the table are the mean values of two different doses. The higher RDF integral indicates the higher absorption preference of the implanted ion. It is seen that the preference of N-ion interaction with the DNA atoms is in an order of OP, O, O', N, C and C'. The shortest r_{max} of OP also indicates the strongest interaction with the incident ion as the distance represents the distance between the atom and the ion, obviously, the shorter the stronger the interaction force. The ranges and medians of bond lengths of eight types were studied. The studied types included oxygen-phosphorus single bonds (O-P), oxygen-phosphorus aromatic bonds (O-P (ar)), carbon-carbon single bonds (C-C), carbon-nitrogen single bond (C-N), carbon-oxygen single bonds (C-O), carbon-carbon aromatic bonds (C-C (ar)), carbon-nitrogen aromatic bonds (C-N (ar)) and carbon-oxygen double bonds (C=O). The maximum, minimum and modal bond lengths in each bombardment were measured. Table III summarizes the main results. It is clearly seen that the O-P bond is the weakest as it has the largest increase in the bond length after ion attack, and following the O-P bond are the C-C, C-C (aromatic) and C-N bonds, whereas the C=O bond is the strongest.

4. Conclusion

Irradiation of naked DNA with low-fluence ions of energy lower than a few keV can induce damage in DNA structure, such as individual single and double strand breaks and multiple double strand breaks, to result in mutation. This is a direct effect of ion interaction with DNA. The breaks of the DNA strand are not random but preferential. Strand poly-AT in the nitrogenous base pairs is more vulnerable than poly-GC and the O-P bond in the phosphate group is the weakest.

Acknowledgements

This work has been supported by Thailand Research Fund, National Research Council of Thailand, and Thailand Center of Excellence in Physics.

References

- [1] YU, L.D., et al. (Eds., English Edition), YU, Z.L. (original in Chinese), Introduction to Ion Beam Biotechnology, Springer Science & Business Media, New York (2006).
- [2] KANBASHI, K., et al., "Frameshifts, base substitutions and minute deletions constitute X-ray-induced mutations in the endogenous *tonB* gene of *Escherichia coli* K12", Mutat. Res. **385** (1997) 259.
- [3] WEI, Z., et al., Nucl. Instr. and Meth. **B 95** (1994) 371.
- [4] YU, L.D., et al., Nucl. Instr. and Meth. **B 206** (2003) 586.
- [5] ZHAO, Y., et al., "Electrophoresis examination of strand breaks in plasmid DNA induced by low-energy nitrogen ion irradiation", Nucl. Instr. and Meth. **B 211** (2003) 211.
- [6] HUNNIFORD, C.A., et al., "Damage to plasmid DNA induced by low energy carbon ions", Phys. Med. Biol. **52** (2007) 3729.
- [7] CHEN, Y., et al., "Formation of plasmid DNA strand breaks induced by low-energy ion beam: indication of nuclear stopping effects", Radiat. Environ. Biophys. **37** (1998) 101.
- [8] LACOMBE, S., et al., "DNA strand breaks induced by low keV energy heavy ions", Phys. Med. Biol. 49 (2004) N65.
- [9] DEND, Z.W., et al., "Beyond the Bragg peak: Hyperthermal heavy ion damage to DNA components", Phys. Rev. Lett. **95** (2005) 153201.
- [10] CHACON, F.A., Ion Induced Radiation Damage on the Molecular Level, Ph.D. Thesis, University of Groningen (2007).
- [11] YU, L.D., et al., "A specialized bioengineering ion beam line", Nucl. Instr. and Meth. **B 257** (2007) 790.
- [12] CHAIVAN, P., et al., "Low-temperature plasma treatment for hydrophobicity improvement of silk", Surf. Coat. Technol. **193** (2005) 356.
- [13] BOEGE, F., et al., "Selected Novel Flavones Inhibit the DNA Binding or the DNA Religation Step of Eukaryotic Topoisomerase I", J. Biol. Chem. **271** (1996) 2262.
- [14] BAILLY, C., "DNA relaxation and cleavage assays to study topoisomerase I inhibitors", Methods Enzymol. **340** (2001) 610.
- [15] CASE, D.A., et al., Amber 8, University of California, San Francisco (2004).
- [16] ACCELRYS, Discovery Studio Release Notes, Release 2.0, Accelrys Software Inc.: San Diego (2007).
- [17] CHALFIE, M., et al., "Green fluorescent protein as a marker for gene expression", Science **263** (1994) 802.
- [18] FOLOPPE, A.D. and MACKERELL, J., "All-atom empirical force field for nucleic acids: I. parameter optimization based on small molecule and condensed phase macromolecular target data", Comp. Chem. **21** (2000) 86-104.
- [19] VOET, D. and VOET, J.G., Biochemistry, John Wiley & Sons, New York (1990), p.19.

Provided for non-commercial research and education use. Not for reproduction, distribution or commercial use.



This article appeared in a journal published by Elsevier. The attached copy is furnished to the author for internal non-commercial research and education use, including for instruction at the authors institution and sharing with colleagues.

Other uses, including reproduction and distribution, or selling or licensing copies, or posting to personal, institutional or third party websites are prohibited.

In most cases authors are permitted to post their version of the article (e.g. in Word or Tex form) to their personal website or institutional repository. Authors requiring further information regarding Elsevier's archiving and manuscript policies are encouraged to visit:

http://www.elsevier.com/copyright

Author's personal copy

Surface & Coatings Technology 204 (2010) 2960-2965



Contents lists available at ScienceDirect

Surface & Coatings Technology

journal homepage: www.elsevier.com/locate/surfcoat



Plasma immersion low-energy-ion bombardment of naked DNA

S. Sarapirom ^a, K. Sangwijit ^b, S. Anuntalabhochai ^b, L.D. Yu ^{a,c,*}

- a Plasma and Beam Physics Research Facility, Department of Physics and Materials Science, Faculty of Science, Chiang Mai University, Chiang Mai 50200, Thailand
- b Molecular Biology Laboratory, Department of Biology, Faculty of Science, Chiang Mai University, Chiang Mai 50200, Thailand
- ^c Thailand Center of Excellence in Physics, Commission on Higher Education, 328 Si Ayutthaya Road, Bangkok 10400, Thailand

ARTICLE INFO

Available online 20 February 2010

Keywords:
Plasma immersion ion implantation and deposition (PIII-D)
Low-energy ion
Naked DNA
Mutation

ABSTRACT

Low-energy ion irradiation of DNA is of great interest in fundamental studies on mechanisms involved in low-energy ion beam induced mutation, plasma sterilization and ionizing radiation risk of lives. We have made the first attempt to use low-energy ions in plasma immersion ion implantation and deposition (PIII-D) to bombard naked plasmid DNA to investigate effect on the DNA structural modification and mutation. Naked DNA samples were immersed in either argon or nitrogen plasma in low pressure and then bombarded by ions in the plasma in different conditions, namely, using a low bias of -2.5 kV, or no bias, in which the sample holder was either grounded or not grounded, to low fluences of 10^{11} , 10^{12} and 10^{13} ions/cm². The plasma-treated DNA was transferred into bacteria *E. coli.* Mutation was found from the bacterial colonies when DNA was bombarded with the bias, but not found when DNA was bombarded without a bias. This indicates that ions with energy only at the order of the thermal energy cannot induce mutation but with low-energy of keV the ions can. Subsequent gel electrophoresis and DNA sequencing analyzed the DNA structural changes and found certain modifications in the DNA forms.

© 2010 Elsevier B.V. All rights reserved.

1. Introduction

Ion beam biotechnology is a newly developed important application of low-energy ion beam physics in biology [1–4]. The applications have included ion beam induced mutation and gene transfer. Mechanisms involved in the applications have however not yet well understood. For the ion beam induction of mutation, as the thickness of the materials covering the genetic substances such as DNA is so greater than the ion range that the ions are seemingly impossible to directly interact with DNA. However, the considerably porous structures of the biomaterials covering DNA may bring a small number of implanted ions to DNA. Therefore, it is necessary to check whether low-energy and low-fluence ions are indeed able to induce mutation of DNA. In our investigation, we simulated the last step of ion interaction with DNA using very low-energy and low-fluence of ions to bombard naked plasmid DNA. With the findings of low-energy ion beam able to induce DNA breakages [5-11], in this study we for the first time applied plasma immersion ion implantation (PIII) technique to bombard naked DNA with low-energy ions from plasma. When DNA is immersed in plasma, the environment is harsher than that of ion beam bombardment. Not only energetic ions, but also electrons, free radicals and X-rays present in plasma can all interact with DNA to cause DNA structural change. Therefore, it is more

E-mail address: yuld@fnrf.science.cmu.ac.th (L.D. Yu).

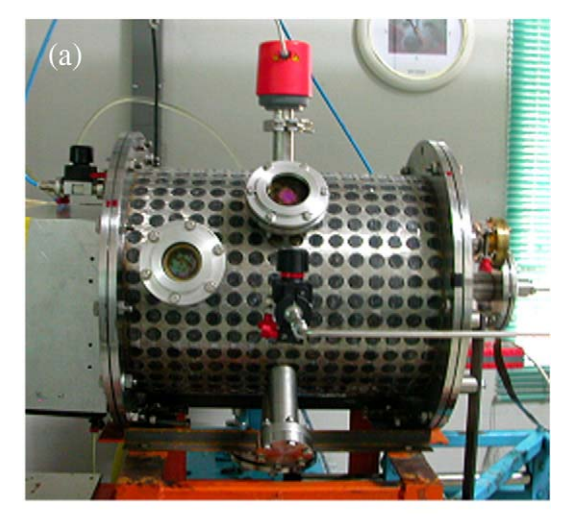
interesting to see how DNA reacts to the plasma environment and bombardment from ions in the plasma.

2. Experiment

An initial sample of DNA plasmid puff, pGFP (plasmid green fluorescent protein, 3344 base pairs), was purchased from Clonetech. The plasmid DNA was replicated following transformation into *Eschericia coli* (*E. coli*) and subsequently extracted and purified using a QIAGEN® Plasmid Purification kit according to the manufacturer's protocol. The plasmid DNA produced by this procedure was dissolved in sterile, de-ionized water resulting in a plasmid concentration of $0.4\,\mu\text{g}/\mu\text{l}$. It was divided into aliquots and later diluted in water as necessary. Aliquots of 9 μ l plasmid DNA solution were deposited in holes of a stainless steel sample holder. The holder was about 5 cm in diameter and had nine holes on it with each in a size of 5 mm in diameter and 5 mm in depth, as shown in Fig. 1. A hole containing the vacuum control was covered by carbon tape. The samples were first dried in laminar flow and then placed in the PIII chamber [12] (Fig. 1) which was then pumped to a pressure <5 × 10⁻⁵ torr.

We used argon or nitrogen plasma for immersion ion implantation with bias voltages of 0 and 2.5 kV and fluences of 0, 10^{11} , 10^{12} and 10^{13} ion/cm², respectively. The ion fluence was controlled by measuring the ion current from the sample holder through an interface I–V converter. When no bias was applied, the sample holder was either grounded or not grounded. The plasma was generated with 50-watt radiofrequency (RF) power and operated with a frequency of 50 Hz and a pulse length of 10 μ s including a rise time of about 2 μ s.

^{*} Corresponding author. Plasma and Beam Physics Research Facility, Department of Physics and Materials Science, Faculty of Science, Chiang Mai University, Chiang Mai 50200, Thailand. Tel.: +66 53 943379; fax: +66 53 222776.



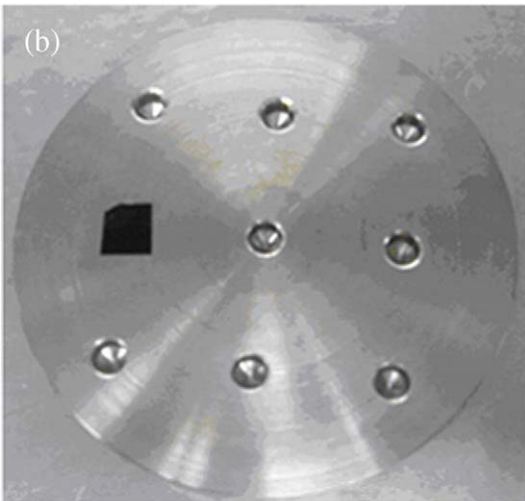


Fig. 1. Photograph of (a) the PIII chamber and (b) the DNA sample holder. The chamber is about 40 cm long and 30 cm in diameter. The sample holder is about 5 cm in diameter. The carbon tape covered hole is for holding the control.

The plasma density was measured by a Langmuir probe. The ion density varied from $1-2.5\times 10^{15}\, ions/m^3$ in the radial axis of the cylindrical PIII chamber with the density peak at the center of the chamber where the sample holder was placed.

After PIII treatment, the DNA samples were individually recovered in 10 µl of de-ionized water for dilution and divided two parts for analysis. The first part was for gel electrophoresis. The samples were added with 2 µl of gel loading buffer (0.25% (w/v) bromophenol blue, 40% (w/v) sucrose) and then loaded onto wells with 1% (w/v) agarose gel made up in TAE buffer (40 mM Tris-acetate, 1 mM EDTA, pH 8.3) pre-strained with 0.002% (w/v) ethidium bromide (EthBr). This gel was run at constant voltage (100 V cm⁻¹) for approximately 1 h. Images of the gels were captured using UV-transilluminator and digital camera. Fluorescence intensity plots were analyzed by OriginLab® software. The intensity corresponding to each form was obtained by integrating the area. A correction factor [13] was applied to the intensity corresponding to the supercoiled form to allow for the increased binding of the EthBr. The intensities were summed and averaged over all the internal controls and the result was used as a measure of the initial quantity of plasmid DNA. The total internal control intensity I_C^T is given by

$$I_C^T = I_C^S + I_C^R + I_C^L, (1)$$

where I_C^S , I_C^R , I_C^L are the intensities of the supercoiled, relaxed and linear bands in the internal control samples [13]. Since the same quantity of

pGFP was used in all internal controls and bombarded samples, $I_{\rm C}^T$ provides a measure of the total quantity of plasmid in each sample. Hence the percentage of each form in the bombarded samples can be calculated by

$$P_i^S = 100 \left[\frac{I_i^S}{I_c^T} \right] \tag{2}$$

$$P_i^R = 100 \left[\frac{I_i^R}{I_c^T} \right] \tag{3}$$

$$P_i^L = 100 \left[\frac{I_i^L}{I_c^T} \right] \tag{4}$$

where P_i^S , P_i^R , P_i^L are the percentages of each form after bombarding and I_i^S , I_i^R , I_i^R , I_i^R are the integrated intensities of the supercoiled, relaxed and linear bands, respectively [13]. Curve fitting was carried out using the OriginLab® software. In another part, plasmid pGFP was transferred into E. coli (strain DH5 α) competent cells. DNA mutation selection was indicated by the white bacterial colonies. White colonies were streaked in 5 generations on plates again to check for their purity and stability of the phenotype. After that, the size of pGFP was checked by electrophoresis and DNA sequencing was performed by First BASE laboratories Sdn Bhd, Malaysia. Three specific primers were used to cover promoter and the complete GFP gene: gfpF1 primer (5'-gct atg acc atg att acg cca a-3') gfpF2 (5'-cac ccc agg ctt tac act tta tg-3') and gfpR2 primer (5'-cac cag aca agt tgg taa tgg ta-3').

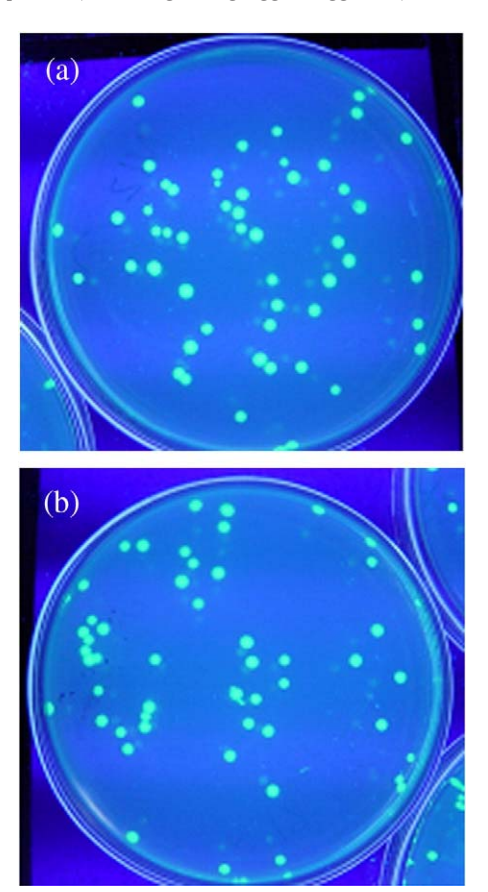


Fig. 2. Growth of *E. coli* transferred with plasmid DNA exposed to vacuum $(10^{-5} \, \text{Torr})$ (a) for 30 min and (b) 60 min. The green color indicates no mutation induced.

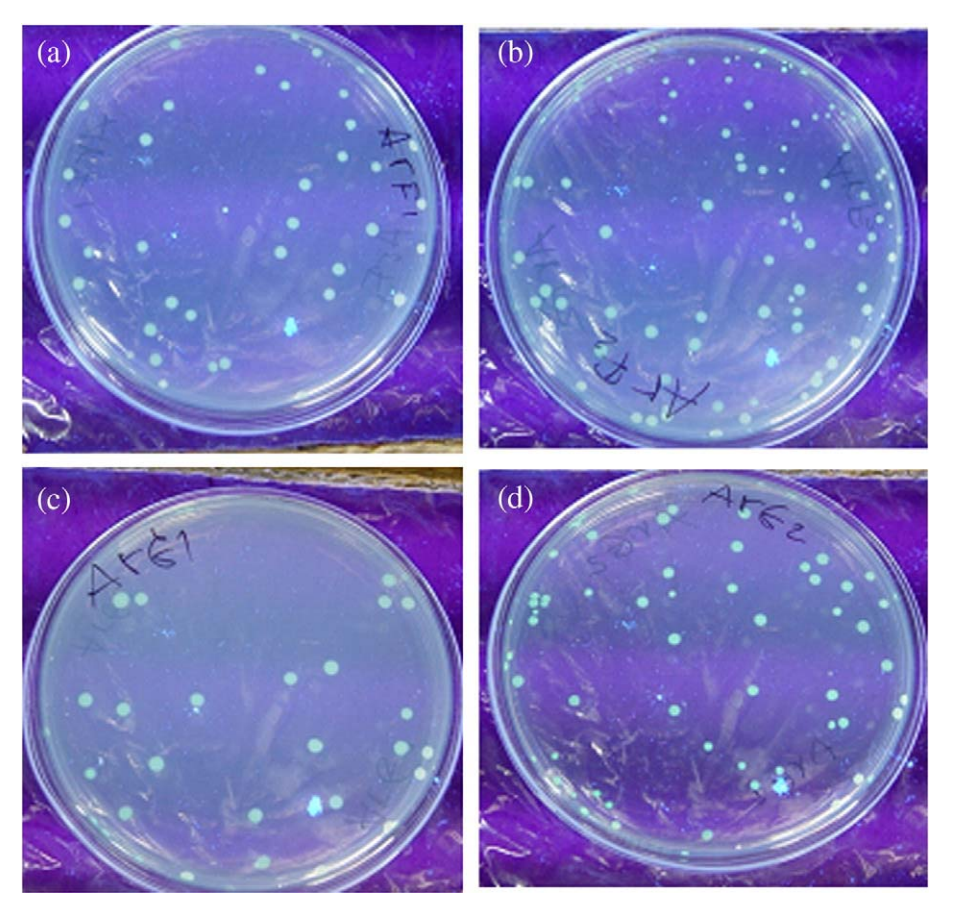


Fig. 3. Demonstration of effect from only plasma on DNA mutation in DNA transferred *E. coli*. Shown here are *E. coli* bacteria transferred with DNA pGFP exposed to Ar plasma in the condition of (a) no grounding for 1 min (corresponding to an ion fluence of 10¹² ions/cm²), (b) no grounding for 10 min (corresponding to an ion fluence of 10¹³ ions/cm²), (c) grounding for 1 min, and (d) grounding for 10 min. The green color indicates no mutation induced.

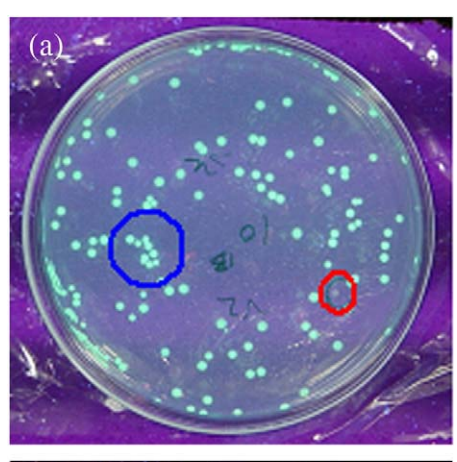
3. Results and discussion

Vacuum effect on damage in DNA and subsequently induced mutation of DNA-transferred bacteria E. coli was first checked. Fig. 2 shows examples of the DNA transferred E. coli after the plasmid exposed to low pressures for various time periods. As the plasmid DNA pGFP contained the green fluorescent protein which would be seen in green color under ultra violet (UV) light, green color observed in pGFP-transferred living materials was the indicator of the presence of the functioning pGFP DNA, whereas no green color, or the original color ("white" in biology term) of the bacterial cells without pGFP transferred, shown should be the indicator of the DNA changed or mutated. No mutation was found from the E. coli transferred with plasmid DNA pGFP which was exposed to vacuum at a pressure of 10^{-5} Torr up to one hour. In fact, under all of the conditions applied (varied low pressures and exposure time lengths), the DNA-transferred E. coli all showed green. This result demonstrates that certain long-time exposure of DNA to vacuum basically has no effect on mutation.

In order to check effect from only plasma (without using bias) on DNA mutation, we placed the DNA samples in the vacuum chamber with argon or nitrogen plasma generated from RF power input but without bias. Two conditions were applied, namely grounding the sample holder and not grounding. In the former case, the ions with only the thermal energy bombarded the DNA, while in the latter case, the ions only "blew" the DNA with the thermal energy. From both conditions, no mutation was found, as shown in Fig. 3. This result means that only with the ion energy of an order of eV, DNA mutation cannot be induced within the treatment time periods.

Fig. 4 shows an example of low-energy ion bombarded DNA induced mutation in *E. coli*. With applying the bias, DNA mutation in

transferred E. coli indicated by the "white" bacterial colonies was indeed observed. Purification of the white colonies with picking up the colonies to grow again in culture media LB in another dish exhibited all cells in "white", demonstrating the white colonies not contaminated but really mutated. However, it was found that the mutation rate was very low as from only one condition of the PIII, i.e. the bias of 2.5 kV and the fluence of 10¹³ ions/cm², among a number of conditions, including various fluences, pressures and gases, the mutation was observed. In biased plasma, there are normally not only ions but probably also electrons, X-ray and free radicals, which may also interact with DNA to induce DNA change in structure. But, from the result of the low mutation rate, we may speculate that the mutation source is the bias-accelerated ions which are implanted into DNA but not others, as if it were the latter, there might also be mutation in other conditions where the factors other than ions were also present. The maximum energy of Ar ions was 2.5 keV and the energy of most N ions was about 1.25 keV (as most N ions were molecular) in our conditions. Therefore, these very low energy ions were able to induce mutation directly. Since mutation is directly related to DNA change, it is reasonable that the higher ion fluence, the more the DNA change and the more the possibility to induce mutation. Hence, low fluence ion bombardment has low mutation rate. It is known that the DNA chain is about 2-3 nm wide and one nucleotide unit is 0.33 nm long [14], or about 1-nm² area for a nucleotide unit. So, on average, for the fluence of 10¹³ ions/cm², every 10 nucleotide units are bombarded by an ion, while for the fluence of 10¹¹ ions/cm², every 1000 nucleotide units are bombarded by only one ion. And furthermore, one collision of an ion with an atom in DNA may not certainly induce DNA change by displacing the atom. This could be the reason that mutation in the lowfluence ion bombardment condition could hardly be observed.



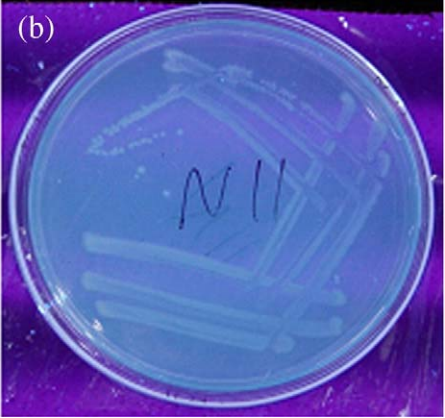


Fig. 4. Demonstration of effect from plasma immersion low-energy-ion bombardment on DNA mutation in DNA transferred $E.\ coli.$ Shown here are $E.\ coli.$ bacteria transferred with pGFP exposed to N-plasma in the conditions of a bias of 2.5 kV and an ion fluence of 10^{13} ions/cm². (a) Mutation selection from the DNA-transferred $E.\ coli.$ "White" colonies as indicated by the red circle are the mutant, compared with the un-mutated green colonies as indicated by the blue circle. (b) Purified $E.\ coli.$ mutant from the red-circled mutant in (a) growing in a new dish with culture media LB to show all of the bacterial cells "white", "White" in biology term means the original color of the bacterial cells without DNA pGFP transferred.

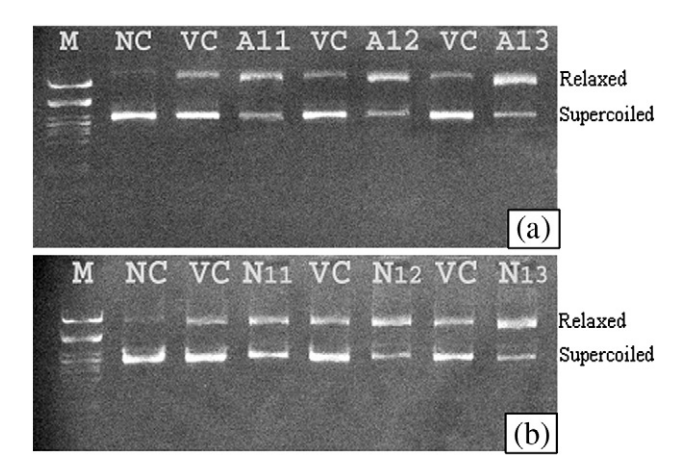


Fig. 5. Electrophoresis results. (a) Effect of argon ion immersion bombardment on naked plasmid DNA pGFP, which was bombarded with 2.5 keV plasma argon at different fluences. Keys: $M-\lambda$ marker, NC-natural control, VC-vacuum control, Ar 11-Ar-ion bombard with fluence 1×10^{11} ions/cm², Ar 12-Ar-ion bombard with fluence 1×10^{12} ions/cm², Ar 13-Ar-ion bombard with fluence 1×10^{13} ions/cm². (b) Effect of nitrogen ion immersion bombardment on naked plasmid DNA pGFP, which was bombarded with 2.5 keV plasma nitrogen at different fluences. Keys: $M-\lambda$ marker , NC-natural control, VC-vacuum control, N 11-plasma nitrogen bombard with fluences 1×10^{11} ions/cm², N 12-plasma nitrogen bombard with fluences 1×10^{13} ions/cm², N 13-plasma nitrogen bombard with fluences 1×10^{13} ions/cm².

Table 1 Percentages of the DNA forms of different types of samples: natural control, internal control (vacuum control) and after bombardment with ether nitrogen or argon ions to fluences of 10^{11} , 10^{12} and 10^{13} ions/cm², calculated from the electrophoresis band intensity by using OriginLab.

Ī	DNA form	Natural control	Vacuum control				Nitroge (ions/c	en ion fl m²)	uence
		(NC)	(VC)	1011	10 ¹¹ 10 ¹² 10 ¹³		1011	10 ¹²	10 ¹³
				(Ar11)	(Ar12)	(Ar13)	(N11)	(N12)	(N13)
Ī	Relaxed Super-coiled	20.5 79.5	33.7 66.3	64.3 35.7	67.2 32.8	71.4 28.6	45.2 54.8	63.3 36.7	70.1 29.9

The DNA forms under various conditions were analyzed with gel electrophoresis (Fig. 5) and quantified based on the fluorescence intensity of the band (Table 1 and Fig. 6). The results clearly show that the supercoiled form decreases while the relaxed form increases as the DNA is treated more and more. The supercoiled form is the original DNA form and normally when a single strand break (SSB) occurs the supercoiled form is relaxed into the relaxed form. Vacuum can cause certain SSBs and the relaxed form increase by about 50% compared with that of the natural control. But, the ion bombardment considerably induces more SSBs with about 200% increase in the relaxed form for the Ar-ion case and 125% increase for the N-ion case at the lowest fluence and the relaxed form further increases as the ion fluence increases. At higher fluences the relaxed forms have almost the same increase for both Ar-ion and N-ion cases. This is a clear indication of the ion direct interaction with DNA responsible for the DNA strand breaks. It is noticed that in our PIII of DNA the linear form of DNA appears negligibly whereas in our pervious experiment on ion beam bombardment of DNA using similar ion energy and fluence the linear form was observed in the electrophoresis [11]. The reason is thought to be that in PIII the ion energy has a distribution with a nonnegligible low-energy component [15], thus the ion fluence with the ion peak energy is actually much lower than that calculated in operation, but in normal ion beam implantation there is no this problem. This fact further demonstrates the direct ion interaction with DNA dominating the DNA breaks. DNA breaks are potentials for mutation to occur. The DNA sequencing analysis as shown in Fig.7

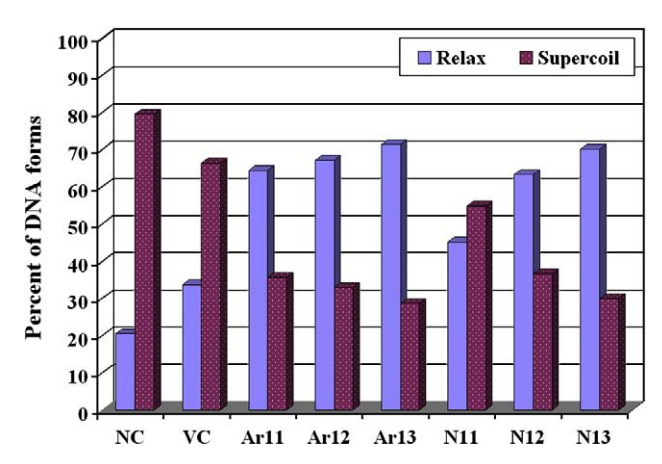


Fig. 6. Graphic percentages of the DNA forms under different conditions: natural control, internal control (vacuum control) and after bombardment with ether nitrogen or argon ions to fluences of $10^{11},10^{12}$ and 10^{13} ions/cm². Keys: $M-\lambda marker,NC-$ natural control, VC - vacuum control, Ar 11- Ar-ion bombarded to 1×10^{11} ions/cm², Ar 12- Ar-ion bombarded to 1×10^{12} ions/cm², Ar 13- Ar-ion bombarded to 1×10^{13} ions/cm², N 11- N-ion bombarded to 1×10^{13} ions/cm², N 13- N-ion bombarded to 1×10^{13} ions/cm², N 13- N-ion bombarded to 1×10^{13} ions/cm², N 13- N-ion bombarded to 1×10^{13} ions/cm².

```
Start codon
Ar318-1 gfpF1
                 -----GCCGGTCAGAAAAATGAGTAAAGG 25
Ar318-4 TgfpF1
                 -----CGGCATCAAAAAACATGTGAAGG 23
Control
                 CATGCCTGCAGGTCGACTCTAGAGGATCCCCGGGTACCGGTA-GAAAAAATGAGTAAAGG 299
Ar318-3 gfpR2
                 CATGCTTGCAGGTCGACTCTAGAGGATCCCCGGGTACCGGCA--GANAAATGAGTAAAGG 167
                 CCTACCTGCCGNNCCAAAAAAAGCCTCCCCTNG-GCCGAAA-GTTTTATTGAGTGAAAA 97
Ar318-2 gfpF2
Ar318-1 gfpF1
                 ACAAAAACTTTTCCCTGGAGTTGTCCCCACTTCCCCGTTCAAATTAAATGGTGATGTTAAT 85
Ar318-4 TgfpF1
                 Control
                 AGAAGAACTTTTCACTGGAGTTGTCCCAATTC--TTGTTGAATTAGATGGTGATGTTAAT 357
Ar318-3 gfpR2
                 AGAAGACCTTTTCACTGGAGTTGTCCCNATTCT-TGTTGAATTAGATTTGCGATGTTAAT 226
Ar318-2 gfpF2
                 GGAAGAACTTTTGACTGAAAATTGACCAAATCT-TCCCTAAAAGGATTTTTACCG--GGT 154
                                  *
                                      **
                                          **
Ar318-1 gfpF1
                 GGGCACAAATTTCTCTGTCAGTGGA-GAGGGTGAAGGTGATGCAACATACGGAAAA-CTT 143
Ar318-4 TgfpF1
                 GGGCA-AAATTTTTTTGTCAGGGAAAGAGGGTGAAGGTGAGGCAAAATACGGAAAAACTT 142
Control
                 GGGCACAAATTT-TCTGTCAGTGGA-GAGGGTGAAGGTGATGCAACATACGGAAAA-CTT 414
                 GGGCACAAATTT-TCTGTCAGTGGA-GAGGGTGAAGGTGATGCAACATACGGAAAA-CTT 283
Ar318-3 gfpR2
Ar318-2 gfpF2
                 GGGAACTGCTTTTTTTGGCGGTGGG-GAAGGGGAAGGCGATGCAACATGGTGTAAA-CTT 212
                 *** *
                        *** * ** * * *
                                      ** ** **** ** ***
                                                            * *** ***
Ar318-1 gfpF1
                 ACCCTTAAATTTATTTGCACTACTGGAAAACTACCTGTTCCATGGCCAACACTTGTCACT 203
Ar318-4 TgfpF1
                 ACCCTAAAGTTTATTTGCACTACGGAAAAACTACCTGTTCCGGGGCCAACACTGGTCAGT 202
Control
                 ACCCTTAAATTTATTTGCACTACTGGAAAACTACCTGTTCCATGGCCAACACTTGTCACT 474
                 ACCCTTAAATTTATTTGCACTACTGGAAAACTACCTGTTCCATGGCCAACACTTGTCACT 343
Ar318-3_gfpR2
Ar318-2_gfpF2
                 ACCCTTTAATTTCTTTGCAGTAAGGGAAAGCGTCCTGNTCCATGGCCATTTCTTGGCATA 272
                 Ar318-1 gfpF1
                 AACTAGCAGACCATTATCAACAAAA---TACTCCAATTGGCGATGGCCCTGTCCTTTTAC 603
Ar318-4 TgfpF1
                 AACTAGCAGACCATTATCAACAAAA---TACTCCAATTGGCGATGGCCCTGTCCTTTTAC 603
                 AACTAGCAGACCATTATCAACAAAA---TACTCCAATTGGCGATGGCCCTGTCCTTTTAC 874
Control
                 AAATAACAAACCCTTCTCCAAAAAA---AAAATCAATTTGGGGTGGCCCTTTTCCTTTTC 758
Ar318-3 gfpR2
Ar318-2 gfpF2
                 ANCTT AT AG ACN AAT AT CT ACAAGAGT ACG AGCAGNT GGGNG AT NGCCAT GT CNTTTT AC 674
                       * **
                            * ** * ** *
                                                *
                                                  * * * *** * *
Ar318-1_gfpF1
                 CAGACAACCATTACCTGTCCCCACAATCTGCCGTTTCGAAAGATCCCAACGAAAA-GAGA 662
Ar318-4_TgfpF1
                 CAGACAACCATTACCTGTCCACACACTCTGCCCTTTCGAAAGATCCCAACGAAAAAGAGA 663
Control
                 CAGACAACCATTACCTGTCCACACAATCTGCCCTTTCGAAAGATCCCAACGAAAA-GAGA 933
Ar318-3 gfpR2
                 CCGACCACCCTTTCCCCTTTCCCCCAAAGGGGCCTTTTGAAAGATTCCCACGGAAA-GAGA 817
Ar318-2 gfpF2
                 CANANAACCATTACCTGTCCACACTATCTACCCT-----
                      *** ** **
                               * * * *
                 Ar318-1 gfpF1
Ar318-4 TgfpF1
                 GACCACATGGNCCTTCTTTGACTTTGTAACAGCTGCTGGGATTACACATGGCATGGATGA 723
                 Control
Ar318-3_gfpR2
                 Ar318-2_gfpF2
                             Stop codon
Ar318-1 gfpF1
                 Ar318-4_TgfpF1
                 ACTATACAAATAGCATTCCTAGAATTCCAACTGAACACCGGTCGCTACCATTACCAAC-T 782
Control
                 ACTAT ACAAATAGCATTCGTAGAATTCCAACTGAGCGCCGGTCGCTACCATTACCAAC-T 1051
Ar318-3_gfpR2
Ar318-2 gfpF2
                 ______
```

Fig. 7. DNA sequencing result. Only are the star-marked locations the same between the the control and the ion-bombardment-induced mutant DNAs.

revealed that some fragments of the DNA extracted from the bacterial mutant was different from those of the original DNA, indicating misrepairs which are responsible for mutation. Fig. 8 shows that the GFP fragment of the extracted DNA from the mutated bacteria is the same as the GFP of the original DNA and thus the mutation is not caused by contamination. So, the DNA sequencing result is trustable.

4. Conclusion

PIII was the first time applied to bombard naked DNA with lowenergy low-fluence ions. This was to simulate the last step of ion beam bombardment of biological cells to induce mutation for understanding relevant mechanism. For a certain time period of exposure of DNA,

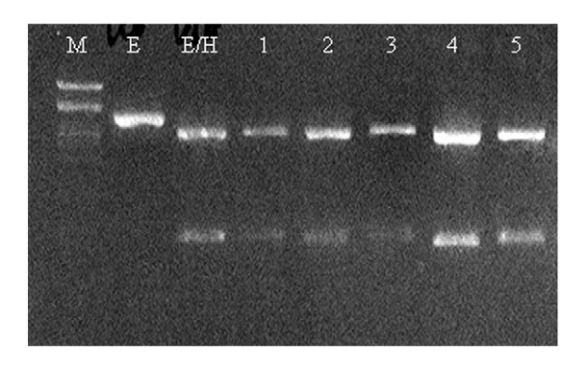


Fig. 8. DNA fragment of GFP gene (714 bp) from "white" colonies (mutant) after cut by restriction enzymes. M: marker, E: pGFP cut by *EcoRI*, E/H: pGFP cut by *EcoRI* and *HindIII*, 1–5: pGFP from "white" colonies cut by *EcoRI* and *HindIII*. The GFP fragments from the "white" colonies indicate that there is pGFP in the host cells.

vacuum was found no effect on DNA mutation for the exposure time up to one hour, and ions with only thermal energy had no effect either for the exposure time corresponding to the fluence of 10^{13} ions/cm². However, low-energy ions at only a few keV even with low fluences can induce DNA mutation. The mechanism of mutation induction is thought to be due to ion direct interaction with DNA to cause DNA breaks.

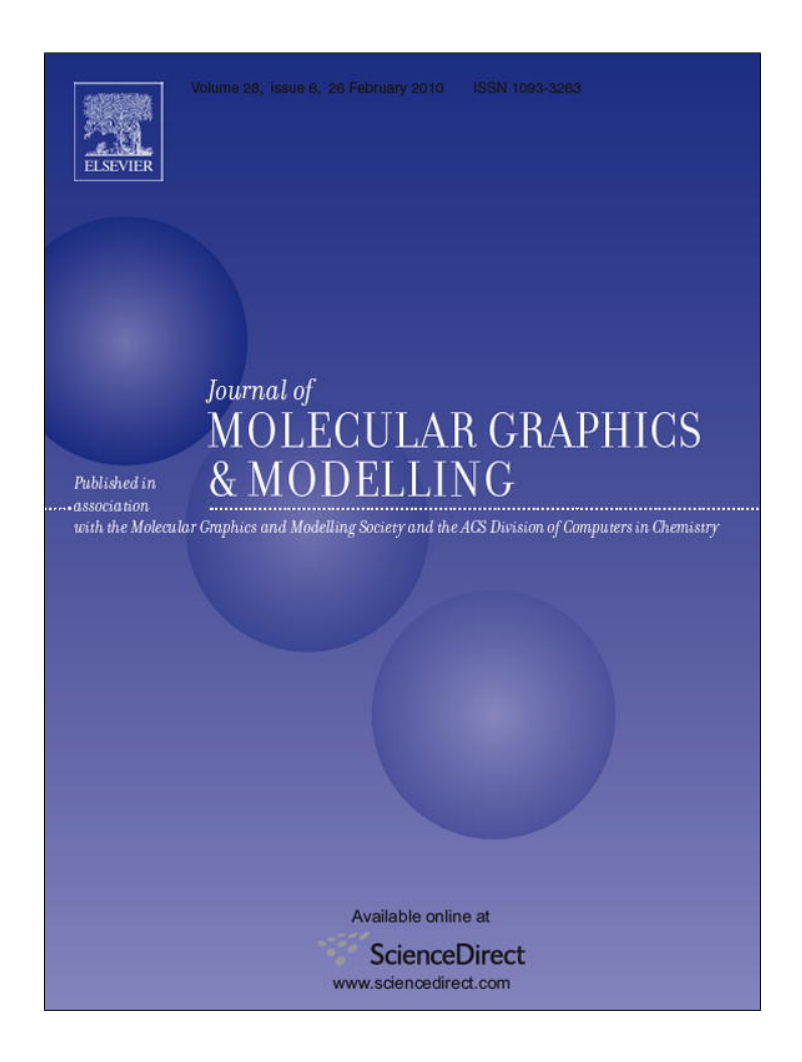
Acknowledgments

This work has been supported by the Thailand Research Fund, Chiang Mai University, Thailand Center of Excellence in Physics and National Research Council of Thailand.

References

- [1] Z.L. Yu, L.J. Qiu, Y.P. Huo, J. Anhui Agric. College 18 (4) (1991) 251.
- [2] Z.L. Yu, IEEE Trans. Plasma Sci. 28 (1) (2000) 128.
- [3] H.Y. Feng, Z.L. Yu, P.K. Chu, Mater. Sci. Eng. R 54 (3-4) (2006) 49.
- [4] L.D. Yu, T. Vilaithong, I.G. Brown, Introduction to Ion Beam Biotechnology, English edition, originally authored by Yu Zengliang in Chinese, Springer Science & Business Media, New York, 2006, English Translators.
- [5] S. Lacombe, C. Le Sech, V.A. Esaulov, Phys. Med. Biol. 49 (2004) N65.
- [6] Z.W. Deng, I. Bald, E. Illenberger, M.A. Huels, Phys. Rev. Lett. 95 (2005) 153201.
- [7] Zengliang Yu, Surf. Coat. Technol. 201 (2007) 8006.
- [8] Fresia Alvarado Chacon, Ion induced radiation damage on the molecular level, Ph.D. Thesis, University of Groningen, 2007.
- [9] C.A. Hunniford, D.J. Timson, R.J.H. Davies, R.W. McCullough, Phys. Med. Biol. 52 (2007) 3729.
- 10] W. Wang, Z.L. Yu, W.H. Su, eprint, arXiv:0807.0079v1 </abs/0807.0079v1>, 2008.
- [11] R. Norarat, N. Semsang, S. Anuntalabhochai, L.D. Yu, Nucl. Instr. Meth. B 267 (2009) 1650.
- [12] P. Chaivan, N. Pasaja, D. Boonyawan, P. Suanpoot, T. Vilaithong, Surf. Coat. Technol. 193 (2005) 356.
- [13] C.A. Hunniford, D.J. Timson, R.J.H. Davies, R.W. McCullough, Conformational Changes to Plasmid DNA Induced by Low Energy Carbon Ions, J. Phys. Conference Ser. 58 (2007) 355.
- [14] M. Mandelkern, J. Elias, D. Eden, D. Crothers, J. Mol. Biol. 152 (1) (1981) 153. See http://www.ncbi.nlm.nih.gov/pubmed/7338906, or http://en.wikipedia.org/wiki/DNA
- [15] M. Nastasi, J.W. Mayer, J.K. Hirvonen, Ion-Solid Interactions: Fundamentals and Applications, Cambridge University Press, 1996, p. 471.

Provided for non-commercial research and education use. Not for reproduction, distribution or commercial use.



This article appeared in a journal published by Elsevier. The attached copy is furnished to the author for internal non-commercial research and education use, including for instruction at the authors institution and sharing with colleagues.

Other uses, including reproduction and distribution, or selling or licensing copies, or posting to personal, institutional or third party websites are prohibited.

In most cases authors are permitted to post their version of the article (e.g. in Word or Tex form) to their personal website or institutional repository. Authors requiring further information regarding Elsevier's archiving and manuscript policies are encouraged to visit:

http://www.elsevier.com/copyright

Author's personal copy

Journal of Molecular Graphics and Modelling 28 (2010) 533-539



Contents lists available at ScienceDirect

Journal of Molecular Graphics and Modelling

journal homepage: www.elsevier.com/locate/JMGM



Molecular simulations of ultra-low-energy nitrogen ion bombardment of A-DNA in vacuum

Chanisorn Ngaojampa ^a, Piyarat Nimmanpipug ^a, Liangdeng Yu ^{b,c}, Somboon Anuntalabhochai ^d, Vannajan Sanghiran Lee ^{a,*}

- ^a Computational Simulation and Modeling Laboratory (CSML), Department of Chemistry and Center for Innovation in Chemistry, Faculty of Science, Chiang Mai University, Chiang Mai 50200, Thailand
- b Plasma and Beam Physics Research Facility (PBP), Department of Physics and Materials Science, Faculty of Science, Chiang Mai University, Chiang Mai 50200, Thailand
- ^c Thailand Center of Excellence in Physics, Commission on Higher Education, 328 Si Ayutthaya Road, Bangkok 10400, Thailand
- ^d Molecular Biology Laboratory, Department of Biology, Faculty of Science, Chiang Mai University, Chiang Mai 50200, Thailand

ARTICLE INFO

Article history:
Received 21 May 2009
Received in revised form 26 November 2009
Accepted 30 November 2009
Available online 4 December 2009

Keywords: Molecular dynamics Monte Carlo Ion bombardment A-DNA

ABSTRACT

For investigating mechanisms involved in low-energy ion beam induced mutation, besides experiments using low-energy and low-fluence ions to bombard naked DNA, molecular simulations were carried out as an effort towards the insight in molecular interactions between ions and DNA. In the current study, Monte Carlo (MC) and molecular dynamics (MD) simulations were applied. The results of MC simulations provide some clues about the interaction energies and sites of preference of N-ion bombardment on an A-DNA short duplex strand. MD simulations of a single N-ion moving towards the same DNA strand with different linear velocities corresponding to bombardment energies of 0.1, 1, 10 and 100 eV revealed information about changes in bond lengths and visibly distorted structures of bombarded nucleotides. The simulations demonstrated that ion-bombardment-induced DNA change in structure was not a random but preferential effect.

© 2009 Elsevier Inc. All rights reserved.

1. Introduction

Recently, low-energy ion beam biotechnology, emerging as a novel and highly interdisciplinary subject, has rapidly been developed [1]. The technology uses low-energy (an order of 10 keV) heavy ion beam, instead of protons, to bombard biological organisms to induce biological effects. The effects can eventually be applied for mutation breeding and gene transfer with high efficiencies. With impressive successes in ion beam biotechnology applications, investigations on relevant mechanisms have followed up. Basically two interaction effects are involved, namely direct and indirect effects [2]. The direct effect comes from the ions direct interacting DNA to cause displacements of the atoms in DNA and therefore bond breakage. The indirect effect is due to ionbombardment-induced secondary effects such as emissions of secondary electrons and X-ray, generation of heat and production of radicals, which can also cause DNA structural changes. There is a puzzle in the issue of the direct effect. In the experiments on ion beam induction of mutation, normally plant seeds with embryos are ion-bombarded. Here, energetic ions must travel through the materials that cover DNA in the cell nucleus before they can directly interact with DNA. Theoretical calculation estimates that the most of the ion energy is lost before the ion can impact with DNA for 30-keV nitrogen ions to pass through organic materials of a-few-hundred nanometers. Questions raised then include whether and how the ultra-low-energy ions are still able to cause DNA damage to induce mutation. Along with experimental efforts, in which keV ions bombarded naked DNA in vacuum and DNA strand breaks and mutation induction were discovered [3–9], molecular simulation is of necessity in studying the interaction between ions even at ultra low energy and DNA at the molecular level to reveal the nature of the interaction. There have been a plenty of studies on ion interaction with solids [10,11] and high-energy radiobiology [12]. However, there are yet lacks of studies on low-energy ion interaction with biological organisms and particularly DNA.

It has been found from experiments that treatments of ion beam on biological matter do not give complete random results, but rather biased ones [13]. For example, in an experiment, the plasmid M_{13} mp18 with the lacZ gene was bombarded by N-ion and transferred into host bacteria JM103 $E.\ coli.$ The results revealed that the dominant type of mutation was from a replacement (95%) while the rest was from the base deletion [14], but no insertion or replication of bases was detected. In addition, it was found that cytosine was the most sensitive residue taking more than 50% of the mutations. Another study using C-ion radiation [15] showed different non-random results with one base-deletions taking 38.5%

^{*} Corresponding author. Tel.: +66 5394 3341; fax: +66 5389 2277. E-mail address: vannajan@gmail.com (V.S. Lee).

of mutations. A comparative study reported a different outcome between N-ion and $^{60}\text{Co-}\gamma$ ray treated *E. coli* containing *rpoB* genes [16]. It was found that CG-to-TA, AT-to-GC and AT-to-TA took majority in the substitution mutations (92.13% or 82/89) in $^{60}\text{Co-}\gamma$ radiation, while N-ion bombardment gave CG-to-TA and AT-to-TA as the major substitutions. Moreover, GC-to-CG and AT-to-GC were found induced by N-ion bombardment only but not by the γ -ray, whereas AT-to-CG was not found after N-ion implantation, but was only found in $^{60}\text{Co-}\gamma$ radiation.

From the above studies, it is clear that there are many distinct molecular mechanisms for radiation-induced mutation which can effect the possible mutations generated from a given mutation method. Ideally to be able to predict and controls of the amount and type of mutation generated by a given method further insight into the mechanisms controlling the processing of mutated DNA is required. Currently, very little knowledge about the molecular mechanisms or pathways of DNA damage during ion beam implantation or other types of radiations has been found [2,15]. To complement the small amount of experimental evidence, some researchers have attempted to use computational methods to investigate the irradiation of DNA. Such studies include simulating accurate structures of mini-circle and super-coiled DNA molecules [19-22], DNA movements [23,24], tracking simulations of radiation particles in DNA molecules [3,25-27] and quantum molecular calculations of DNA damaged by radiation [28,29]. However, no such work has been done with ion beams induced mutation.

In this study, molecular modeling methods were selected to investigate the molecular interactions and elementary processes of DNA during irradiation by ion beam. To complement the experiment work done with N⁺ ion beam irradiation, we chose this form of ion beam particles to examine computationally. The study was divided into two main parts: (i) a Monte Carlo (MC) simulation of N^+ on a DNA strand and (ii) a molecular dynamics (MD) simulation of the effect of N⁺ implantation on a DNA strand. The MC simulations aimed to specify the preferred sites of N⁺ implantation around an arbitrary short strand of DNA using commercial software packages. The MD simulation aimed to investigate possible changes in the structure of the same DNA molecules after the bombardment. In both parts of the experiment, the DNA was in the A-form to best resemble real world experimental conditions, in which naked solid state DNA samples were bombarded by ion beam under vacuum [9]. Predominantly, this study focused on low-energy ion irradiation, because highenergy (above 10² keV) ion irradiation can cause very strong interactions with the DNA structure resulting in extensive damage to the DNA. By focusing our investigation on low-energy ion irradiation, the interaction of ions on DNA molecular sites allows identifying details of the effect of ion interactions to DNA structural changes.

2. Methods

2.1. DNA preparation

A 30-base-pair-long DNA duplex with sequence 5'-AAGAATG-GAA TCAAAGTTAA CTTCAAAATT-3' was constructed in A-form which was the form commonly observed in the dehydrated samples of DNA under vacuum condition with a pressure of 10^{-4} Pa for ion-bombardment experiments on the glass surface as well as in crystallographic experiments. The selected residues numbered between 760 and 789 bps of the green fluorescent protein plasmid (pGFP) from GenBank, sequenced by Chalfie et al. [30]. This portion of DNA contained the sequence that translates into the flourophore of the functioning protein (green fluorescent protein, GFP). The DNA duplex was built in Discovery Studio 1.7.1

software [31]. The CHARMm27 force field [32] was applied on this molecule. To obtain the DNA structure in the equilibrium state in vacuum, DNA was neutralized with Na-ion. The energy minimization, heating, equilibration and production MD simulation were performed using the Standard Dynamic Cascade protocol. The steps of energy minimization were divided into two parts: 1000 steps of the steepest descent minimization, and 4000 steps of the adopted bases Newton–Raphson minimization. Afterwards, heating was performed for 60 ps from 0.0 to 323.0 K according to the experimental temperature. Then, the equilibration was performed for 2900 ps at 323.0 K. And finally, the production was performed for 40 ps at the same constant temperature. All processes were done in NPT ensemble with the total simulation time of 3 ns. The final DNA structure from the MD simulation was used as the substrate for the adsorption of N⁺.

2.2. Monte Carlo simulations of N⁺ around a DNA strand

In Materials Studio 4.3 [33], the minimized DNA structure was imported, and the N $^+$ ion was constructed. The COMPASS force field [34,35] was assigned to both DNA and ion. Then, the adsorption calculations using the Adsorption Locator module were performed for ion fluences of 18 and 27 ions on one DNA molecule (corresponding to 6×10^{13} and 9×10^{13} ions/cm 2 as in the ion-bombardment experiment [9], respectively). In the calculation, the simulated annealing algorithm was performed for 5 cycles, with 15,000 MC simulation steps for each cycle as in Supplementary Fig. S1. The initial temperature was 1000 K before cooling down gradually to 323.0 K during the simulations. The simulation searched for the 10 best configurations of adsorption along with their interaction energy.

The starting configuration was adjusted to the current temperature for many iterating steps. Applying the Metropolis Monte Carlo method decided whether to accept or reject the change of N^+ position. The probability to transform from configuration m to n defined as P_{mn} is:

$$P_{mn} = \min\left[1, \exp\left\{\frac{E_n - E_m}{k_B T}\right\}\right] \tag{1}$$

where k is the Boltzmann constant and T is the simulation temperature [36]. The total energy of configuration m (E_m) is calculated by the following sum:

$$E_m = E_m^{AA} + E_m^{AS} \tag{2}$$

where E_m^{AA} is the intermolecular energy between the adsorbate molecules (N⁺) and E_m^{AS} is the interaction energy between the adsorbate molecules and the substrate (DNA) [37].

After the simulations, the results were shown as the equilibrium structure of DNA substrate, radial distribution function (RDF) plots (g(r)), distances of maximum RDF (r_{max}) and RDF integrals in the interval of 0.0–4.0 Å $(I_{4\dot{A}})$. The RDFs were measured from the N⁺ to each of the rest of atom types in the DNA. The atom types were arbitrary defined in the discussion (shown in Fig. 1). The results point out that N⁺ ions have specific sites of adsorption preference.

2.3. Molecular dynamics simulations of N^+ ion bombardment of DNA

In Materials Studio, the final structure of the DNA strand adsorbing 27 ions (corresponding to fluence of 9×10^{13} ions/cm²) with the best interaction energy (the lowest or most negative energy) was used as the initial structure for the simulations of N⁺ bombardments. All the nitrogen ion residues were deleted except for the one in the middle of the DNA strand as shown in Fig. 2a. The ion was moved 10 Å further from the strand by editing its Cartesian coordinate in the program database (PDB) file. The classical MD

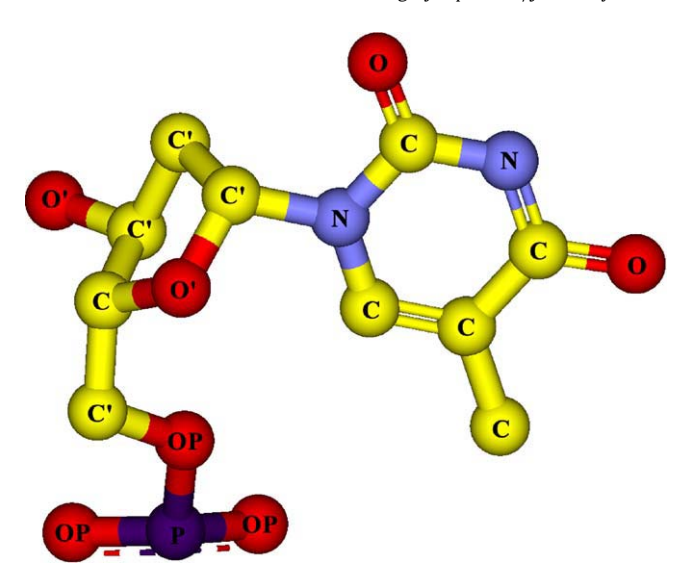


Fig. 1. Atom type definition of the nucleotide. For clear illustration of the MDs constructed DNA, the neutralization is not shown.

simulations of NPT (*N*: number of atoms, *P*: pressure, and *T*: temperature) ensembles at 323 K and 0 atm were performed for bombardments with energy of 0.1, 1, 10, and 100 eV in AMBER 9 [38]. The forcefields for DNA had partial charges explicitly parameterized for solution conditions, and thus might require modification for a vacuum condition. From the previous study by Rueda et al. [38,39], the charges of nucleobases in vacuo were scaled by a factor of 0.8 and the calculations showed that the changes in forcefield parameters had little effect in the conformational transition of the DNA duplex. The time step was 1 fs. The non-bonded cutoff was 9.0 Å. The residues 1–8, 22–38 and 52–60 at the end chains were held fixed. The velocity vectors applied in AMBER were calculated from the ion energy (*E*) and mass (*m*) using the equation:

$$v = \left(\frac{E}{2m}\right)^{1/2} \tag{3}$$

where v is the magnitude of the velocity (scalar quantity) and the unit vector for velocity direction was specified as well. The directions of the velocities were assumed to be in the direction from the ion to an arbitrary target atom in DNA calculated using the known coordinate of N^+ and the target atom.

3. Results and discussion

3.1. Ion and DNA interaction

From the energy report calculated by Adsorption Locator shown in Table 1, it was found that the best configuration of the DNA molecule adsorbing 27 N $^+$ ions had the interaction energy of -26.19 kcal/mol, which was 4.38 kcal/mol lower than the interaction energy of the one adsorbing 18 N $^+$ ions. The negative values of both fluences indicated that the adsorptions of N $^+$ on DNA molecules were thermodynamically favorable. The lower (more negative) interaction energy of the DNA molecule adsorbing 27 N $^+$ points out

Table 1The interaction energies of the best configuration for each ion fluence.

Ion beam fluence $(\times 10^{13} \text{ ions/cm}^2)$	Equivalent number of N ⁺	Interaction energy (kcal/mol)
6	18	-21.810
9	27	-26.192

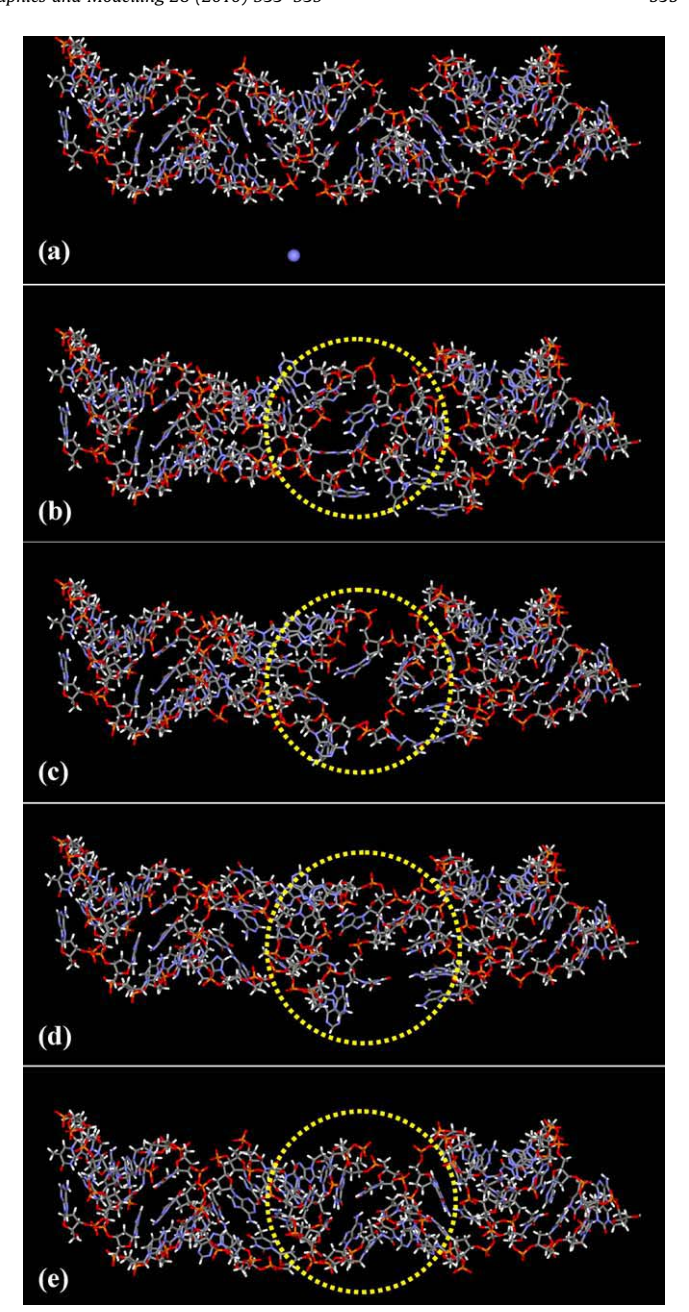


Fig. 2. The initial structure of DNA and the structures after bombardment with varied N-ion energy from selected simulation snapshots. (a) Initial structure; the particle at the low part represents the incident ion. (b) 0.1 eV at 4 ps. (c) 1 eV at 4 ps. (d) 10 eV at 4 ps. (e) 100 eV at 1 ps. The dash-circled areas are the main ion-bombardment-induced change parts.

that the 18 N $^+$ does not fill the DNA molecule's adsorption capacity since it releases even more energy when adsorbing an extra 9 ions. Moreover, it could be said that the adsorption capacity for the molecule was at least equal to 27 ions, or experimentally, 9×10^{13} ions/cm 2 . According to the experiment result reported earlier [9], when the ion fluence increases, the amount of DNA in the supercoiled form decreases and the amount in the linear form increases for N-ion bombardment. This indicates that nitrogen ions even with lower energy are effective in producing double strand breaks and thus more than capable of inducing gene mutation.

3.2. Radial distribution functions

Specific sites adsorption preference of N⁺ ions interacting with DNA from simulation was detailed. Table 2 summarizes the values

Table 2 Summary of the distance of maximum radial distribution functions, r_{max} , and the integral of radial distribution functions from 0.0 to 4.0 Å, $I_{4Å}$, of each atom type.

Fluence (×10 ¹³ ions/cm ²)	Atom type	r _{max} (Å)	$I_{4 ilde{A}}$
6	N	4.15	1.77
	0	6.25	1.46
	0′	5.15	1.48
	OP	3.25	3.20
	С	3.95	1.65
	C'	4.05	0.96
9	N	3.55	1.89
	0	3.25	4.15
	0′	3.75	3.73
	OP	3.35	3.30
	С	3.85	1.34
	C'	3.95	1.90

of r_{max} and I_{AA} for the best configuration at each fluence level. This table shows that, for fluence values equal to 6×10^{13} ions/cm², OP (O in phosphate) has the highest RDF integral value of 3.20, approximately twice as large as other cases. This pointed a fact that N⁺ preferred to be adsorbed at OP sites in phosphate groups of DNA. A straightforward explanation can be made from the basic chemical knowledge that oxygen atoms in phosphates have negative charge, which can bind strongly with positively charged species by electrostatic interaction. The distances of maximum radial distribution functions, r_{max} , also give similar results. OPs are suggested to have the strongest interaction with N⁺, as they have the least r_{max} while other atom types give far greater r_{max} values.

Different results were observed for the fluence of 9×10^{13} ions/ cm². Here, the three highest RDF integral values were all from oxygen atoms: O (O in bases), O' (O in sugars) and OP. The integral values for the three atom types were 4.15, 3.73 and 3.28, respectively. This might be because a larger number of ions increase the chance of interacting with other oxygen sites. Hence, oxygen is still the atom of preference for N⁺ irradiation. Other atom types give considerably smaller integral values. For this fluence, the values of r_{max} do not show as large differences as found with the previous fluence value. This might also be because of the more ions and thus the more chances to interact with other atoms. Still, oxygen atoms gave smaller value of r_{max} (3.25, 3.75 and 3.35 for O, O' and OP respectively) compared with those of other atom types (3.55, 3.85 and 3.95 for N, C and C', respectively). The results also agreed with the fact that oxygen atoms have large electronegativity, a measure of the ability of an atom to attract electrons it is sharing with another, and usually strongly polarize the formed bonds. Therefore, bonds with oxygen atoms are negative dipoles with partially negative charge on the oxygen side and thus they can still attract positively charged species. The RDF plots with the r_{max} reported in Table 2 indicate that N⁺ ions are likely to interact with OP, C, C', N, O' and O, respectively. The radial distribution function of N⁺ around OP in phosphates with a) the fluence of 6×10^{13} ions/ cm² and b) the fluence of 9×10^{13} ions/cm² was provided in Supplementary Fig. S2.

3.3. Molecular dynamic simulations

Our study used molecular dynamics to monitor the change in bond lengths within the DNA as the biomolecule was subjected to ion bombardment, and observed enormous changes in the bond length as described below. Large bond length changes might lead to bond breakage. However, the breakage of covalent bonds cannot be accounted from the simulation due to the limitation of classical MD. A quantum mechanics approach would be a solution for such simulation; however, it requires very small DNA duplexes in the simulation and also some approximations as well. Another

limitation of our approach as already mentioned in the method section resides in the forcefield for DNA, in which its partial charges parameterized for solution conditions may not be suitable in vacuo. Nevertheless, molecular dynamics techniques allow detailed time and space resolution for carefully selected systems which could provide details of the structural change in DNA after ion bombardment. The root mean square deviations (RMSD) were collected for every time step of the simulations to study the overall movement of the DNA structures during the simulation. The initial structure of DNA and the structures after bombardment with varied N-ion energy of 0.1, 1, 10, and 100 eV from selected simulation were snapshotted as shown in Fig. 2. At the simulation time of 4 ps, it is clearly seen large structural changes (Fig. 2b-d) in DNA for 0.1, 1, and 10 eV N-ion bombardment. For the highest ion energy of 100 eV, the ion seems to pass through DNA too quickly to snapshot for the change in the DNA structure and the structure even at 1 ps as illustrated in Fig. 2e does not show change compared with the initial structure shown in Fig. 2a. From the RMSD plots in Fig. 3, all bombardments exhibited rapid changes in RMSD during the simulations whereas the RMSDs for the unbombarded system at 298 and 323 K were smaller. At 100 eV ion bombardments, the RMSD peaked after 1.5 ps. Since large RMSD values represent a large movement and flexibility of the DNA structure, it is suggested that the flexibility might result in the simultaneous breakages of chemical bonds in DNA. The upcoming sections will present the changes in each type of bond lengths after the rapid changes in the RMSD.

The ranges and medians of the bond lengths of eight bond types were studied. The studied types included oxygen-phosphorus single bonds (O-P), oxygen-phosphorus aromatic bonds (O-P (ar)), carbon-carbon single bonds (C-C), carbon-nitrogen single bond (C-N), carbon-oxygen single bonds (C-O), carbon-carbon aromatic bonds (C-C (ar)), carbon-nitrogen aromatic bonds (C-N (ar)) and carbon-oxygen double bonds (C=O). The maximum, minimum and modal bond lengths in each bombardment were measured and reported in Tables 3–5. Relative deviations from the equilibrium lengths were noted in the parentheses on the right of the measured bond lengths. The results for the 100 eV bombardments were not presented because the simulation lasted for too short a time to notice bond length changes.

From the tables, the maximum bond lengths of all types were far higher than the equilibrium lengths for all bombardments. The bombardment producing the largest maximum bond lengths was the one with the 1 eV ion beam, followed by ones with 0.1 eV and 10 eV ion beams respectively. This indicates that the energy of 1 eV can cause the most stretching to all the bonds. In the same manner, the bombardment resulting in the largest minimum bond lengths

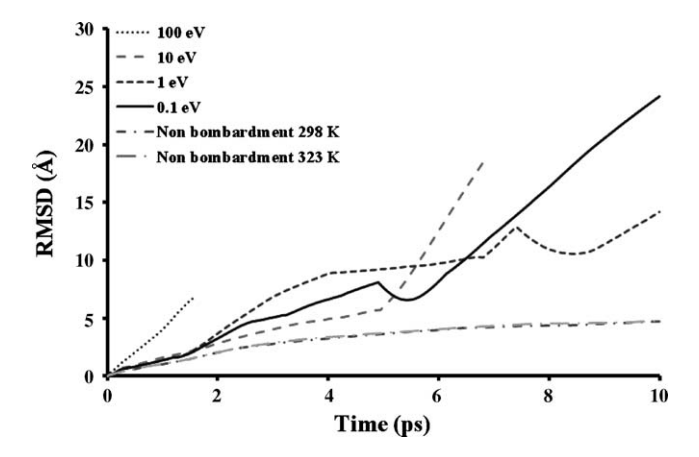


Fig. 3. RMSD plots for the MD simulations of ion bombardments at different ion energies in comparison with the unbombarded systems at 298 and 323 K.

Table 3Bond length maxima, minima and modes after 10 ps of 0.1 eV bombardment simulations.

Bond	Average	Bond le	Bond length after 0.1 eV bombardment (Å)				
type	equilibrium length (Å)	Maximum		Minimum		Mode	
O-P	1.582	1.817	(+15%)	1.411	(-11%)	1.618	(+3%)
O-P (ar)	1.486	1.606	(+8%)	1.306	(-12%)	1.498	(+1%)
C-C	1.518	1.800	(+19%)	1.398	(-8%)	1.560	(+3%)
C-N	1.490	1.664	(+12%)	1.405	(-6%)	1.489	(-0%)
C-O	1.433	1.566	(+9%)	1.302	(-9%)	1.445	(+1%)
C-C (ar)	1.387	1.557	(+12%)	1.329	(-4%)	1.426	(+3%)
C-N (ar)	1.351	1.604	(+19%)	1.088	(-19%)	1.388	(+3%)
C=O	1.230	1.528	(+24%)	1.133	(-8%)	1.220	(-1%)

Table 4Bond length maxima, minima and modes after 10 ps of 1 eV bombardment simulations.

Bond	Average	Bond le	Bond length after 1 eV bombardment (Å)					
type	equilibrium length (Å)	Maxim	Maximum		Minimum			
O-P	1.582	2.838	(+80%)	1.382	(-13%)	1.702	(+8%)	
O-P (ar)	1.486	2.236	(+50%)	0.971	(-35%)	1.498	(+1%)	
C-C	1.518	2.409	(+58%)	0.939	(-38%)	1.570	(+3%)	
C-N	1.490	2.153	(+44%)	1.398	(-6%)	1.543	(+4%)	
C-O	1.433	2.373	(+66%)	0.829	(-42%)	1.432	(-0%)	
C-C (ar)	1.387	2.116	(+53%)	1.116	(-20%)	1.408	(+2%)	
C-N (ar)	1.351	2.097	(+55%)	0.745	(-45%)	1.381	(+2%)	
C=0	1.230	1.787	(+45%)	0.958	(-22%)	1.221	(-0%)	

Table 5Bond length maxima, minima and modes after 6 ps of 10 eV bombardment simulations.

Bond	Average	Bond le	Bond length after 10 eV bombardment (Å)				
type	equilibrium length (Å)	Maximum		Minim	Minimum		
O-P	1.582	1.909	(+21%)	1.471	(-7%)	1.698	(+7%)
O-P (ar)	1.486	1.798	(+21%)	1.271	(-14%)	1.481	(-0%)
C-C	1.518	1.702	(+12%)	1.304	(-14%)	1.544	(+2%)
C-N	1.490	1.618	(+9%)	1.396	(-6%)	1.515	(+2%)
C-0	1.433	1.713	(+20%)	1.223	(-15%)	1.459	(+2%)
C-C (ar)	1.387	1.648	(+19%)	1.310	(-6%)	1.399	(+1%)
C-N (ar)	1.351	1.548	(+15%)	1.145	(-15%)	1.336	(-1%)
C=0	1.230	1.319	(+7%)	1.054	(-14%)	1.218	(-1%)

is still the one with 1 eV ion beam, followed by ones with 10 and 0.1 eV ion beam respectively. It is suggested that this energy gives the strongest shrinkage in overall bonds lengths. However, the bond lengths for 10 eV bombardments were measured at 6 ps since the simulation halted after that. So, the bond lengths due to this bombardment could be further elongated, and, by a rough approximation, the bond lengths could be close to ones bombarded if the simulation had lasted as long as 10 ps.

It was found that the bond type most sensitive to the ion bombardments was the O-P bonds. The maximum and modal lengths of this bond type had the largest deviation amongst all bond types, especially in 1 eV bombardment, where the bonds could elongate to as long as 2.838 Å (80% stretched from the equilibrium length). This corresponds to very large changes in overall RMSDs since the O-P bonds are a part of the DNA backbones. The DNA double helix could have an extreme stretching to twice of its normal length before its base pairs break, demonstrated by both theoretical modeling and nanomanipulation experiments [40]. As the DNA double helix is a multiply bonded structure, a nearly 100% stretching of the bond such as the one obtained above might cause breakage which can affect the overall structures and movements of DNA.

For further analysis of the bond lengths, the relative number of the elongated bonds for each type was recorded in order to study the changes of the bond lengths with changes of time. The percentages of the elongated bonds in DNA during the simulation of each bombardment were reported as line curves in Fig. 4. The percentage is calculated by dividing the counts of the elongated bonds (the bonds with more than 5% elongation) by the total counts of the bonds of the specific type. For example, if the total count of the O–P in the structure is 116, and the count of elongated O–P is 20, then the percent of the elongated bonds for the O–P in this structure is calculated as 20/116 = 17.2%.

From the figures, it was found that most of the bonds in the DNA tended to be elongated as time went by. This could be seen in the rising curves throughout the simulations. Some of the curves (especially for 0.1 eV bombardments) declined during some periods because the criterion of 5% elongation might still be too small for bond breakages. Furthermore, the three bond types with the largest percentage of the elongated bonds were O–P, C–C and C–C (*ar*) (navy, scarlet and orange graphs, respectively). And, the two types with the least percent of the elongated bonds were O–P (*ar*) and C=O (magenta and blue graphs respectively). So, major breakages would most probably occur in O–P, C–C and C–C (*ar*) as

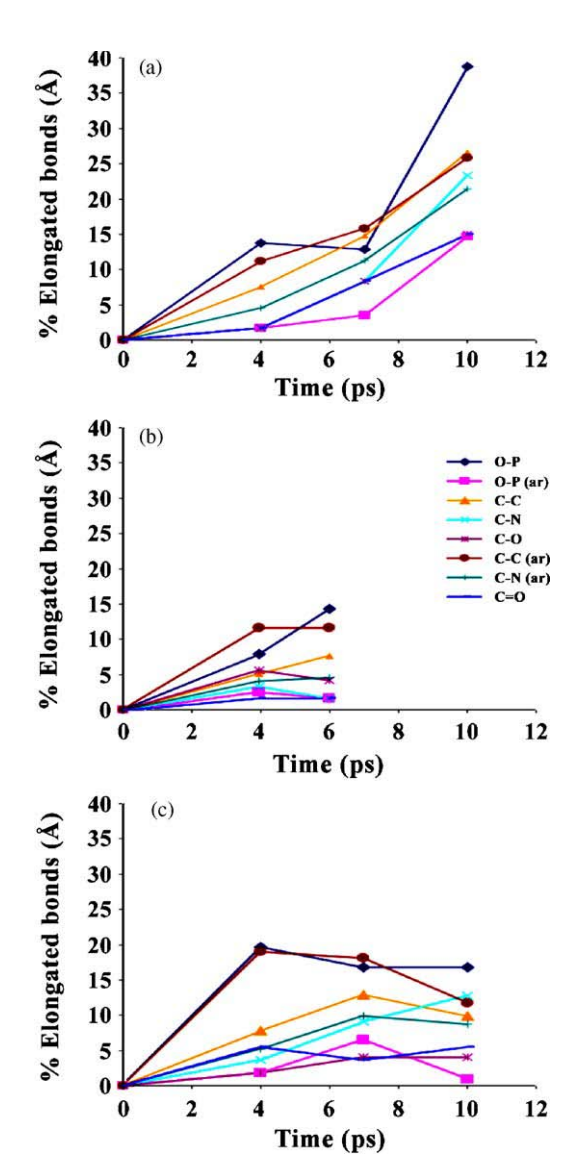


Fig. 4. Percentages of the elongated bonds in DNA during the simulation of (a) 10 eV, (b) 1 eV, and (c) 0.1 eV bombardments.

C. Ngaojampa et al./Journal of Molecular Graphics and Modelling 28 (2010) 533-539

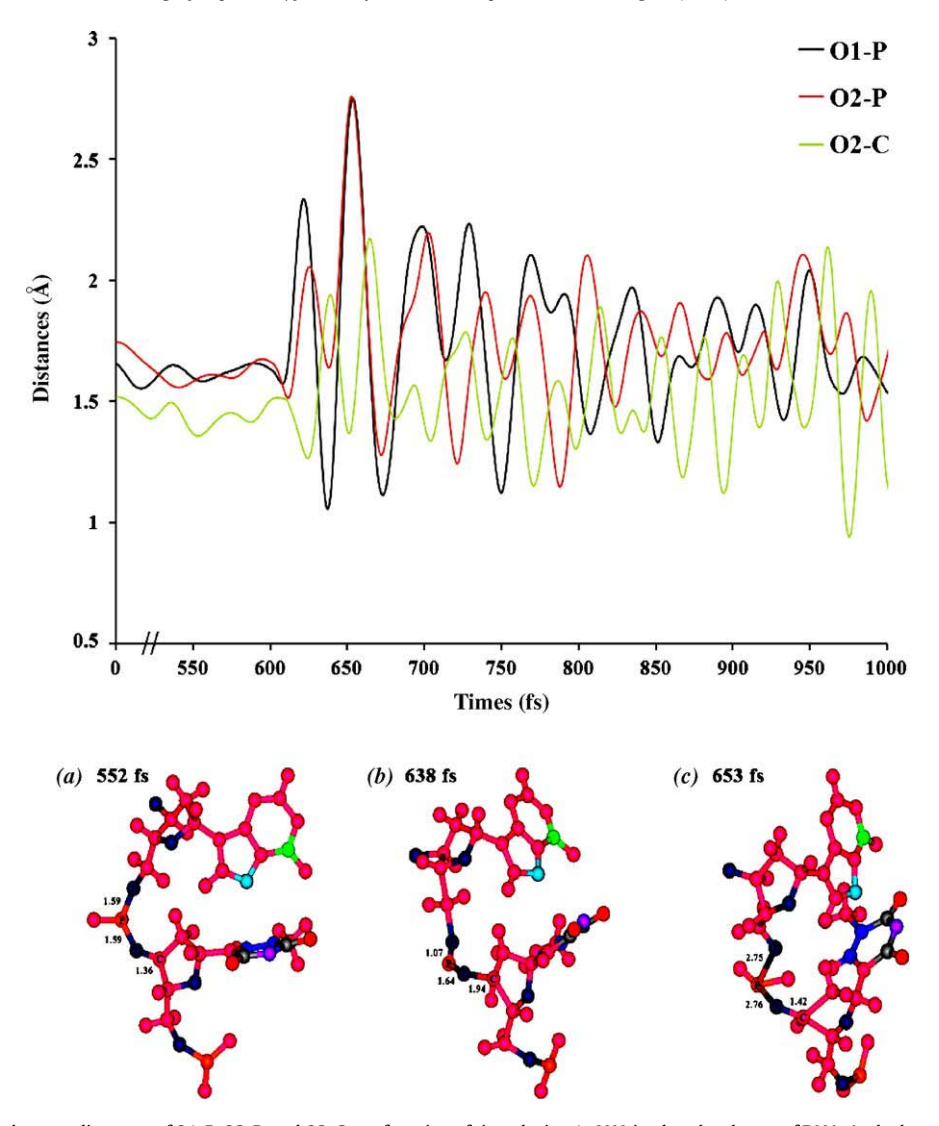


Fig. 5. Demonstration of the elongate distances of O1-P, O2-P, and O2-C as a function of time during 1 eV N-ion bombardment of DNA. At the lower part are the pictures of the structure (O1-P, O2-P and O2-C) selected at time of 552, 638, and 653 fs, respectively.

the DNA was bombarded, thus causing DNA damage. The elongate distances between O1-P, O2-P, and O2-C were observed during the first 1-ps trajectory of 1-eV N-ion bombardment of DNA as demonstrated in Fig. 5. The large displacement was started at 638 fs when the N-ion impacted on the DNA. The selected structure at 552, 638, and 653 fs showed the dynamics of the three breakable bonds at O1-P, O2-P and O2-C. From the usual thermal fluctuations, O-P and O-C fluctuation of the unbombarded system showed low RMSD below 0.5 at 298 and 323 K (the data is not shown). The counter ions were not included in the figure since they were distributed in other locations. The observation agrees well with the $RMSD\ results\ shown\ in\ Fig.\ 3, which\ corresponded\ to\ rapid\ changes$ in the structures after ion bombardment in comparison with the lower RMSD observed in the unbombarded system at 298 and 323 K. The graphs of the bond lengths also showed sudden changes at a corresponding time (7-10 ps). This can be explained that if breakages occurred in the DNA molecule, the molecular structure would have more freedom to move. On the other hand, for the 10 eV bombardments, Fig. 3 shows a correspondence of the graphs with the RMSD only for O-P. In contrast, the 0.1 bombardment did not show such a correspondence.

When comparing the energies of ion bombardments with the mean bond enthalpies (normally a few hundreds to no more than a thousand kcal/mol) [30], we found that most of the mean bond

enthalpies were in the range of the energies of bombardments (0.1–10 eV corresponding to the energy range of 10–932 kJ/mol). The relevance of the ranges indicated the sensibility of the simulations.

4. Conclusion

Ultra-low-energy ion bombardment of DNA in vacuum condition was simulated with the example of 0.1–100 eV nitrogen ions to study effects of the ion-DNA interaction on DNA damage. Monte Carlo simulations of adsorption of N⁺ on DNA revealed some information of interactions of $N^{\scriptscriptstyle +}$ with DNA. The fluence of 9×10^{13} ions/cm² due to its lower interaction energy with DNA resulted in stronger adsorption of N⁺ on DNA molecule than the fluence of $6\times 10^{13}~ions/cm^2.$ From the RDF analysis, $N^{\scriptscriptstyle +}$ ions are likely to interact with OP, C, C', N, O', and O site in DNA. MD simulations of the N⁺ bombardment on DNA molecules exhibited some interesting behavior of the DNA after collisions with N⁺. Firstly, the RMSDs of the DNA bombarded by N⁺ showed rapid increases after collisions. This might be due to the stretching and then probable breakage of bonds in the structures leaving the molecules more flexible. Further investigation of the stretching bonds was also studied using bond length analysis. The analysis of the bond length maxima, minima and modes showed that all types of bonds had stretching and shrinkage after the bombardment. Additionally, the

modes also gave the same tendency. The bombardment energy of 1 eV resulted in the most extreme maxima and minima, as well as the largest values of the modes of the bond lengths. The analysis also pointed out that the O–P bonds were the most sensitive to the collision. Lastly, the bond length changes with time for each bombardment were also studied. The O–P, C–C and C–C (ar) were the most vulnerable bonds in the DNA strands to ion bombardment. The bond enthalpies of these bond types corresponded well with the applied energy.

Acknowledgements

This research was supported by the Institute of Promotion of Science and Technology Teaching (IPST), the Thailand Research Fund (TRF), the Center for Innovation in Chemistry (PERCH-CIC), and the Thailand Center of Excellence in Physics (ThEP). The software resource is the courtesy of National Nanotechnology Center (NANOTEC), Thailand.

Appendix A. Supplementary data

Supplementary data associated with this article can be found, in the online version, at doi:10.1016/j.jmgm.2009.11.009.

References

- L.D. Yu, T. Vilaithong, I. Brown, Introduction to Ion Beam Biotechnology. English edition, originally authored by Yu Zengliang in Chinese, Springer Science & Business Media, New York, 2006.
- [2] Z. Wei, H. Xei, G. Han, Nucl. Instrum. Methods B95 (1994) 371.
- [3] Y. Zhao, Z. Tan, G.Y. Qiu, Y.H. Du, Nucl. Instrum. Methods B211 (2003) 211.
 [4] C.A. Hunniford, D.J. Timson, R.J.H. Davies, R.W. McCullough, Phys. Med. Biol. 52
- (2007) 3729. [5] Y. Chen, B. Jiang, X. Ding, X. Liu, C. Chen, X. Guo, G. Yin, Radiat. Environ. Biophys. 37
- [5] Y. Chen, B. Jiang, X. Ding, X. Liu, C. Chen, X. Guo, G. Yin, Radiat. Environ. Biophys. 37 (1998) 101.
- [6] S. Lacomb, Sech C. Le, V.A. Esaulov, Phys. Med. Biol. 49 (2004) N65.
- [7] Z.W. Deng, I. Bald, E. Illenberger, M.A. Huels, Phys. Rev. Lett. 95 (2005) 153201.
- [8] F.A. Chacon, Ion induced radiation damage on the molecular level, Ph.D. Thesis, University of Groningen, 2007.
- [9] R. Norarat, N. Semsang, S. Anuntalabhochai, L.D. Yu, Very low-energy and low-fluence ion beam bombardment of naked plasmid DNA, Nucl. Instrum. Methods B 267 (2009) 1650–1653.
- [10] H. Ryssel, I. Ruge, Ion Implantation, Wiley Chichester, 1996.
- [11] M. Nastasi, J.W. Mayer, J. Hirvonen, Ion-Solid Interactions: Fundamentals and Applications, Cambridge University Press, 1996.
- [12] E. Hall, Radiobiology for Radiobiologists, Lippincott Williams & Wilkins, 1993.
- [13] Z. Yu, Study on the interaction of low-energy ions with organisms, Surf. Coat. Technol. 201 (2007) 8006–8013.

- [14] J. Yang, L. Wu, L. Li, et al., Sequence analysis of lacZ? mutations induced by ion beam irradiation in double-stranded M₁₃mp₁₈ DNA, Sci. China C. Life. Sci. 40 (1997) 107–112.
- [15] Q. Wang, G. Zhang, Y.H. Du, Y. Zhao, G.Y. Qiu, Low-energy (30 keV) carbon ion induced mutation spectrum in the lacZ gene of M13mp18 double-stranded DNA, Mutat. Res. Fundam. Mol. Mech. Mutagen. 528 (2003) 55–60.
- [16] C.X. Xie, A. Xu, L.J. Wu, et al., Comparison of base substitutions in response to nitrogen ion implantation and ⁶⁰CO-γ ray irradiation in *Escherichia coli*, Genet. Mol. Biol. 27 (2004) 284–290.
- [19] E.A. Kummerle, E. Pomplun, A computer-generated supercoiled model of the pUC19 plasmid. Eur. Biophys. I. 34 (2005) 13–18.
- [20] C. Bouchiat, M. Mezard, Elastic rod model of a supercoiled DNA molecule, Eur. Phys. J. E. 2 (2000) 377–402.
- [21] F. Lankas, R. Lavery, J.H. Maddocks, Kinking occurs during molecular dynamics simulations of small DNA minicircles, Structure 14 (2006) 1527–1534.
- [22] W.K. Olson, V.B. Zhurkin, Modeling DNA deformations, Curr. Opin. Struct. Biol. 10 (2000) 286–297.
- [23] L.J. Maher, Mechanisms of DNA bending, Curr. Opin. Struct. Biol. 2 (1998) 688–694.
- [24] H. Nikjoo, C.E. Bolton, R. Watanabe, et al., Modelling of DNA damage induced by energetic electrons (100 eV to 100 keV), Radiat. Prot. Dosimetry 99 (2002) 77–80.
- [25] H. Nikjoo, D. Emfietzoglou, R. Watanabe, S. Uehara, Can Monte Carlo track structure codes reveal reaction mechanism in DNA damage and improve radiation therapy? Radiat. Phys. Chem. 77 (2008) 1270–1279.
- [26] R. Watanabe, H. Nikjoo, Modelling the effect of incorporated halogenated pyrimidine on radiation-induced DNA strand breaks, Int. J. Radiat. Biol. 78 (2002) 953–966.
- [27] H. Nikjoo, P. O'Neill, W.E. Wilson, D.T. Goodhead, Computational approach for determining the spectrum of DNA damage induced by ionizing radiation, Radiat. Res. 156 (2001) 577–583.
- [28] X. Li, M.D. Sevilla, L. Sanche, Density functional theory studies of electron interaction with DNA: can zero eV electrons induce strand breaks? J. Am. Chem. Soc. 125 (2003) 13668–13669.
- [29] J.M. Falcone, D. Becker, M.D. Sevilla, S.G. Swarts, Products of the reactions of the dry and aqueous electron with hydrated DNA: hydrogen and 5,6-dihydropyrimidines, Radiat. Phys. Chem. 72 (2005) 257–264.
- [30] M. Chalfie, Y. Tu, G. Euskirchen, W.W. Ward, D.C. Prasher, Green fluorescent protein as a marker for gene expression, Science 263 (1994) 802–805.
- [31] Discovery studio 1.7.1, Accelrys Software Inc., San Diego, CA, 2006.
- [32] N. Foloppe, A.D. MacKerell Jr., All-atom empirical force field for nucleic acids: I. Parameter optimization based on small molecule and condensed phase macromolecular target data, J. Comput. Chem. 21 (2000) 86–104.
- [33] Materials Studio Modeling 4.3, Accelrys Software Inc., San Diego, CA, 2008.
- [34] H. Sun, Compass: an ab initio force-field optimized for condensed-phase applications; overview with details on alkane and benzene compounds, J. Phys. Chem. B 102 (1998) 7338–7364.
- [35] D. Rigby, H. Sun, B.E. Eichinger, Computer simulations of poly-(ethylene oxide): force field, PVT diagram and cyclization behavior, Polym. Int. 44 (1997) 311–330.
- [36] N. Metropolis, A.W. Rosenbluth, M.N. Rosenbluth, A.H. Teller, E. Teller, Equation of state calculations by fast computing machines, J. Chem. Phys. 21 (1953) 1087– 1092.
- [37] D.A. Case, T.A. Darden, T.E. Cheatham Iii, et al., AMBER 9 (2004).
- [38] M. Rueda, S.G. Kalko, F.J. Luque, M. Orozco, The structure and dynamics of DNA in the gas phase, J. Am. Chem. Soc. 125 (2003) 8007–8014.
- [39] M. Rueda, F.J. Luque, M. Orozco, Nature of minor-groove binders DNA complexes in the gas phase, J. Am. Chem. Soc. 127 (2005) 11690–11698.
- [40] A. Lebrun, R. Lavery, Modelling extreme stretching of DNA, Nucl. Acids Res. 24 (12) (1996) 2260–2267.

Low-Energy Ion Beam Biotechnology at Chiang Mai University

L.D. Yu^{1,2}* and S. Anuntalabhochai³

- ¹ Plasma and Beam Physics Research Facility (PBP), Department of Physics, Faculty of Science, Chiang Mai University, Chiang Mai 50200, Thailand
- ² Thailand Center of Excellence in Physics, Commission on Higher Education, 328 Si Ayutthaya Road, Bangkok 10400, Thailand
- ³ Molecular Biology Laboratory, Department of Biology, Faculty of Science, Chiang Mai University, Chiang Mai 50200, Thailand

(*Corresponding author: Email: yuld@fnrf.science.cmu.ac.th)

ABSTRACT

MeV-ion beam has long been applied to research and applications in biology for many decades as highly energetic ions are undoubtedly able to interact directly with biomolecules to cause biological changes. However, low-energy ion beam at tens of keV and even lower has also been found to have significant biological effects on living materials. The finding has led to applications of ion-beam induced mutation and gene transfer. From the theoretical point of view, the low-energy ion beam effects on biology are difficult to understand since the ion range is so short that the ions can hardly directly interact with the key biological molecules for the changes. This talk introduces interesting aspects of low-energy ion beam biology, including basis of ion beam biotechnology and recent developments achieved in Chiang Mai University in relevant applications such as mutation and gene transfer and investigations on mechanisms involved in the low-energy ion interaction with biological matter such as eV-keV ion beam bombardments of naked DNA and the cell envelopes.

INTRODUCTION

Plant seeds were carried by spacecrafts and sent to the space for mutation purpose because high-energy cosmic particles might irradiate and penetrate the seeds to induce mutation. However, scientists have found that they can achieve the same effect on the earth ground using low-energy particle bombardment of the seeds in a much cheaper, easier and more effective way. That is the initiation of the low-energy ion beam technology application in biology. Low-energy ion beam biotechnology (IBBT) is such a technique that uses energetic ion beams (a few tens of keV in energy being enough), generated and transported by an ion accelerator, to bombard biological organisms in vacuum to induce mutation breeding and gene transfer for increasing applications of the biological substance as well as to detect and analyze characteristics of biological organisms [1]. Ion beam interaction with biological living organisms is so different from that with normal solid materials. Biological organisms are living, and ion beam treatment should not kill them. Fresh cells contain a large amount of water, which essentially evaporates in vacuum, and the evaporation causes differences in the target status from that in normal atmosphere. Biological material structures are highly porous and inhomogeneous, and ions penetrate and sputter abnormally more than for normal condensed materials. The functioning structures of organisms are very complicated and different ion-beam treated locations have different responses, and hence in order to get a certain response, ion beam should be precisely controlled to target the location. Biological organisms are extremely sensitive to ion irradiation,

will actively respond to the irradiation and thus highly produce secondary effects, which can greatly affect consequences of ion beam bombardment. Organisms have recovery ability, and ion beam radiation damage may be repaired and thus ion beam effects may disappear in a certain time period. Different parts of an organism may have communications and an ion-beam treated location may produce unexpected effects. This is a highly interdisciplinary field of physics, biology, agriculture and medical science. It is an extension of ion beam modification of conventional solid materials and an extension of high-energy radiobiology. This review talk introduces interesting aspects of low-energy ion beam biology, including basis of ion beam biotechnology and recent developments achieved in Chiang Mai University (CMU) in relevant applications such as mutation and gene transfer and investigations on mechanisms involved in the low-energy ion interaction with biological matter.

IBBT FACILITIES AT CMU

A bioengineering-specialized ion beam line has been self-developed, which possesses special features [2]: vertical main beam line, low-energy (30 keV) ion beams, double swerve of the beam, a fast pumped target chamber, and an *in-situ* atomic force microscope (AFM) system [3] chamber, as shown in Fig.1. The whole beam line is situated in a bioclean environment, occupying two stories. The quality of the ion beam has been studied. It has proved that this beam line has significantly contributed to our research work on low-energy ion beam biotechnology. Another facility is a non-mass-analysis ion implanter [4], which was originally developed for industrial applications and later modified for bioengineering purpose as well. This installation is featured with high current, low-to-medium energy applicability, large implantation area, and versatile sample holder and stage with water cooling. This facility is particularly used for ion beam mutation induction.

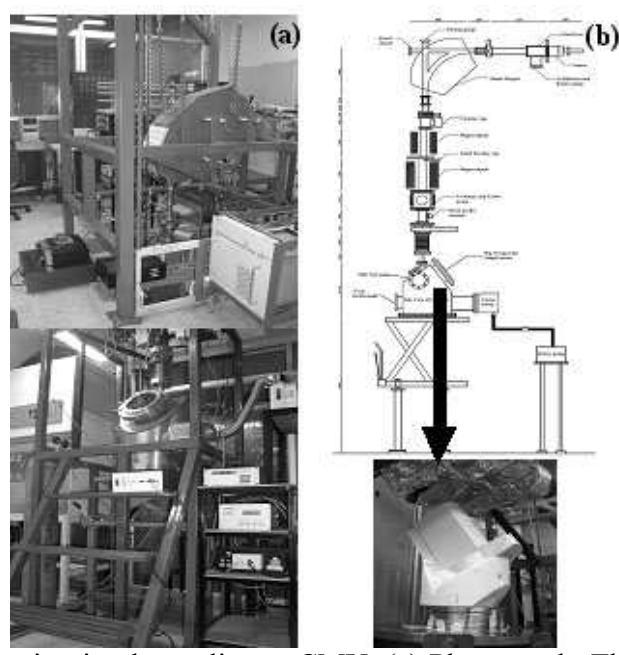


Figure 1. The bioengineering ion beam line at CMU. (a) Photograph. The upper one is the part upstairs and the lower one is the part downstairs. (b) Schematic diagram with a photo of the *insitu* AFM sitting inside the chamber.

ION BEAM INDUCTION OF GENE TRANSFER

Introduction

Using ion beam bombardment is a physical method to induce DNA transfer in cells. In the method, the ion beam parameters such as ion species, energy and fluence are precisely controlled so that the ions can only bombard the cell envelope to crate radiation-damage-induced special structures which are expected to act pathways for exogenous macromolecules to pass through. The range and extent of the radiation damage for the target material of the cell envelope depend on the ion beam parameters as mentioned above. Therefore, the ion beam parameters should be carefully designed for treating different biological cell species which have different cell envelope thicknesses. The post biological treatment for DNA transfer is carried out immediately after ion beam bombardment normally in standard biological procedures.

DNA transfer

Using the critical ion beam conditions, we succeeded in DNA transfer in bacterial cells of E. coli [5,6]. Fig. 2 shows the introduction of pGEM-T easy and pGFP plasmids, containing Lac z and GFP genes respectively, into E. coli strain DH5α bombarded by Ar ions at an energy of 26 keV and a fluence of 2×10^{15} ions/cm². In the experiment, the bacterial cells were directly bombarded by the Ar-ion beam in vacuum, followed by a standard DNA transfer process in solution. We observed the plasmid DNA indeed transferred in the ion-bombarded bacterial cells but not in the unbombarded control. The blue and green colonies observed under UV at the bacteria incubated in medium are the indicators of the marker genes Lac z and GFP, respectively, and thus demonstrate that the DNA has been indeed transferred into the bacterial cells. The subsequently measured DNA molecular sizes further confirm that the transferred DNA is the original exogenous DNA. In another work, two marker genes, GFP and lipoic acid synthetase, were chosen to transfer into yeast (Saccharomyces cerevisiae strain W303C, MATa ura3-52 his3-∆200 lys2-801) [7]. The yeast cells were bombarded by nitrogen ions at energy of 50 keV with fluences of 0.5, 1, and 2×10^{16} ions/cm², and subsequently the bombarded yeast cells were incubated with both plasmids, pYGFP and pYlip plasmids, carrying GFP and lipoic acid synthetase genes separately. The expression of GFP gene in yeast was observed by green yeast colonies under UV light (Fig. 3a), while the expression of lipoic acid synthetase gene was analyzed using SDS-PAGE method. A gene's product at 34 kDa was detected only in the bombarded yeast with the pYlip (Fig. 3b). The expression of both genes was induced by culturing the yeast cells in YPD (yeast potato dextrose) media supplemented with galactose for 10 hrs. These evidences demonstrated that nitrogen ions assisted gene transfer into the yeast cells.

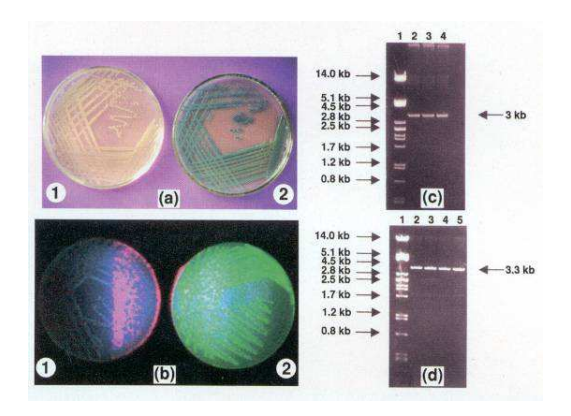
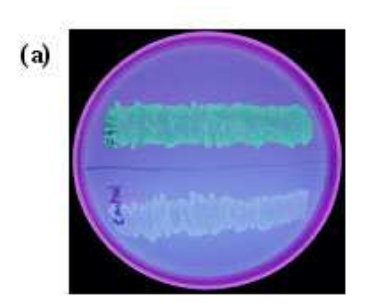


Figure 2. Expression of the ion-beam-induced gene transfer in the cells of bacteria *E. coli* [(a), (b)] and the corresponding molecular size measurement [(c), (d)] by electrophoresis. (a) and (c): transferred pGEM-T easy plasmid. (b) and (d): transferred pGFP plasmid. (1) *E. coli* without gene, and (2) with gene transferred. In (c) and (d), lane 1 shows the standard molecular size markers, and other lanes show the DNA molecular sizes measured by various restriction enzymes.



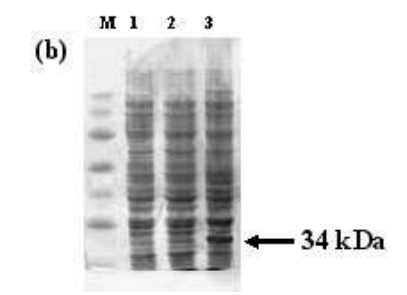
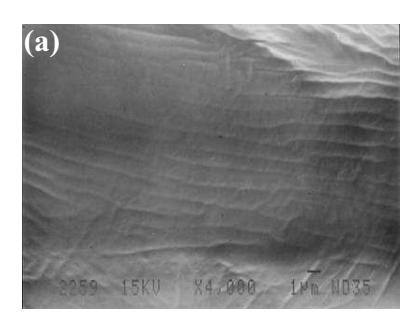


Figure 3. Demonstration of ion-beam-induced transfer of plasmid DNA, pGFP and pYlip containing *GFP* and *lipoic acid synthetase* genes, respectively, in yeast (*S. cerevisiae* strain W303C) bombarded by nitrogen ions at energy of 50 keV and fluences of 2 × 10¹⁶ ions/cm². (a) A green colony of yeast indicates an expression of *GFP* gene in the yeast cells. (b) SDS-PAGE analysis of *lipoic acid synthetase*; (1) *S. cerevisiae* wild-type, (2) transformed but non-induced, (3) transformed and induced recombinant *S. cerevisiae*, and (M) molecular mass marker. The arrow indicates the band (M~34 kDa) corresponding to recombinant lipoic acid synthetase. The gel was stained with Coomassie blue to visualize the protein bands.

Investigations on mechanism

Mechanisms involved in ion beam induction of gene transfer have been investigated. We found that subjected to ion bombardment, micro- and nano-craters were formed on the biological cell surface of either plants or bacteria [3,8-10], as shown in Fig. 4. These tiny craters might function as pathways for the exogenous macromolecule to transfer into cells. A physical model was set up for ion implantation of the cell wall materials to explain abnormally great ion range and sputtering in the cell wall [11]. The model demonstrated that with appropriately low ion energy and fluence, ions were able to penetrate through the cell envelope and possibly create the pathways.

For separately investigating ion bombardment effect on the cell envelope materials, we used chemically similar chitosan and cellulose membranes to substitute for the cell envelope subjected to ion bombardment. It was found that the electric impedance decreased and the capacitance increased and these electric property changes enhanced DNA transfer through the membrane [12]. Electron-neutralized ion beam was also applied to bombard the membranes to check charge effect. It was found that the neutralized beam reduced the impedance pronouncedly compared with the ion beam [13].



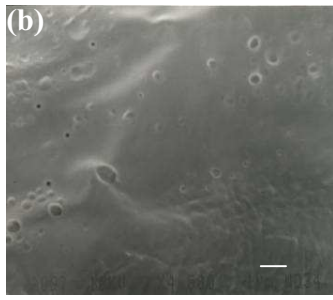


Figure 4. Low-energy ion bombardment induced formation of micro/nano-craters in the plant cell envelope. (a) SEM photograph of the surface of the unbombarded onion skin cells. (b) *Ex-situ* SEM photograph of the 30-keV Xe-ion bombarded onion skin cell. Bar scale: 2 μm.

ION BEAM INDUCTION OF MUTATIONS

Introduction

Induction of mutation by external energetic particles stems from the idea that the particles penetrate through the coat of the germinating parts of biological organisms such as the embryo of a seed or the buds and then interact with the genetic substance in the cells of the germinating parts. In normal operation conditions, biological organisms are put in vacuum environment and subjected to ion beam bombardment. Therefore, special measures should be taken. In the case of seeds, if the seed is big and its coat is thick, it is better to remove the seed coat covering the embryo part beforehand to directly expose the embryo part to the ion beam for high-efficiency mutation induction. In case the seed is too small, if the embryo location is known it is better to orient the embryo part towards the ion beam; if the embryo location is unknown, the seeds have to be positioned in random for ion bombardment. In the case of tissues such as buds, the non-critical parts of the tissue should be well wrapped to prevent the water-evaporation worsening the vacuum and to expose only the germinating part to the ion beam. Here we introduce some examples of our successes in ion-beam-induced mutations and relevant studies on mechanisms.

Mutation induction

Two varieties of local rice (Oryza sativa indica) [14], purple glutinous rice (Kum Doi Saket) and Thai jasmine rice (KDML 105) [15], were chosen for the mutation induction purpose. Thousands of seeds of the rice were implanted with nitrogen ions at energy of 30-60 keV to fluences of an order of 10¹⁶ ions/cm² and mutants were selected from grown plants of the seeds. For the purple glutinous rice, seedlings with green pigment were observed in M1 generation while the wild type was purple. Seeds in the M1 generation were harvested and cultivated for M2 generations. Their phenotypes were divided into 3 groups: 1) the whole plant was still green, 2) only the stem was green while the leaf blade and sheath were purple, and 3) the whole plant was purple. It was also observed that the pigment of the seat coat and pericarp were not purple as was found in the wild type (Fig. 5). In a mutant, the starch content in the harvested seeds showed a blue-black color versus the normal color when stained with I₂ solution (Fig. 5). This indicated that low energy ion beam induced mutation of glutinous rice. Analysis of the DNA fingerprint revealed genotypic differences among rice samples in the M2 generation, indicating genetic modification occurring in their genome. For Thai jasmine rice, various mutants were obtained after screening. Fig. 6 shows one of the examples in the straw stem height change. DNA sequencing analysis obtained two DNA sequences. One belonged to a member of flavonoid

3'hydroxylase of *O. sativa japonica* with the highest identity of 60%. The flavanoid 3'hydroxylase is the enzyme that is involved in anthocyanin biosynthetic pathway. Anthocyanin pigments display color ranging from bright red/purple to blue. Color variation of the main red/purple in various tissues such as leaf sheath, collar, auricles, ligule, and pericarp, and light brown in starchy endosperm may be induced from mutation in genes controlling the purple/red to blue. Another was 61 % identity to cytochrome P450 of *O. sativa japonica*. It is a member of cytochrome P450, playing significant role in biological systems, such as hormonal regulation, phytoalexin synthesis, as well as flower petal pigment biosynthesis, probably resulting in the phenotypic variations.

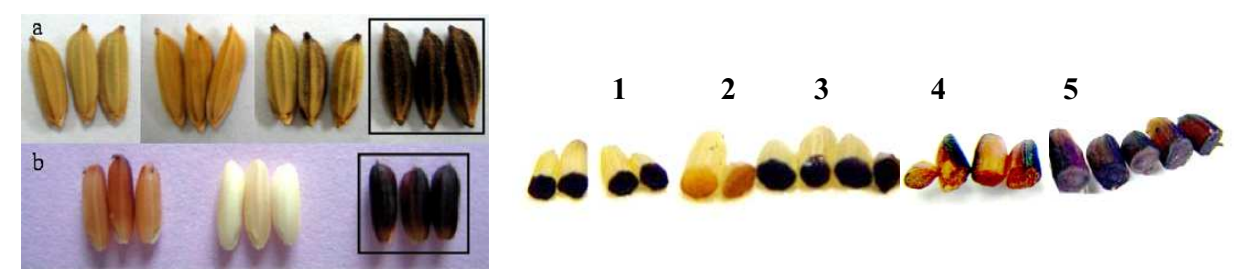


Figure 5. Ion-beam-induced mutations of purple rice. Left: phenotypes of M2 seeds. Pigment of seed coat (a) and pericarp (b) were not dark purple as in wild type (square box). Right: Starch content in purple rice seeds. After staining with aliquot of iodine solution the blue-dark color was observed in non glutinous rice seeds bombarded by nitrogen. Non glutinous Thai jasmine rice seed control (1), bombarded purple rice seeds with white pericarp from the same panicle (2 and 3), purple rice seed control (4) and non-glutinous black rice seeds (5).

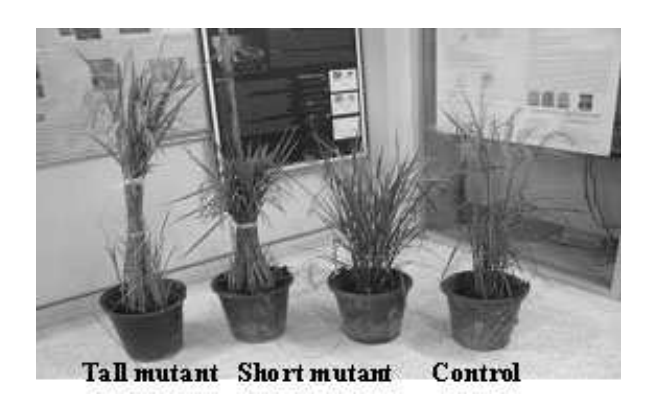


Figure 6. Photograph of the ion-beam-induced mutants in M_5 generation, showing the straw stem height change.



Figure 7. One of the examples in ion-beam-induced color change in Gerbera flower petal. Note that the original color should be all in red.

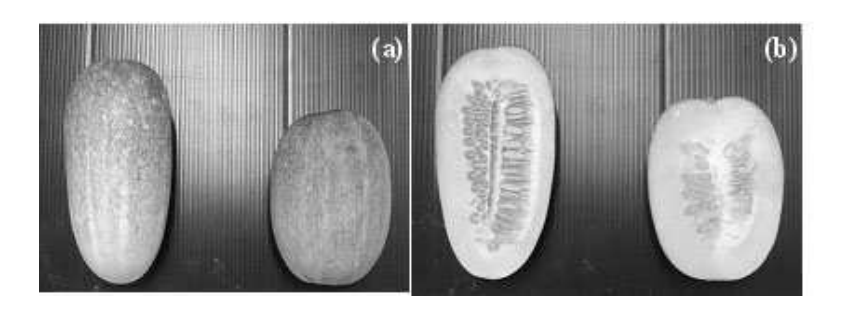


Figure 8. Effect of ion beam on reproductive organ of cucumber. (a) Size comparison of whole fruit of cucumber between control (left) and hybrid (right). (b) Fresh meat of control (left) and hybrid (right).

Seeds and buds of various local flowers such as petunia, rose, gerbera and chrysanthemum were bombarded by nitrogen ion beams at energies of 30-60 keV and fluences of $1 \times 10^{16} - 5 \times 10^{17}$ ions/cm² in vacuum [16]. After ion beam treatment, the seeds or buds were cultured to grow. After screening, various mutants were found with features of changes in the flower shape, color, petal shape and size, and petal color (Fig. 7). DNA analysis revealed different polymorphic bands in the mutants from in the control. Seeds of two vegetable species, cucumber (*Curcumis sativus*) and mung bean (*Vigna radiata*) were bombarded by N-ion beam at several tens of keV to fluences ranging from 10^{16} to 10^{18} ions/cm². For cucumber, about 3% of bombarded plants at 2×10^{17} ions/cm² showed their size of female reproductive organ (ovary) greater than control and some were transformed into male reproductive organ. Crossing pollination between the greater organ to male organ of wild type resulted in short of fruit size but normal fresh meat. (Fig. 8). For bean, the ion-beam-induced mutants showed less stem height, number of leaves, growth rate and dry mass than the control significantly.

Gene cloning

Anthracnose, caused by the fungus *Colletotrichum* sp., is one of the important diseases affecting flowers. The use of natural antagonists has recently been applied for biological control. In the study, the target material was *Bacillus* (B.) *licheniformis* (a kind of bacteria) isolated from hot springs in Chiang Mai, showing its activity to suppress conidia germination of the fungus and reduce symptom caused by the disease in flower plants. N-ions at energy of 28 keV were used to bombard the bacteria to a fluence range of $1 - 10 \times 10^{15}$ ions/cm². After ion bombardment, mutants were screened and one of the mutants with loosing its antagonistic property was obtained. For this mutant DNA fingerprint analysis was carried out. The additional band of the mutant in the DNA analysis was subcloned into pGEM-T easy vector and sequenced. Partial sequence analysis revealed that this fragment was a gene encoding enzyme lipase. Regarding to the lipase gene sequence, pair of specific primer was designed from the B. licheniformis database to amplify the entire sequence of the gene using its genomic as template. In order to determine the expression of the lipase gene in yeast, the entire lipase gene was subcloned into pYES2 and named pYES2-LicLip, then transferred into yeast cell via low energy ion beam. The result showed that only the yeast transformed with pYES2-Liclip induced colonies and *B. licheniformis* induced colonies presented antifungal activity to plant pathogen, collectotrichum musae [17].

Investigation on mechanisms

How low-energy ion beam can induce mutation is yet a puzzle. Theoretical calculations predict the ion range in the materials that cover DNA such as seed coat and cell envelope considerably shorter than the material thickness and thus it is impossible for the low-energy ions to act with DNA. However, the reality may be far deviated from the assumption. The plant seed coat may be significantly porous and hence the stopping power of the seed coat to the incident ions is significantly lower than that of a homogenously dense seed coat material as assumed by the computer program. Furthermore, we have found that there exist a number of cracks in the plant seed coat or the embryo membrane, as shown in Fig. 9, particularly under ion bombardment. These cracks may be channels for incident ions to penetrate deeply into the embryo.

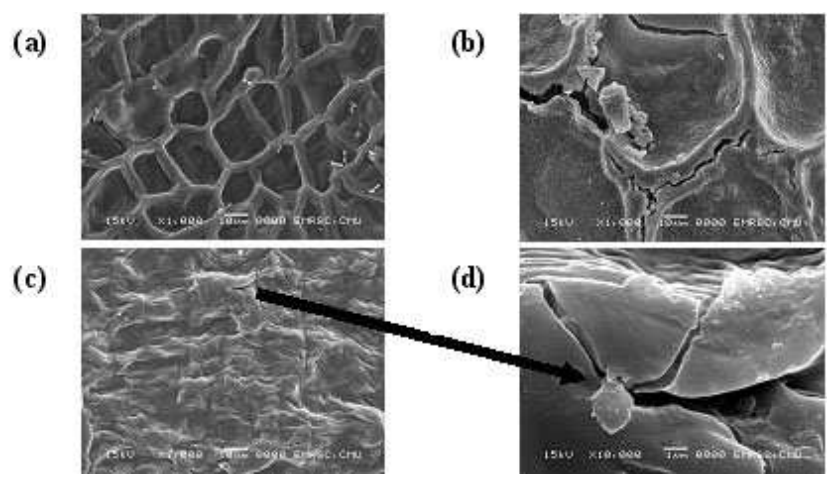


Figure 9. SEM microphotographs of the surfaces of (a) rice seed embryo, (b) flower petunia seed coat, (c) green bean seed embryo, and (d) zoom of the crack from (c).

When ions are implanted into biological matter, depositions of energy and mass and exchanges of momentum and charge combinatively work to produce unexpected effects much more than in condensed matter [1]. The existing and created biological channels can lead to direct interaction of ions with DNA. Ion implantation induced heat, secondary electron and X-ray emissions and produced free radicals as secondary effects may interact with the genetic substance to cause mutation. Some of these have primarily been theoretically discussed [18], but further experimental investigations are needed to provide evidence to support these suppositions. We have carried out some basic studies on this issue.

In order to simulate the final stage of ions interact with DNA, very low-energy and low-fluence nitrogen and argon ions of 1-5 keV from with ion beam or plasma with fluences of orders of $10^{11} - 10^{13}$ ions/cm² were used to bombard naked plasmid DNA in vacuum. After ion bombardment, gel electrophoresis and DNA sequencing were operated on the DNA. It was found that low-energy low-fluence ions could indeed produce DNA damage in the forms of single strand break, double strand break and multiple double strand breaks to cause mutation. Lighter active nitrogen ions are found more effective in induction of mutation than heavier inert argon ions, probably due to more biological effects. The results confirm that one of the physical mechanisms in ion beam mutation is a small portion of incident ions capable of penetrating the materials covering the nucleus to directly interact with DNA and thus cause mutation [19].

Since at present it is technically difficult in determining the intrinsic features of ion-induced DNA changes, computer simulation becomes a very useful tool to assist in finding answers. Molecular dynamics simulation (MDS) of low-energy ion interaction with DNA has also been involved in the research at CMU [20]. In the MDS, carbon and nitrogen ions at energy of 0.1 – 100 eV bombarded A-DNA (Fig. 10) to simulate the ion interaction with DNA in vacuum. The results show that for the nitrogenous base pairs, poly-AT is more sensitive to argon ion bombardment than poly-GC; for the phosphate group, deoxyribose (sugar) and bases, nitrogen ions interact in the preference sequence with OP, O (in base), O' (in sugar), N, C (in base) and C' (in sugar) atoms and most easily break the O-P bond and followed by C-C, C-C (aromatic) and C-N bonds. The findings demonstrate that low-energy ion beam induced DNA structural modification is not a random but preferential effect.

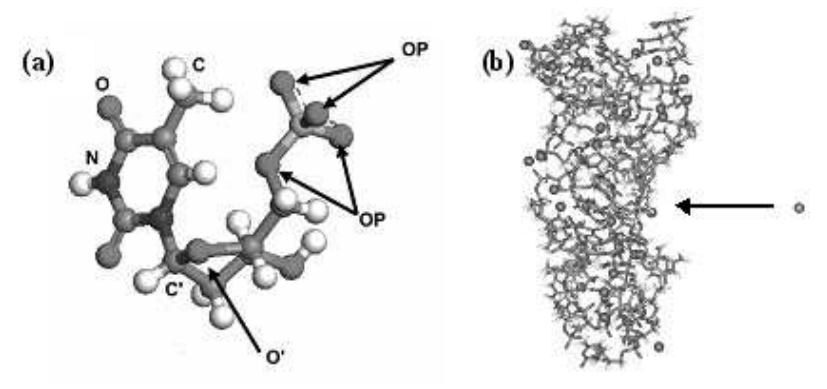


Figure 10. MDS of ion bombardment of A-DNA. (a) Atom type definition of the nucleotide. (b) Ion incidence to DNA.

CONCLUSION

Low-energy ion beam has been demonstrated to have effective multiple effects on induction of mutation and gene transfer due to its multi-factor interaction with biological organisms. The induced mutation is in a broad spectrum and the gene transfer is in a high efficiency. These have brought significant applications to agriculture, horticulture, microbiology and medical science. Relevant mechanisms are being explored. Direct interaction between ions and genetic substance leading to mutation is involved and found that the ion interaction with DNA is preferential in atomic locations and chemical bond types. Electric property changes in the cell envelope induced by ion implantation cause assistance in gene transfer.

ACKNOWLEDGEMENTS

We wish to thank our research staffs for their contributions to the projects, particularly named T. Vilaithing, P. Apavatjrut, A. Krasaechai, B. Phanchaisri, V.S. Lee, P. Nimmanpipug, and R. Chandej. Special thanks are also presented to international collaborators, particularly named Z.L. Yu, I.G. Brown, S. Sangyuenyongpipat, etc. The research has been supported by Thailand Research Fund, National Research Council of Thailand and Thailand Center of Excellence in Physics.

REFERENCES

- [1] Yu Zengliang, Eng eds.: Yu Liangdeng, Thiraphat Vilaithong, Ian Brown, *Introduction to Ion Beam Biotechnology* (English Edition), (Springer Science & Business Media, New York, 2006).
- [2] L.D. Yu, S. Sangyuenyongpipat, C. Sriprom, C. Thongleurm, C. Tengsirivattana, R. Suwanksum, and T. Vilaithong, *Nucl. Instr. Meth.* **B 257**, 790-795 (2007).
- [3] S. Sangyuenyongpipat, L.D. Yu, T. Vilaithong, I.G. Brown, *Nucl. Instr. Meth.* **B 257**, 136-140 (2007).
- [4] S. Davydov, L.D. Yu, B. Yotsombat, S. Intarasiri, C. Thongleurm, V. A-no, T. Vilaithong, M.W. Rhodes, *Surf. Coat. Technol.* **131**, 558-562 (2000).
- [5] S. Anuntalabhochai, R. Chandej, B. Phanchaisri, L.D. Yu, T. Vilaithong, I.G. Brown, *Appl. Phys. Lett.* **78(16)**, 2393-2395 (2001).
- [6] B. Phanchaisri, L.D. Yu, S. Anuntalabhochai, R. Chanej, P. Apavatjrut, T. Vilaithong, I.G. Brown, *Surf. Coat. Technol.* **158-159**, 624-629 (2002).
- [7] S. Anuntalabhochai, R. Chandej, M. Sanguansermsri, S. Ladpala, R.W. Cutler and T. Vilaithong, *Surf. Coat. Technol.* **203**, 2521-2524 (2009).
- [8] T. Vilaithong, L.D. Yu, P. Apavatjrut, B. Phanchaisri, S. Sangyuenyongpipat, S. Anuntalabhochai, I.G. Brown, *Rad. Phys. Chem.*, **71/3-4**, 927-935 (2004).
- [9] S. Sangyuenyongpipat, L.D. Yu, T. Vilaithong, A. Verdaguer, I. Ratera, D.F. Ogletree, O.R. Monteiro and I.G. Brown, *Nucl. Instr. Meth.* **B 227**, 289-298 (2005).
- [10] S. Sangyuenyongpipat, L.D. Yu, T. Vilaithong, I.G. Brown, *Nucl. Instr. Meth.* **B 242(1-2)**, 8-11 (2006).
- [11] L.D. Yu, T. Vilaithong, B. Phanchaisri, P. Apavatjrut, S. Anuntalabhochai, P. Evans, I.G. Brown, *Nucl. Instr. Meth.* **B 206**, 586-590 (2003).
- [12] K. Prakrajang, P. Wanichapichart, S. Anuntalabhochai, L.D. Yu, *Nucl. Instr. Meth.* **B 267**, 1645-1649 (2009).
- [13] K. Prakrajang, P. Wanichapichart, D. Suwannakachorn, L.D. Yu, *Thai J. Phys.* (2010), in press.
- [14] S. Anuntalabhochai, R. Chandej, B. Phanchaisri, L.D. Yu, S. Promthep, S. Jamjod, and T. Vilaithong, *Proceedings* of *the 9th Asia Pacific Physics Conference*, Hanoi, Vietnam, October 25-31, 2004, Session 10: Applied Physics, 10-24C.
- [15] B. Phanchaisri, R. Chandet, L.D. Yu, T. Vilaithong, S. Jamjod, S. Anuntalabhochai, *Surf. Coat. Technol.* **201**, 8024-8028 (2007).
- [16] A. Krasaechai, L.D. Yu, T. Sirisawad, T. Phornsawatchai, W. Bundithya, U. Taya, S. Anuntalabhochai, T. Vilaithong, *Surf. Coat. Technol.* **203**, 2525-2530 (2009).
- [17] S. Mahadtanapuk, M. Sanguansermsri, L.D. Yu, T. Vilaithong and S. Anuntalabhochai, *Surf. Coat. Technol.* **203**, 2546-2549 (2009).
- [18] Z.Q. Wei, H.M Xie, G.W. Han, W.J. Li, Nucl. Inst. and Meth. **B 95,** 371-378 (1995).
- [19] R. Norarat, N. Semsang, S. Anuntalabhochai, and L.D. Yu, *Nucl. Instr. Meth.* **B 267**, 1650-1653 (2009).
- [20] C. Ngaojampa, L.D. Yu, T. Vilaithong, P. Nimmanpipug, V.S. Lee, *The Proceedings of the 12th Annual Symposium on Computational Science and Engineering* (ANSCSE 12), 27-29 March 2008, Ubon Rajathanee, Thailand, 127-133.



Low-energy ion beam bombardment of naked DNA and induction of mutation

R. Norarat¹, N. Semsang², S. Anuntalabhochai², L. D. Yu^{1,*}

¹Fast Neutron Research Facility, Department of Physics, Faculty of Science, Chiang Mai University, Chiang Mai 50200, Thailand ²Molecular Biology Lab, Department of Biology, Faculty of Science, Chiang Mai University, Chiang Mai 50200, Thailand

This study employed low-energy ion beams to bombard naked plasmid DNA. In the experiments, nitrogen ions at 2.5 keV bombarded naked plasmid DNA pGFP to low fluences of an order of 10¹³ ions/cm². Subsequently DNA states were analyzed using electrophoresis. Results provided evidenced that the low-energy ion bombardment indeed altered the DNA structure from supercoiled to relaxed form (single strand breaks) and short linear fragments (multiple double strand breaks) and thus induced mutation.

Keywords: Low-energy ion beam bombardment, Naked DNA, Plasmid, Mutation, Electrophoresis

1. INTRODUCTION

Ion beam bombardment of biological organisms has been recently applied to mutation breeding of both agricultural and horticultural plants at Chiang Mai University. Understanding of mechanisms involved in ion interaction with living cells responsible for the mutation is far behind the rapid pace of the application developments. Mutation can be introduced to DNA as a result of enzymatic processing of DNA lesions of post-bombarding replication. However, the mechanisms of low-energy ion bombardment-induced mutations are not well clarified at the molecular level [1]. Many experiments using tens of keV ion beams have achieved mutations. The range of such low-energy ions is limited within hundreds of nanometers in normal biological organism materials. Provided that a very small portion of ions can penetrate through the materials covering the genetic substances to reach DNA, their energy must be already extremely low due to energy loss in their traveling paths. Hence a question raised is whether the very few low-energy ions can induce mutation for DNA. A good way to approach the mechanism is to bombard the DNA in vitro, then analyzing with electrophoresis [2, 3] and transfect the DNA to host cells to determine the mutation spectra [1, 4]. There have been some reports on low-energy ions able to produce plasmid DNA strand breaks [2, 3, 5-7]. In this study we used nitrogen ions at 2.5 keV with very low fluences for the first time to bombard naked plasmid DNA pGFP, and then analyzed the DNA with electrophoresis and transferred the DNA to host cells to determine the mutation spectra. The experiments aimed at simulation of ion beam bombardment of real cells to induce mutation.

2. EXPERIMENT

2.1 DNA Preparation and Bombardment

An initial sample of plasmid pGFP (3344 base pairs) was purchased from Clontech. This was replicated following transformation into Escherichia coli and

*Corresponding author. Tel.: +66 5394 3379; fax: +66 5322 2776 E-mail: yuld@firef.science.cmu.ac.th subsequently extracted and purified using a QIAGEN[®] Plasmid Purification kit according to the manufacturer's protocol. The plasmid DNA produced by this procedure was dissolved in sterile, de-ionized water resulting in a plasmid concentration of 1 μg/μl. This was divided into aliquots and later diluted in water as necessary.

Aliquots of 1 μl plasmid DNA solution (containing 1 μg DNA unless otherwise indicated) was deposited on the glass sample holder (see Fig. 1.) which consisted of nine rings (5 mm diameter; 5 mm depth). The sample was then dried by heating to 60 °C for 5 minute before bombarding. DNA samples were exposed under vacuum (<1×10⁻⁵ mbar), with 2.5 keV nitrogen ions at different fluencies of 3×10¹³, 6×10¹³ and 9×10¹³ ions/cm² bombarding naked plasmid DNA. In most experiments, for every sample placed in the bombarding position another sample was placed in the chamber under the same vacuum conditions but in a position that was not exposed to bombarding (Internal control).

2.2 Electrophoresis

After bombardment, the sample chamber was brought to atmospheric pressure and the sample plate was removed. The samples of the control and bombardment were individually recovered in 10 µl of de-ionized water for dilution and divided into two parts for analyzing. The first part stored at -20 °C for transformation into (Escherichia coli) E.coli and the other, then added to it 2 μl of gel loading buffer (0.25% (w/v) bromophenol blue, 40% (w/v) sucrose). The ten samples (six irradiated and four controls) were then loaded onto a 16 well, 1% (w/v) agarose gel made up in TAE buffer (40 mM Tris-acetate, 1 mM EDTA, pH 8.3) pre-strained with 0.002% (w/v) ethidium bromide (EthBr). Preliminary studies demonstrated that the use of pre-strained gel provided better resolution in regard to band width and intensity. This gel was run at constant voltage (100 V/cm) for approximately 1 hr. Images of the gels were captured using UV-transilluminator (for viewing DNA in agarose gels stained with ethidium bromide) and digital camera (for capturing). Fluorescence intensity plots were obtained using the Scion Image for Windows.

R. Norarat et al. 77

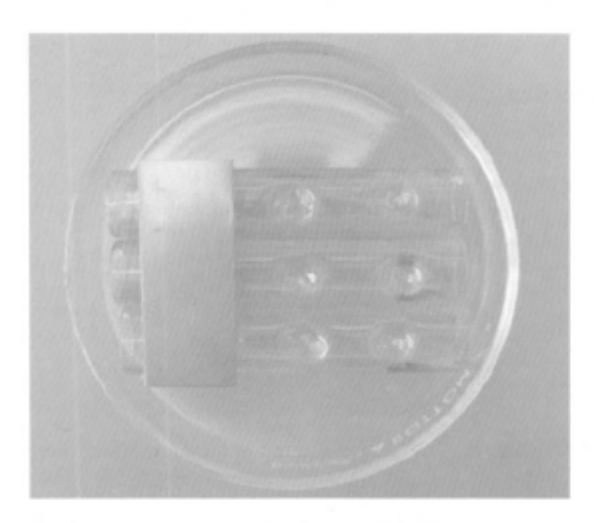


FIGURE 1. The glass sample holder.

The following sample treatments were analyzed: (1) bombarded, (2) internal control, (3) solution control and (4) digested control. The internal control samples were subjected to the same preparation, vacuum and collection procedures as the bombarded samples but were not subject to bombarding. The solution control consisted of the same quantity of plasmid as the internal controls but it was not subjected to the deposition, vacuum and collection procedures. The digested control consisted of a sample of pGFP digested with restriction enzyme EcoRI (Sigma) in order to act as a marker for full length linear plasmid.

The intensity corresponding to each form was obtained by integrating the area under the corresponding peak. A correction factor [8, 9] was applied to the intensity corresponding to the supercoiled form to allow for the increased binding of the EthBr. The intensities were summed and averaged over all the internal controls and the result was used as a measure of the initial quantity of plasmid DNA, I_C^T the total internal control intensity is given by:

$$I_C^7 = I_C^5 + I_C^R + I_C^L$$
 (1)

where I_C^S , I_C^R and I_C^L are the intensities of the supercoiled, relaxed and linear bands in the internal control samples. Since the same quantity of pGFP was used in all internal controls and bombarded sample, I_C^T provides a measure of the total quantity of plasmid in each sample. Hence the percentage of each form in the bombarded samples may be calculated by:

$$P_b^S = 100 \left[\frac{I_b^S}{I_s^T} \right] \qquad (2)$$

$$P_b^R = 100 \left[\frac{I_b^R}{I_b^T} \right] \qquad (3)$$

$$P_b^R = 100 \left[\frac{I_b^R}{I_L^R} \right] \qquad (4)$$

where P_b^S , P_b^R and P_b^L are the percentages of each form after bombarding and I_b^S , I_b^R and I_b^L are the integrated intensities of the supercoiled, relaxed and linear bands respectively. Curve fitting was carried out using the Microsoft Office Excel 2007.

2.2 Selection of DNA Mutation

The bombarded sample which was stored at -20 °C was transferred into E.coli JM109 competent cells. And the transformation mixture, containing 200 µg/ml IPTG (isopropyl β -D-thiogalactoside), was plated on plates. After overnight incubation at 37 °C, white plaques were picked out and plated on plates again to check for their purity.

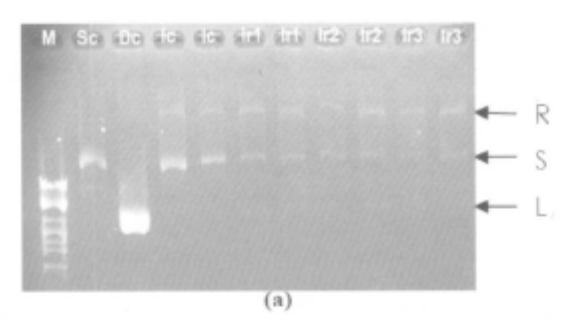
3. RESULTS AND DISCUSSIONS

From electrophoresis analysis as shown in Fig. 2, it is seen that the majority of the DNA in the unbombarded sample remained in the supercoiled form. It is known that when a single-strand breaks (SSB) is induced, the plasmid converts into relaxed form, and when a double strand break (DSB) or multiple DSBs are produced, the plasmid converts to linear full-length form or fragments. Nitrogen ion bombardment induced both SSB and DSB, as demonstrated by the increased amount of relaxed and full-length linear plasmid. However, we found increased amount of relaxed band in the internal control when compared with solution control. This vacuum effect on DNA converting into relaxed form should be further confirmed and analyzed.

It can be seen that the large reduction in the supercoiled plasmid was not balanced by an increase in the relaxed and full-length linear plasmid. These facts suggest that the relaxed and full-length linear plasmid was not only a transient product and they must be further converted to a form that was not detected [2]. Other reasons may include that these fragments will move more rapidly than full length linear strands and may be lost due to migration out of studied area of the gel [3].

After bombardment, DNA was transferred into *E.coli* JM109 and grown in IPTG, after overnight incubation at 37 °C. The result shows that green (non-mutant) and white (mutant) colonies were produced. White colony was picked out and plated on plates again to check for its purity as shown in Fig. 3. This result confirms that low-energy nitrogen ion beam bombardment induced DNA mutation.

Note that the ion fluence was in the order of 10¹³ ions/cm², about three orders lower than that applied for normal ion bombardment induction of mutation. This is corresponding to, on average, one ion hitting the DNA per 1000 incident ions. This low fluence means about 1/10 ions hitting the DNA at per 1 nm². It is well known that the DNA chain is about 2-3 nm wide and one nucleotide unit is 0.33 nm long [10], or about 1 nm² area for a nucleotide unit. So, on average, every 10 units are bombarded by only one ion. This low probability of hitting has already caused significant changes in the DNA structure, demonstrating how sensitive and effective the low-energy ions are capable of inducing mutation.



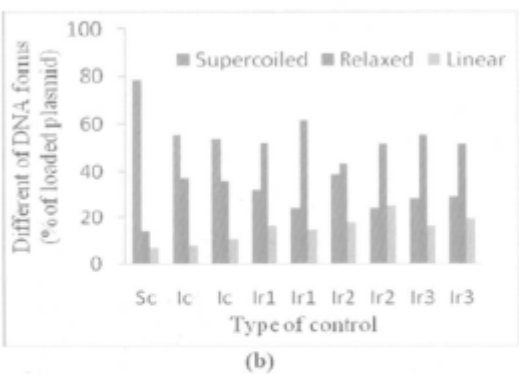


FIGURE 2. Electrophoresis results. (a) Effect of nitrogen ion on plasmid DNA. Naked plasmid DNA pGFP was bombarded with 2.5 keV nitrogen ions at different fluences, separated on 1.4% agarose gel and visualized by ethidium bromide staining. Keys: S-supercoiled, R-relaxed, L-linear, Sc-solution control, Dc-EcoRI digested control, Ic-internal control, Ir-bombard with fluences: Ir1-3×10¹³, Ir2-6×10¹³, Ir3-9×10¹³ ions/cm². (b) Quantitation of the various form of plasmid DNA after nitrogen ion bombardment.

4. CONCLUSION

We have studied the effect of low-energy ion beam bombardment of naked DNA. Our work demonstrates that low-energy low-fluence nitrogen ions with 2.5 keV can efficiently produce DNA damage in the forms of Fig. 3: Characterization of plasmid containing green fluorescence protein (pGFP) DNA was transferred into *E.coli*. White colony is mutant DNA, and green colony is control (non-mutant).

ACKNOWLEDGMENTS

We wish to thank C. Seprom for assistance in ion beam operation and equipment maintenance. This work is supported by the Thailand Research Fund.

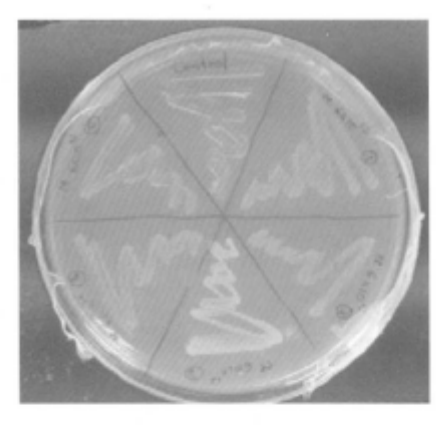


FIGURE 3. Characterization of plasmid containing green fluorescence protein (pGFP) DNA was transferred into *E. coli*. White colony is mutant DNA, and green colony is control (non-mutant).

- K. Kanbashi, X. Wang, J. Komura, T. Ono, K. Yamamoto, Frameshifts, base substitutions and minute deletions constitute X-ray induced mutations in the endogenous tonB gene of Escherichia coli K12, Mutat. Res. 385, 259-267 (1997).
- Y. Zhao, Z. Tan, G.-y. Qiu, Y.-h. Du, Electrophoresis examination strand breaks in plasmid DNA by low-energy nitrogen ion irradiation, Nucl. Instrum. Methods Phys. Res. B in press, (2003).
- C. A. Hunniford, D. J. Timson, R. J. H. Davies and R. W. McCullough. Damage to plasmid DNA induced by low energy carbon ions. *Phys. Med. Biol.* 52, 3729-3740 (2007).
- B. Hoebee, J. Brouwer, P. van de, H. Loman, J. Retel, ⁶⁰CO γrays induce predominantly C/G to G/C transversions in doublestranded M13 DNA, Nucleic Acids Res. 16, 8147-8156 (1998).
- Y. Chen, B. Jiang, Y. Chen, X. Ding, X. Liu, C. Chen, X. Guo, G. Yin, Formation of plasmid DNA strand breaks induced by low-energy ion beam: indication of nuclear stopping effects, *Radiat. Environ. Biophys.* 37, 101-106 (1998).
- S. Lacomb, C. Le Sech and V. A. Esaulov, DNA strand breaks induced by low keV energy heavy ions. *Phys. Med. Biol.* 49, N65-73 (2004).
- Z. W. Deng, I. Bald, E. Illenberger and M. A. Huels, Beyond the Bragg peak: hyperthermal heavy ion damage to DNA components. *Phys. Rev. Lett.* 95, 153201 (2005).
- F. Boege, T. Straub, A. Kehr, C. Boesenberg, K. Christiansen, A. Andersen, F. akob and J. Kohrle, Selected novel flavones inhibit the DNA binding of the DNA relegation step of eukaryotic topoisomerase I, J. Biol. Chem. 271, 2262-70 (1996).
- C. Bailly, DNA relaxation and cleavage assays to study topoisomerase I inhibitors, Methods Enzymol. 340, 610-623 (2001).
- Mandelkern, M., Elias, J., Eden, D., Crothers, D., The dimensions of DNA in solution, J Mol Biol 152 (1), 153–61



Chitosan and cellulose membrane characteristics modification by ion beam for simulation of ion bombardment of plant cell envelope

K. Prakrajang^{1,*}, P. Wanichapichart², L. D. Yu¹

¹Fast Neutron Research Facility, Department of Physics, Faculty of Science, Chiang Mai University, Chiang Mai 50200, Thailand

²Membrane Science and Technology Research Center, Department of Physics, Faculty of Science, Prince of Songkla University, Songkhla 90110, Thailand

Ion beam biotechnology has been developed for induction of DNA transfer into biological cells. Mechanisms involved in the ion interaction with the cell envelope to create pathways for exogenous DNA to transfer are not yet well understood. In order to separately investigate effects of ion interaction with plant cell envelope, this study uses chitosan and cellulose membrane to simulate the cell envelope, base on very similar chemical structure and composition of both materials, to characterize behavior of the membrane modified by ion beam. Chitosan and cellulose membranes were bombarded with argon ion beams at energy of 15 to 25 keV to fluencies in orders of to 1015 ion/cm2. The membrane surface morphology was investigated with atomic force microscopy. The membranes contact angle was also measure for their biocompatibility. The membrane electric characteristics were studied with a two-chamber membrane measurement system. Results showed that subjected to ion bombardment, the membrane impedance decrease, the conductance and capacitance increased. The membrane characteristics modification by ion beam explains effects of ion bombardment of plant cell envelope on induction of DNA transfer in terms of electric properties. Real onion skin cell envelopes were also used in the same experiments for a comparison with the results obtained from using the chitosan and cellulose membrane. Result demonstrated applicability of the simulation using chitosan and cellulose membrane.

Keywords: Chitosan, Cellulose, Membrane, Ion beam, Modification, Plant cell envelope

1. INTRODUCTION

Ion beam bioengineering is a relatively new application area of ion beam physics and technology. An interesting and potentially important development that has been demonstrated is the ion-beam-induced transfer of DNA into biological cells [1-4]. Here, a low-energy ion beam in tens of keV range bombarded biological cells to perforate the cell envelope, through which exogenous macromolecules can be introduced into cell interior in a subsequent post-bombardment biological processing step. However, a consistent physical mechanism for this significant result has not yet been developed. Questions are how the exogenous DNA macromolecules enter the cell and how bombardment creates the pathways, the nature of the pathway structure and geometry. Based on the similarly chemical structure and compositions of both chitosan (C6H11O4N) and cellulose in the plant cell wall (C6H12O6), this study uses chitosan membrane and cellulose membranes to simulate the plant cell envelope to characterize relevant behavior in order to separately investigate effects of ion interaction with plant cell envelope. Chitosan is a remarkable material that has been known for a long time. It is taken from chitin, a polysaccharide found in the exoskeletons of crustaceans. The typical thickness of chitosan membranes is about 40-80 μm [5].

Corresponding author. Tel.: +66 8667 12915; fax: +66 5322 2776 E-mail: kittikun@fnrf.science.cmu.ac.th

2. EXPERIMENT

2.1 Ion Beam Bombardment

Chitosan membranes and cellulose membranes were prepared by the Membrane Science and Technology Research Center, Prince of Songkla University, Thailand. The preparation method was published in elsewhere [5-6]. Square samples of the membranes of a size about 4×4 cm² were bombarded with argon ions accelerated by 15-25 kV to fluences at order of 10¹⁵ ions/cm².

2.2 Membrane Characterization

The membrane surface morphology was investigated with atomic force microscope in dynamic mode. The contact angle of the membrane was also measured for their biocompatibility. Bombarded membranes were characterized by electrical membrane impedance spectroscopy by using two-chamber system to study the membrane electrical properties under 10mM KCl solution condition [6].

3. RESULTS AND DISCUSSIONS

The atomic force microscope images of membrane surface morphology and membrane surface roughness are shown in Fig. 1 and Table 1, respectively. From the results, the chitosan membrane surface is smoother than cellulose membrane surface. By increasing the fluences, the membrane surface morphology seems to be roughned and their surface roughness is increased. With increasing ion energy, the roughness is decreased. It is known that the ion sputtering yield is higher when the ion energy is lower and the surface sputtering loss is proportional to the ion fluence.

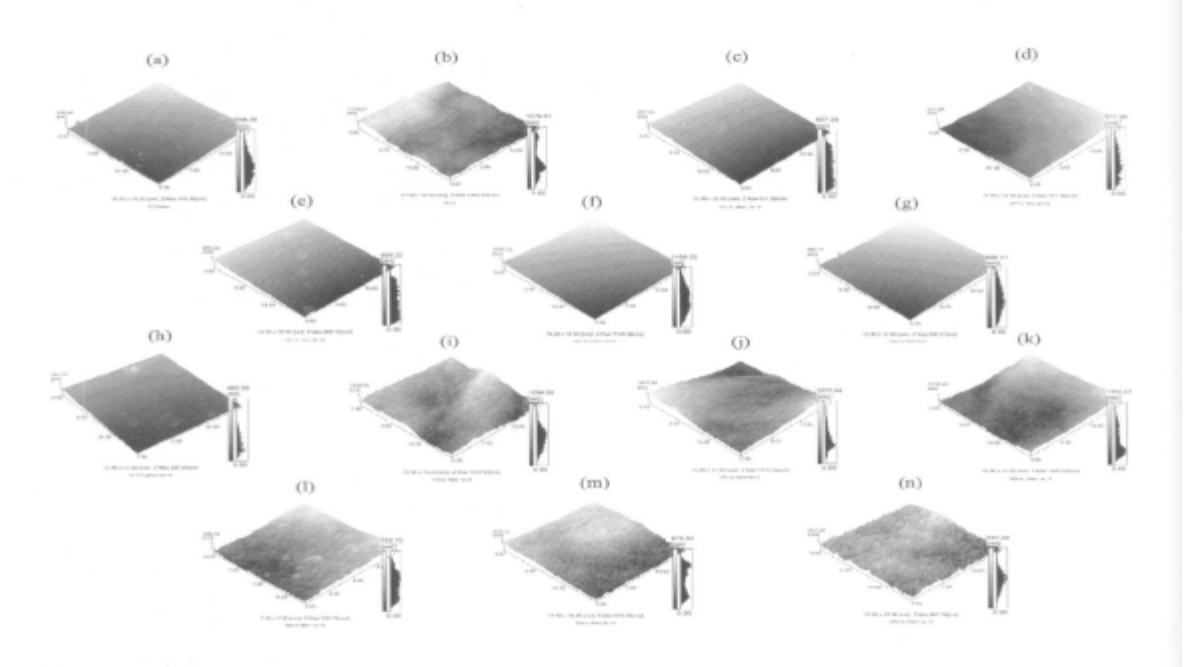


FIGURE 1. Atomic force microscopic image and roughness analysis graph of the chitosan and cellulose membrane surface, (a) chitosan control (b) cellulose membrane control (c)-(e) chitosan 15 keV Ar at 1, 2, 4 ×10¹⁵ (f)-(h) chitosan 15 keV Ar at 1, 2, 4 ×10¹⁵ (i)-(k) cellulose 15 keV Ar at 1, 2, 4 ×10¹⁵ (l)-(n) cellulose 25 keV Ar at 1,2,4 ×10¹⁵ ions/cm².

TABLE 1. The Membrane Surface Roughness Measured by AFM Section Analysis.

	Roughness, rms (nm)	
Conditions	Chitosan Membrane	Cellulose Membrane
Control	11.89	66.37
15 keV 1×1015 ions/cm2	19.87	112.9
15 keV 2×1015 ions/cm2	21.36	132.31
15 keV 4×1015 ions/cm2	19.13	142.76
25 keV 1×1015 ions/cm2	15.78	97.70
25 keV 2×1015 ions/cm2	17.47	100.07
25 keV 4×1015 ions/cm2	18.56	112.46

From the results we can then say that the increase in surface roughness is caused from the high sputtering yield of argon. So, the ion bombarded roughened surface has more surface area that is active and more compatible with biology application such as DNA transfer.

The measurement results of the contact angle of the membrane are shown in Fig. 2 and Table 2. The results show that the contact angle of cellulose membrane is smaller than the chitosan membrane. When bombarded with the ion beam, the contact angle was decreased. Low ion energy, the contact angle was depressed generally more than at high ion energy. These results indicate that the cellulose membranes are more biocompatible than chitosan membrane because small surface contact angle is better in biocompatibility. The changes in the contact angle are seen related to the membrane surface roughness, the rougher the smaller the contact angle and the more biocompatible.

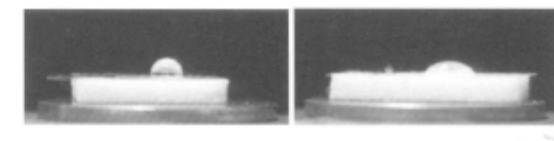


FIGURE 2. The photograph of membrane contact angles of (left) chitosan membrane, and (right) cellulose membrane.

TABLE 2. The Membrane Contact Angle.

Conditions	Contact Angle (degree)	
	Chitosan Membrane	Cellulose Membrane
Control	92	47
15 keV 1×1015 ions/cm2	85	35
15 keV 2×1015 ions/cm2	73	39
15 keV 4×1015 ions/cm2	66	19
25 keV 1×1015 ions/cm2	82	31
25 keV 2×1015 ions/cm2	68	60
25 keV 4×1015 ions/cm2	70	52

The membrane impedance spectroscopy shows the value of impedance, conductance and capacitance of the membranes (Fig. 3). These values are the electrical properties of the membrane. It is seen from the results that, when bombarded with argon the impedance of both membranes was slightly decreased, the conductance and the capacitance were increased. The changes for cellulose membranes are more pronounced than those for chitosan membranes. Compared with the data of onion skin membrane, the data from the cellulose are closer to those of the onion membranes.

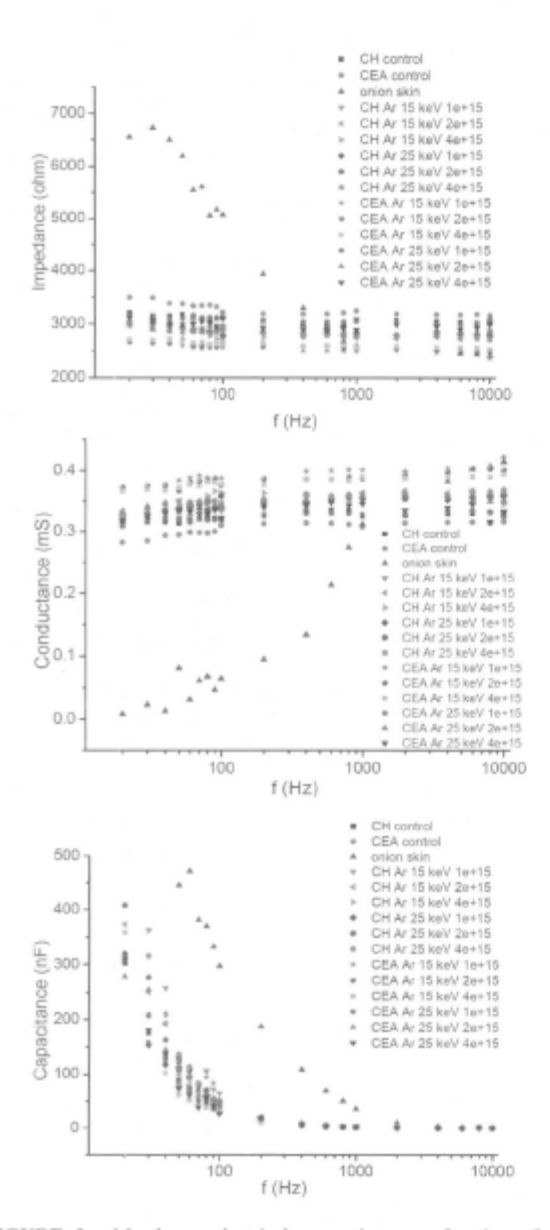


FIGURE 3. Membrane electrical properties as a function of testing frequency for different beam conditions. (a) Impedance, (b) conductance, and (c) capacitance. CH: chitosan. CEA: cellulose. Data of onion skin membrane for a reference.

This indicates that the cellulose membranes should be more similar to the real plant cell envelope. Or, we may speculate that for the real plant cell envelope, the changes would be much more pronounced. Compared with the data from N-ion implantation [5], it is found that the changes caused by Ar-ion implantation done in this experiment are considerably more pronounced, indicating that heavier ion bombardment is more effective to the cell envelope modification than lighter ion bombardment. The changes in the electrical properties show that the effect of ion bombardment can increase the membrane ion selectivity ability in solution that may explain on the induction of DNA in plant cell envelope in terms of electrical effects.

4. CONCLUSIONS

The increasing of the surface roughness and the decreasing of surface contact angel indicate that chitosan and cellulose membrane are biocompatible and demonstrated applicability for the plant cell envelope simulation. The decrease of the membrane impedance shows the ability to use the chitosan and cellulose membrane for the simulation in DNA transfers application.

ACKNOWLEDGMENTS

We wish to thank C. Seprom for assistance in ion beam operation and equipment maintenance. This work has been supported by Thailand Research Fund (TRF) and TRF-RGJ Ph.D. Scholarship.

- T. Vilaithong, L. D. Yu, C. Alisi, B. Phanchaisri, P. Apavatjrut and S. Anuntalabhochai, Surface and Coatings Technology 128-129, 133-138 (2000).
- L. D. Yu, B. Phanchaisri, P. Apavatjrut, S. Anuntalabhochai, T. Vilaithong and I. G. Brown, Surface and Coatings Technology 158-159, 146-150 (2002).
- L. D. Yu, T. Vilaithon, B. Phanchaisri, P. Apavatjrut, S. Anuntalabhochai, P. Evans and I. G. Brown, Nuclear Instruments and Methods in Physics Research B 206, 586-590 (2003).
- S. Sangyuenyongpipat, S. Anuntalabhochai and I. G. Brown, Radiation Physics and Chemistry 71, 927-935 (2004).
- P. Wanichapichart and L. D. Yu, Surface and Coatings Technology 201, 8165-8169 (2007).
- P. Rakbamrung and P. Wanichapichart, 31st Congress on Science and Technology of Thailand.

Charge Effect on Membrane Impedance Modification of Ion Bombarded Cellulose-Mimetic Plant Cell Envelope

K. Prakrajang¹, K. Sangwijit², S. Sarapirom¹, S. Anuntalabhochai², P. Wanichapichart^{3,4}, D. Suwannakachorn^{1,4}, L.D. Yu^{1,4,*}

Abstract

Ion beam biotechnology has been applied to induce gene transfer into biological cells. Mechanisms involved in the ion interaction with the cell envelope to create pathways for exogenous DNA to transfer are not yet well understood. Studies have found ion implantation resulting in modifications of the surface morphology and electric properties of the plant cell envelope membranes to favor the gene transfer. How the modifications occur is yet to explain. This study focuses on the charge effect brought by ion implantation on the modifications. Membranes of cellulose, the main chemical composition of the plant cell envelope, used to mimetic the cell envelope, were bombarded with ion or electron-showering-neutralized beam of argon and nitrogen at energy of 10 keV to fluences in an order of 10¹⁵ ions/cm². The membrane electric characteristics were studied with a two-chamber membrane measurement system. Results clearly showed charge effect on the modifications of the membrane. Generally, the charge input from ion implantation reduced the decrease in the impedance of the membrane. The change in the impedance was not related to the membrane surface wettability represented by the contact angle. The radiation-induced impedance decrease of the membrane was demonstrated to be the key mechanism for ion-beam-induced DNA transfer.

Keywords: Charge effect, Cellulose membrane, Ion beam, Neutralize, Cell envelope, Gene transfer

Email: yuld@fnrf.science.cmu.ac.th

^{*} Corresponding authors: Tel.: 053 943379, Fax: 053 222776,

1. Introduction

Ion beam bioengineering is a relatively new application area of ion beam physics and technology [1]. An interesting and potentially important development that has been demonstrated is the transfer of DNA into plant or bacterial cells [2,3]. A low-energy ion beam in a few tens of keV bombarded cells to perforate the cell envelope, through which exogenous macromolecules can be introduced into the cell interior in a subsequent postbombardment biological process. However, a consistent physical model for this significant result has not yet been developed. Questions on this aspect may include how the exogenous DNA macromolecules enter the cell and how ion bombardment creates the pathways, and what the nature of the pathway structure and geometry is. Base on the fact that the major composition of the plant cell envelope is cellulose (C₆H₁₂O₆), this study uses cellulose membranes to mimetic the cell envelope for characteristic behavior in order to separately investigate effects of ion interaction with the plant cell envelope. In our previous studies, we have demonstrated that changes in the electric properties of the cell envelope membrane materials contribute to the exogenous macromolecule transfer into the cells [4]. But, a question on this result is how the changes in the electric properties are caused by the ion beam. Ion beam brings multiple factors to the biological materials, namely mass, energy, momentum and charge [1]. In this study, we focus our interest in the charge effect, i.e. whether charge of the ion beam can play some role in inducing the changes in the electric properties of the cell envelope materials.

2. Experiment

An electron shower was designed, constructed and installed to our bioengineering ion beam line [5] for neutralization of ion beam. The working principle of the electron shower was that when an electric current was applied to a graphite filament, electrons were emitted from the filament to the insulating sample surface that was being ion implanted and thus neutralized the charge of ion beam. Figure 1 shows the electron shower used in our experiment. After the electron shower was installed in the target chamber, the electron showering effect was tested. It was found that the effect on ion charge neutralization depended on the distance between the electron shower and the sample surface and the ion energy as well. If the electron shower was placed fairly away from the sample surface, the ion current measured at the sample was increased, which was opposite to our expectation. This meant that the electrons from the shower did not neutralize the ion charge but further ionized the ions. This effect was thought to be caused by collisions between the electrons and the energetic ions in the beam that had not yet reached the target surface to increase the ionization of the ions. When the electron shower was placed very close to the sample surface and also to the ion beam, the ion current at the sample was indeed decreased, indicating charge neutralization realized. It was also found that when the ion energy was lower than 10 keV, even though the filament was placed somehow far away from the sample surface, the ion beam could be neutralized. This effect demonstrated again our speculation that the electrons from the filament directly ionized further the ions in the beam when the filament was far away from the sample surface, but when the ion energy was lower, the interaction energy between the electrons and the ions became lower so that the ionization could be reduced. In the experiment, the distance between the graphite filament of the electron shower and the sample surface was normally controlled at a few millimeters.

Cellulose membranes were supplied by the Membrane Science and Technology Research Center, Prince of Songkla University. The membrane preparation methodology has been published elsewhere [6,7]. Square samples of the membranes in a size about 4×4 cm² and about 30 µm in thickness were mounted on a stainless steel holder. The membranes were bombarded with nitrogen and argon ions with energy of 10 keV to fluences of 1, 2, 4×10^{15} ions/cm² at room temperature. For each ion bombardment condition, control samples were placed away from the ion beam in the target chamber during ion bombardment. Note that both nitrogen and argon ion beams were previously used to achieve gene transfer in plant and bacterial cells [2,3]. The ion bombardment was carried out using the bioengineering ion beam line at Chiang Mai University [5], which was featured as a vertical setup with a doubly magnetic steering system to remove the neutrals from the finally applied ion beam. The beam was focused onto the target without using any aperture. During ion bombardment, the ion beam was fixed but the sample stage was repeatedly translated for a uniform and large area bombardment and also prevention from beam heating caused damage in the membrane. The bombarding time was normally around some ten minutes for fluences of the order of 10¹⁵ ions/cm². During ion implantation, a current of 5 A was provided to the graphite filament to shower electrons to the sample surface.

Bombarded membranes were characterized by electrical membrane impedance spectroscopy by using a two-chamber system to study the membrane electrical properties under 10mM KCl solution condition [6,7]. The contact angle of the membrane was also measured for checking wettability change.

An experiment of plasma low-energy-ion implantation in bacterial cells was conducted to demonstrate the impedance change of the cellulose membrane to be the dominant mechanism for ion beam induced DNA transfer. *Escherichia coli* (*E. coli*) cells were bombarded by argon or nitrogen ions in a plasma immersion ion implantation (PIII) chamber using -2.5 kV bias, 50 Hz pulsing frequency and 20 µs pulse length to fluence orders of 10¹², 10¹³ and 10¹⁴ ions/cm². After PIII, the bacteria were mixed with solution of plasmid DNA pTZ57R (size of 2,886 bp) or pBI121 (size of 13 kbp), both of which possessed antibiotic resistance, for conventional DNA transfer, followed by checking the bacterial survival in Lysogeny broth (LB) media containing antibiotic ampicillin and kanamycin.

3. Results and Discussion

Figure 2 shows the measured impedance of the cellulose membranes.

Figure 2(a) shows changes in the impedance of the membrane after bombarded with using the electron shower compared to the un-bombarded membrane. It is seen that the impedance of the membrane when bombarded with neutralized ions is decreased. This is in the same trend with the ion beam bombardment effect we obtained before [4], indicating that whether charge input or not does not affect the impedance decrease. This result implies the cause of the induced impedance decrease intrinsically not much related to the input charge.

Figure 2(b) shows a comparison between the membrane bombarded with normal ion beam and that bombarded in cooperation with using the electron shower. It is clearly seen that neutralized ions have effect on decreasing the impedance considerably more than ion beam. The impedance decrease of the polymeric membranes is generally caused by structural modification of the polymers, such as the formation of cross-links and conjugated double and triple bonds due to irradiation induced damage [8]. The delocalized π -electrons in the conjugated bonds are loosely bound and thus more mobile than the covalent σ -bond electrons. When ions carrying charge are implanted in polymeric materials, the positive charge will combine with the released electrons to decrease the conductivity induced by ion implantation, while after the charge is neutralized by electron showering the combination of the charge with the delocalized electrons no longer occurs and thus the ion-implantation-induced conductivity further increases or the impedance more effectively decreases. An interesting phenomenon seen in this figure is that the impedance decreases due to Ar and N ion bombardments are quite different, the decrease from the former much less than the latter, whereas the impedance decreases when ion neutralization is applied have no significant difference (actually, there is some difference as shown below). This may be interpreted by the fact that argon has higher ionization energy, 15.8 eV required to split off the loosest bound electron of the atom, while nitrogen has lower ionization energy, 14.5 eV [9]. During ion implantation. N ions may not only more easily capture electrons but also loose electrons after they capture the electrons and are subjected to subsequent collisions with either further implanted ions or recoiled atoms than Ar ions. Hence, in the N-ion bombarded membrane there are still more electrons than in the Ar-ion bombarded membrane, leading the former to have more conductivity or lower impedance than the latter. However, after the ions are sufficiently neutralized and thus become stable atoms, only those delocalized electrons contribute to the conductivity.

Figure 2(c), the zoom of the lower part of Figure 2(a), shows details of the impedance of the bombarded membrane with using the electron shower. The neutralized Ar ions exhibit effect generally more than neutralized N ions on decreasing the impedance. This is in the same trend as that induced by ion beam bombardment we obtained before [4]. As a heavier ion species, Ar-ion implantation may produce heavier damage than lighter N-ion implantation in materials and thus more electrons delocalized than the case of N-ion implantation. As for the fluence dependence of the impedance, it does not show a monotonic relationship instead a complicated one though the differences among different fluences are not significant. This may be related to the cross-linking formation induced by ion bombardment. The low-fluence ion bombardment may induce the greatest or saturated amount of the cross-links. When the fluence increases, some cross-links may be damaged by scission; when the fluence further increase, some cross-links form further again. The competition between the formations of cross-links and scissions finally results in the complicated fluence dependence.

Figure 3 shows the contact angles of the cellulose membranes. Generally speacking, no significant differences can be seen between the ion beam and neutralized beam bombarded membranes. This can be easily explained by the fact that the contact angle only depends on the material surface structure and charcteristics but not the charge. The contact angle was generally increased when bombarded with nitrogen beam, but decreased when bombarded with argon beam with the exception of the highest fluence,

no matter with using or not using the electon showering. Contact anlge is normally related to the wettability of the material surface. For polymeric material surface, normally hydrophobicity is related to high portion of cross-links and hydrophilicity related to high portion of scissions. Hence, it indicates that the observed charge effect on the change in the impedance of the membrane is not substaintially related to the surface wettability, or hydrophobicity and hydrophilicity. That is why we do not either see significant differences in the charge effect among different fluences as mentioned above because different fluences only alternatively modify the near-surface structure between crosslinks and scissions and thus the wettbility. But, the decreasing in the contact angle or increasing in the hydrophilicity for the Ar-ion bombarded surface compared with the increasing in the contact angle for the N-ion bombarded surface seems related to the more decrease in the impedance for the Ar-ion bombarded surface. However, the difference in the contact angle change between Ar and N cases is rather obvious compared with the small difference in the impedance change between the two cases. Therefore, it is difficult to attribute the impedance change to the surface wettbility change. The obtained result shown here on the contact angle implies that the impedance decrease due to ion bombardment is dominantly caused by irradiation damage induced conjugated double and triple bonds whereas ion bombardment induced formation of cross-links plays a minor role.

The result of the experiment using low-energy ions from PIII to bombard bacteria E. coli for induction of DNA transfer shows successful subsequent DNA transfer into the bacteria. Some bacteria were found survival in the LB media, indicating the DNA that had the antibiotic resistance property was indeed transferred into the bacteria, as shown in Figure 4. N-plasma treated bacteria were found to be more effective in transferring the DNA than Ar-plasma treated bacteria. For the smaller DNA pTZ57R, N-plasma treatment had four of five successes in DNA transfer, but Ar-plasma treatment had only two of five. For the larger DNA pBI121, only N-plasma treatment could succeed in DNA transfer but Ar-plasma could not. This result is suprising. A traditional idea on ion-beaminduced DNA transfer is that the ions that should have enough energy and fluence bombard the biological cells, penetrate deeply enough in the cell envelope and create certain radiation damage which will serve as pathways for exogenous DNA molecules to pass through [1,3]. Previous experiments normally applied ions of a few tens of keV (to fluences in an order of 10¹⁵ ions/cm²) to induce DNA transfer [3], because the ions with this energy could penetrate several tens of nanometers which were similar to the thickness of the cell envelope. However, this time in our experiment the ion energy was only a few keV and the ion fluences were only one tenth down to one thousandth that formerly used. For the low-energy and low-fluence ion bombardment, it is impossible for the ions to penetrate deeply in the cell envelope and create considerable damage in the envelope. In this case, the traditional idea seems not working. In our previous study, we found that ion implantation in the cell envelope materials could modify the electric properties of the materials and demonstrated that the modification could be reponsible for ion-beam-induced DNA transfer [4]. The result of our this experiment then demonstrates that the ion-implantation induced impedance decrease of the cell envelope materials is the dominant mechanism for ion-beam-induced DNA transfer. Particularly, our previous results showed that N-ion bombardment was more effective in decreasing the impedance than Ar-ion bombardment. The result of this experiment very well agreeing our previous finding strongly supports our conclusion mentioned above. In PIII, there exists probability of certain neutralization of positive charge in the target built up during the implant pulse accomplished by exposure of the target to plasma between implant pulses [10]. Therefore, in PIII the impedance change effect is more noticeable than in beam-line ion implantation, which has been tried by us also using low-energy ion beam but with no successes in induction of DNA transfer.

4. Conclusion

Ion charge indeed has effect on change in impedance of the cellulose membrane which is used as the mimetic of the plant cell envelope to study mechanisms involved in ion beam induced gene transfer. The charge introduced by the ions dilutes the concentration of the delocalized electrons due to ion bombardment induced radiation damage and thus reduces the ability to decrease the impedance of the membrane. The change in the impedance is dominantly related to ion irradiation damage induced conjugated double and triple bonds but not substaintially related to the membrane surface wettability. The impedance decrease induced by ion bombardment is the dominant mechanism for ion beam induced DNA transfer.

Acknowledgements

This work has been supported by Thailand Research Fund, Thailand Center of Excellence in Physics and Chiang Mai University. We thank C. Seprom for technical assistance.

References

- [1] L.D. Yu, T. Vilaithong, I.G. Brown (Eng. Eds.), *Introduction to Ion Beam Biotechnology*, English edition, originally authored by Yu Zengliang in Chinese, Springer Science & Business Media, New York, 2006.
- [2] Z.L. Yu, J.B. Yang, Y.J. Wu, B. Cheng, J. He, Y.P. Huo, *Nucl. Instr. Meth.* B 80/81 (1993) 3128.
- [3] S.Anuntalabhochai, R. Chandej, B. Phanchaisri, L.D. Yu, T. Vilaithong, I.G. Brown, *Applied Physics Letters*, Vol.78, No.16 (April 16, 2001) 2393-2395.
- [4] K. Prakrajang, P. Wanichapichart, S. Anuntalabhochai, L.D. Yu, presented to *The* 16th International Conference on Ion Beam Modification of Materials, Aug. 31 Sep. 5, 2008, Dresden, Germany; Nucl. Instr. Meth. B 267 (2009) 1645-1649.
- [5] L.D. Yu, S. Sangyuenyongpipat, C. Seprom, C. Thongleurm, R. Suwanksum, N. Tondee, K. Prakrajang, T. Vilaithong, I.G. Brown, H. Wiedemann, *Nucl. Instr. Meth.* B 257 (2007) 790-795.
- [6] P. Wanichapichart, L.D. Yu, Surf. Coat. Technol. 201 (2007)8165-8169.
- [7] P. Wanichapichart, S. Kaewnoparat, W. Phud-hai, K. Buaking, *Songklanakarin J. Sci. Technol.* 24 (Suppl.) (2002) 855-862.

- [8] Eal H. Lee, Nucl. Instr. and Meth. B 151 (1999) 29-41.
- [9] C. Nordling and J. Osterman, Physics Handbook, 4th ed., Studentlitteratur, Lund, 1987.
- [10] Peter L. Kellerman, Michael P. Bradley and Shu Qin, Active charge control in PIII—enlarging the process space, *Surface and Coatings Technology* 156(1-3) (1 July 2002) 77-82.

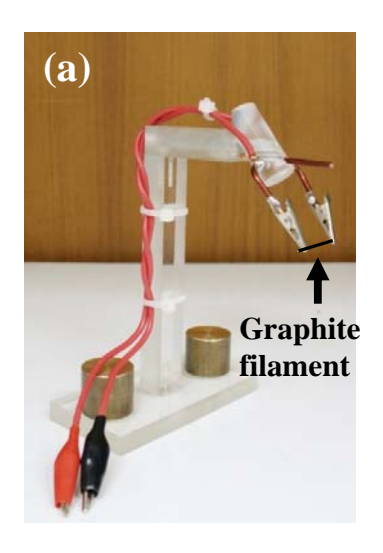
Figure Captions

Figure 1. Photographs of the electron shower. (a) At the bench test. (b) Installed inside the target chamber.

Figure 2. Impedance of the cellulose membranes under various conditions. (a) Comparison between the neutralized beam bombarded and the control membranes. (b) Comparison between different neutralized beams. (c) Comparison between the neutralized beam and ion beam bombardments. "+e": with the electron shower used.

Figure 3. Membrane contact angles. "+e": with the electron shower used.

Figure 4. Bacteria *E. coli* which were nitrogen-PIII treated and subsequently transferred with plasmid DNA pTZ57R survived in the LB media that contained ampicillin and kanamycin. The blue color is the indicator of the functioning of the plasmid DNA pTZ57R.



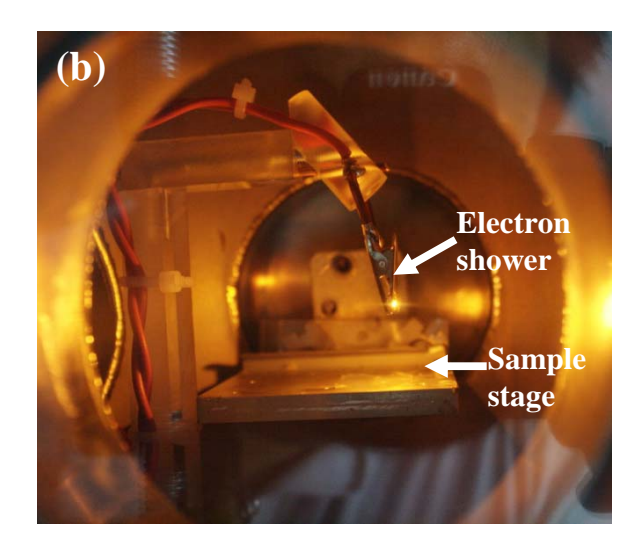


Fig. 1

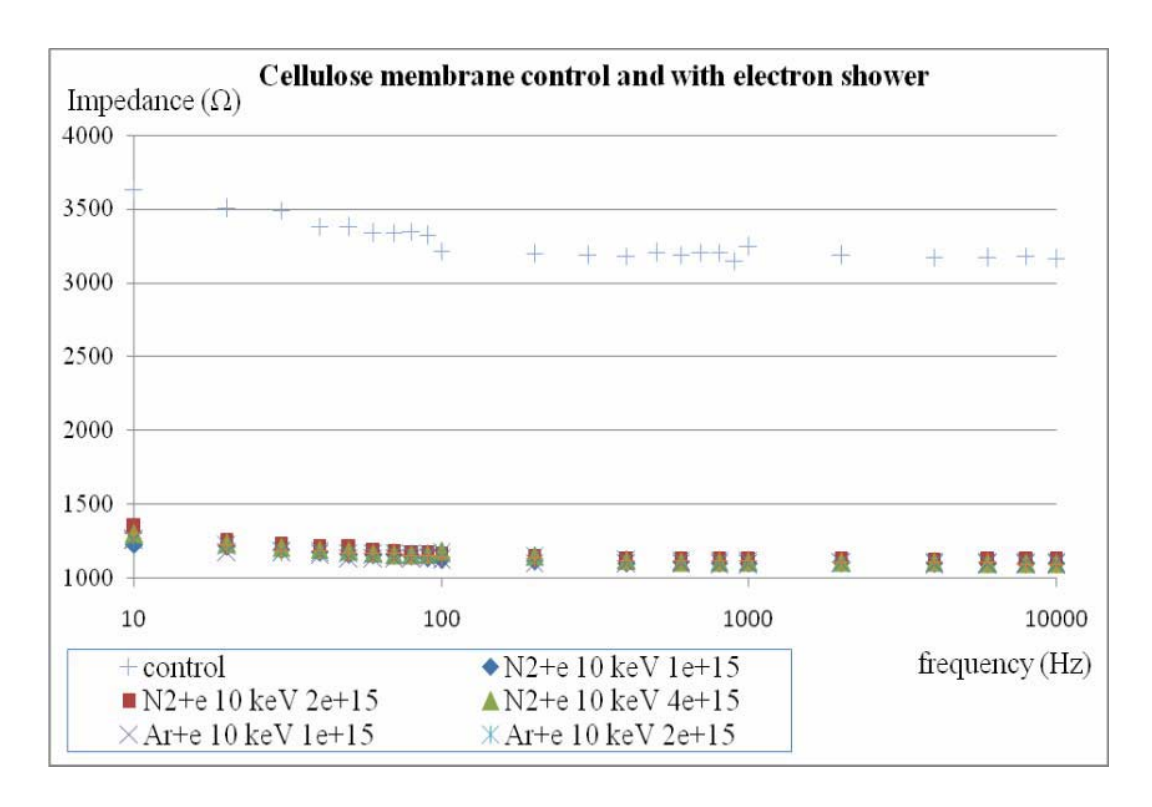


Fig. 2(a)

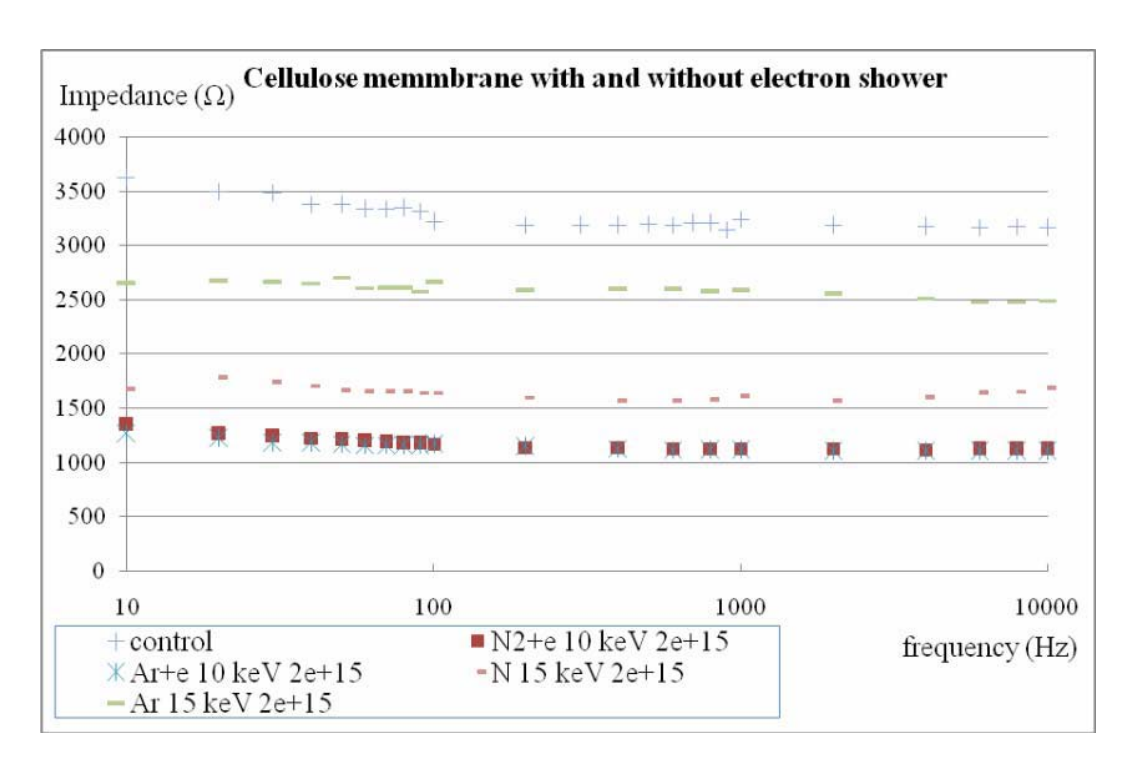


Fig. 2(b)

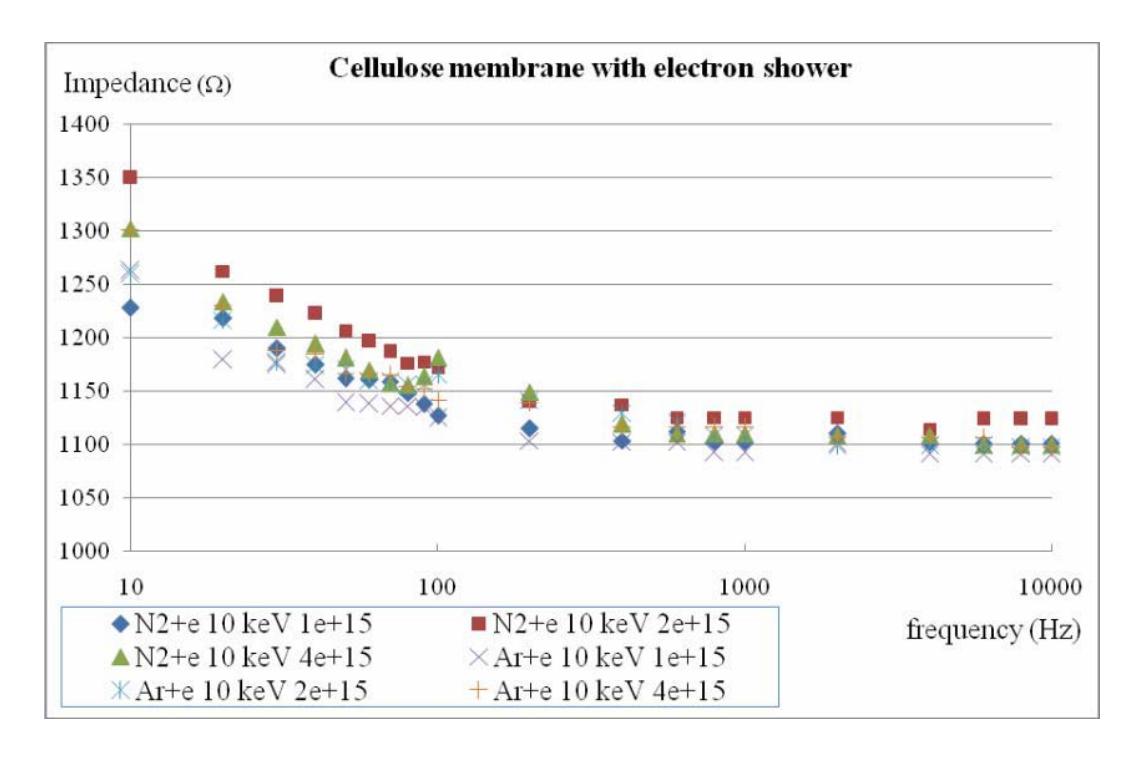


Fig. 2(c)

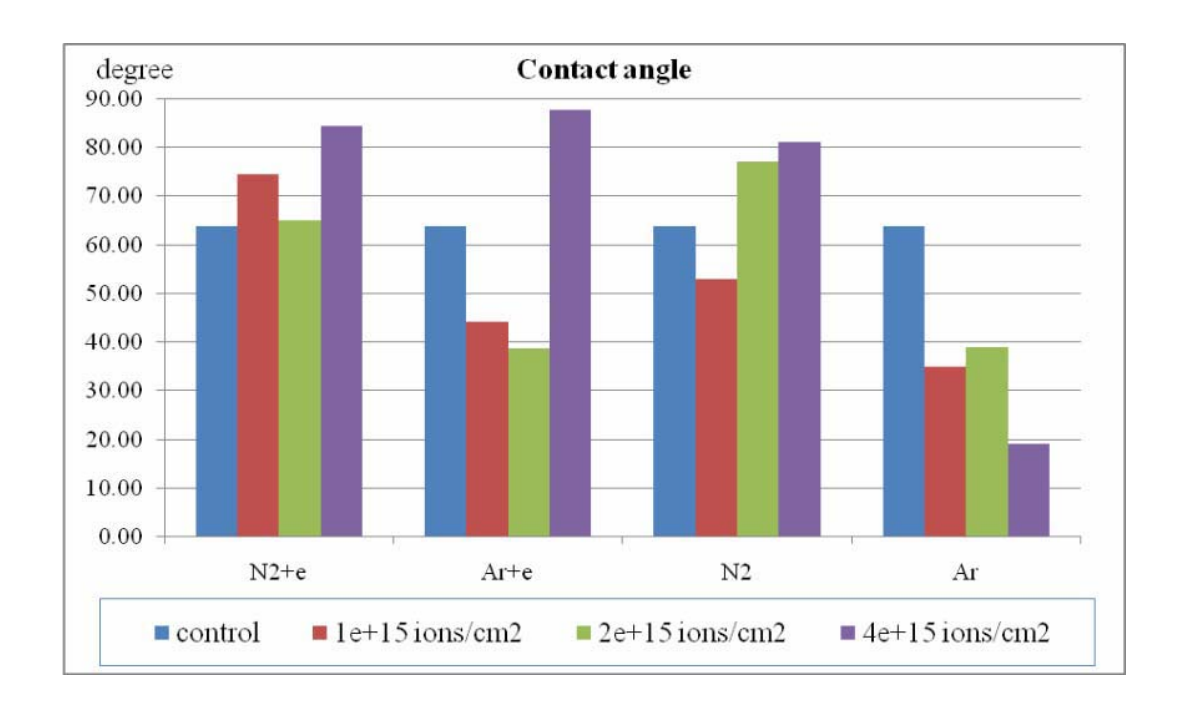


Fig. 3

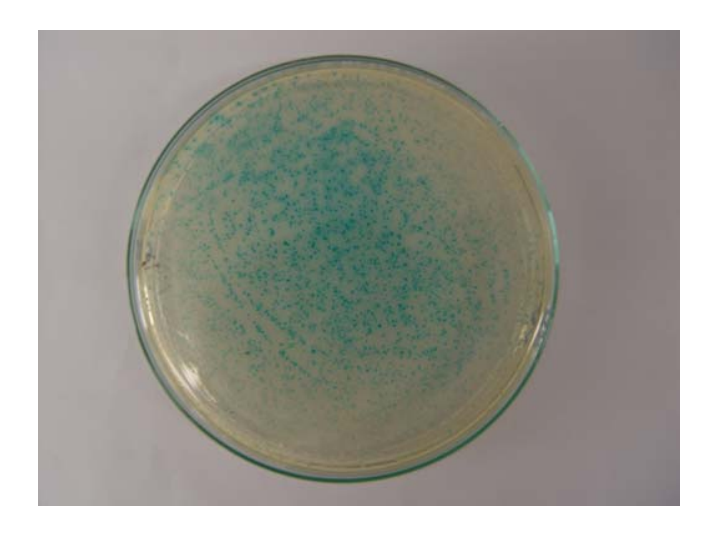


Fig. 4

Cloning of Thioredoxin Reductase Gene in Antagonistic Bacteria Using a Low-Energy Ion Beam

S. Mahadtanapuk $^{(1)}$, W. Teraarusiri $^{(1)}$, M. Sanguansermsri $^{(2)}$, W. Nanakorn $^{(2)}$, L. D. Yu $^{(3)}$ and S. Anuntalabhochai $^{(4)}$

(1) School of Agriculture Natural Resources and Environment, Naresuan University Phayao, Tumbol Maeka, Muang, Phayao, 56000, Thailand,

⁽²⁾Naresuan University Phayao, Tumbol Maeka, Muang, Phayao, 56000, Thailand²,

(3) Fast Neutron Research Facility, Department of Physics, Faculty of Science,

Chiang Mai University, Chiang Mai 50200, Thailand

⁽⁴⁾Department of Biology, Faculty of Science, Chiang Mai University, Chiang Mai 50200, Thailand⁴

Corresponding Author: Somboon Anuntalabhochai (phone): 66 053 943346, (Fax):66 054 466 663

(e-mail):burinka@hotmail.com

Abstract

Bacillus licheniformis is a potential antagonistic bacterium property in *Curcuma* alismatifolia Gagnep. Here, we cloned thioredoxin reductase (trx) genes from B. licheniformis, using a low-energy ion beam by accelerating nitrogen ions at energy of 30 keV with a fluence range of 10¹⁴–10¹⁶ ions/cm². After this treatment, The HAT-RAPD marker revealed the modified polymorphism fragment presenting in the wild type but not in the bacterial mutant. These polymorphism bands were subcloned into a pTZ57R/T plasmid and sequenced. One of the fragments conserved in the wild type and lost in the mutant bacteria was found to code for the thioredoxin reductase gene. To investigate expression of this gene, RT-PCR was used for gene analysis by specific primer. The result was shown trx gene from B. licheniformis was highest expression when co-cultivated with the bacteria and fungi disease.

Keywords

Ion beam bombardment, cloning, mutation, thioredoxin reductase

1. Introduction

Now a day, ion beam biotechnology is a newly founded interdisciplinary field between applied nuclear physics and biology, where physical ion beams are utilized for biological engineering or processing [1]. The ion beam application has been recently extended to the field of biology and agriculture. The important mechanism of ion beam biotechnology is the use of energetic charged particles to produce radiation damage, which acts as a new mutagenic source for genetic modification in organisms in the way of either directly inducing mutation or creating physical injuries for exogenous molecules transferring by energy deposition, momentum transferring, foreign particle implantation and charge exchange [2].

Since then, Low-energy, low-dose and pulsed-beam are the main features of the ion beams employed for biological purposes. The ion-beam energy is generally a few ten keV or lower (high energies may cause negative effects as mentioned later), the ion dose is mostly around 10¹⁵-10¹⁶ ions/cm² and the operating beam is in pulsed modes with the pulse interval around 10⁻⁵ second [3]. The structure of an ion implanter for biotechnology application is relatively simpler than the machines used for other conventional surface modification purposes. More over, a study on effects of N-ion implantation on microbial mutagenesis of strains of *Streptomyces roseflavus* (Huang *et al.*, 1994) [4] has found that the average total and positive mutation rates by the ion-implanted germs. The ion implantation offered two strains with stable and high potency. Products of the two strains showed a satisfactory effect in preventing and controlling the chicken diarrhea and piglet bowel complaint. Recently, this technique was applied in Thai in order to investigate the antagonistic property of *Bacillus licheniformis* on Anthracnose, a disease causing by *Colletotirchum* sp. in *Curcuma alismatifolia* Gagnep, [5].

Colletotirchum is a large genus of Ascomycete fungi, containing species that are amongst the most successful plant pathogenic fungi, causing significant economic damage to crops in tropical, subtropical, and temperate regions [6]. The current method to protect against this disease has been through the application of synthetic fungicides, but alternative methods to combat this disease could potentially be less harmful to human health and the environment [7], and one such method has already achieved considerable success utilizing antagonism [8].

The antagonism biocontrol involves the use of naturally occurring nonpathogenic microorganisms that are able to reduce the activities of plant pathogens and thereby suppress diseases. The antagonistic microorganisms can complete with pathogens for nutrients, inhibit pathogen multiplication by secreting antibiotics or toxins, or reduce pathogen population through parasitism. Moreover, some of these microorganisms can induce generalized resistance in plants, which enables the plant hosts to better defend themselves against pathogens [9].

Bacillus spp., a potential antagonistic bacteria have been applied to control anthracnose in many plants [10], As Bacillus spp. have the characteristics of omnipresence in soils, high thermal tolerance, rapid growth in liquid culture, ready formation of resistant spores, and are considered to be a safe biological agent, their potential as a biocontrol agent is considered to be high. [11]. However, the mechanism of suppression to plant pathogens by Bacillus spp. has not been extensively investigated and the report about gene involving antipathogenicity is very rare.

In this study, *Bacillus licheniformis* obtained from hot spring Chiang Mai province showed its activity to suppress of the fungus. To mutate of *B. licheniformis*, the bacteria was performed by low energy ion beam bombardment. N-ions were chosen to bombard the bacteria under vacuum condition at energy of 30 keV with fluences range of 1-10 x 10⁵ ions/cm². Genetic alternation in the bombarded bacteria loosing their antagonistic property was investigated by HAT-RAPD technique. Our results revealed that the fingerprint profiles

of the bombarded bacteria and wild type were different. Moreover, the research has been focus on gene(s) and their functions involving in their antagonistic activity.

2. Experimental

Media and Culture Conditions

The plant disease fungi, *Colletotichum musae* initially isolated from Curcuma bract (Fig. 1A,B) and another economic fungal disease such as *Pyricularia grisea*, *Pyricularia oryzae* initially isolated from rice, *Penicillium digitatum* initially isolated from orange, *C. gloeosporioides* initially isolated from chilly, were routinely subcultured onto potato dextrose agar (PDA). The fungi was stored at 4 °C and was routinely cultured on slants of PDA. The *Bacillus licheniformis* strain with highly antagonistic activity against fungal diseases on Curcuma were isolated from hot spring Suynkam Paeng Chiang Mai Province. The bacteria was tested for antagonistic activity on dual culture (Fig.2) and on planta (Fig.1 C,D). After testing the bacteria was cultured on slants of Luria-Bertani (LB) at 4 °C for using in induction mutation by low energy ion beam implantation.

Median lethal dose (LD50) determination

For median lethal dose (LD50) determination, one loop of cells of *B. licheniformis* was transferred into 100 ml of Luria–Bertani medium, LB [Trypton (10 g), yeast extract (5 g), NaCl (10 g), water (1 l)] in a 500 ml flask. For solid LB medium plate, 18 g agar was added. The culture was incubated for 24 h at 37 °C with rotating speed of 120 rpm. The cells of *B. licheniformis* were centrifuged to precipitate the cells and spread as a single-cell layer on a sterile adhesive tape which was attached to a Petri dish and then placed inside a sample holder. The holder was capable of sequentially exposing a number of samples to the ion beam, as well as housing the unbombarded control sample. Ion bombardment was carried out using

the bioengineering applicable heavy-ion-implantation facility at Chiang Mai University (Fig.3). Nitrogen ions were chosen for ion bombardment in the an energy of 30 keV and ions were delivered at fluences of 10^{14} – 10^{16} ions/cm² with a normal ion flux of an order of 10^{13} ions/cm²/sec which was low enough to maintain the cells survival according to reported experience [12]. Inside the target chamber the temperature of the target was about 0 °C as both low ion flux and water cooling was used. The samples were maintained under these conditions for about 1.5–2 h, allowing for system pump-down and ion bombardment.

After implantation, each sample with fluence combination were separately suspended in 5 ml of LB medium and incubated for 1 h at 37°C on a rotating shaker until about OD₆₀₀. These cell suspensions were subsequently 10-fold diluted to form samples at concentrations ranging from 10⁻¹ to 10⁻¹¹ and grown on solid LB medium. All culture plates were then incubated for 1 day at 37°C to ensure cell viability. Then the number of cells for the same dilution of different fluences was compared for the survival determination.

Induction mutation in B. licheniformis by low ion beam bombardment

The *B. licheniformis* cells grown in complete LB solid medium were smeared on sterile adhesive tape and placed on a Petri dish. The dish was then placed on an ion beam sample holder for bombardment. The ion source was N⁺ ions with energies 30 keV and the dose for implantation ranged at LD50 was used for the experiment.

The bombarded cells were cultured with LB medium. Subsequently, bacterial mutant loosing their antagonistic ability were analysed against the fungi. Genetic alteration of the bombarded bacteria was detected by HAT-RAPD [13] in comparison to wild type.

Cloning and sequencing of the gene

The polymorphic fragment from HAT-RAPD fingerprint with an absence of DNA bands in comparison between the mutant bacteria and wild type bacteria was reamplified by

PCR. The PCR product was electrophoretically resolved on a 1% (w/v) agarose gel, and the appropriate DNA fragment recovered with an Agarose Gel DNA Extraction kit (Roche, Germany). The purified DNA fragment was ligated into a pTZ57R/T plasmid system, according to the manufacturers' recommendations, transferred into *E. coli* DH5α competent cells, and plated on LB agar plates containing 100 mg/ml ampicillin. A clone containing the correct insert was identified by restriction enzyme analysis, and denoted pTZ57R-*Trx1*. The nucleotide sequence of the pTZ57R-*Trx1* was conformed to *B. licheniformis* (*trx* gene) by sequencing method and used for gene expression analysis.

Culture and preparation of bacteria cell for gene expression analysis

For analysis of the expression of thioredoxin reductase (*trx*) gene from *B. licheniformis*. The bacteria cells were grown in LB medium at 37 °C for 24 h in incubator shaker. Then cells were used for a dual culture method as described by Supuk et al, 2007 [14]. Briefly, the bacteria and pathogenic fungi were inoculated dually on PDA medium in petri dishes 2-2.5 cm apart. The inhibition of actively growing fungus by the bacteria on PDA plates was quantified as the distance of radial growth in centimeters. The cultures were incubated at room temperature, and growth of the fungus towards and away from the bacterium was allowed for 5, 7, 10 days after incubation. The cells of bacteria at different time incubation with fungal were used for RNA extraction for gene expression analysis.

Gene expression by RT-PCR analysis

Total RNA from *B. licheniformis* at different time incubation with fungal was extracted by using RNeasy[®] Mini Handbook (QIAGEN). The RNA was used as template for reverse transcriptase (RT-PCR), specific forward and reverse primers were designed from sequences *B. licheniformis* (*trx* gene). PCR reaction mixture contained 20 ng of the cDNA, 200 μM dNTPs, 25 mM MgCl₂, 20 mM Tris-HCl, 0.25 μM of each primer and 2 unit of Taq

polymerase buffer in a 20 µl total volume. Amplification was carried out with a thermal cycler (Perkin Elmer, Gene Amp PCR 2400) for 30 cycles at 94°C for 1 minute, 67 °C for 1 minute and 72 °C for 1 minute. A final elongation step was carried out at 72°C for 5 minutes. PCR products were separated by electrophoresis on 1% agarose gels.

3. Results and Discussion

On the knowledge of genomic damage or the result of mutation, when the damage cannot be repaired, the DNA duplication will induce mutation at the molecular level. Therefore, studies of ion- implantation- induce mutation and their application is very interesting in biology field. The essential reason for the mutation effects is that the ion beam can damage the bases and break sugar phosphate bonds in a nucleotide, the units of DNA. The base damage can change the genetic code, and the release of inorganic phosphate induces strand breaking of DNA [15].

In this study, to fogus on gene(s) and their functions involving in *B. licheniformis*, antagonistic activity, and the bacteria was performed by low energy ion beam bombardment. Genetic alternation in the bombarded bacteria loosing their antagonistic property was investigated by HAT-RAPD technique.

In part of induction mutation, the median lethal dose (LD50) was determined, the nitrogen ions were chosen for ion bombardment in the energy range of 30 keV and ions were delivered at fluences of 10^{14} – 10^{16} ions/cm². The LD50 determination result was showed that at 10^{16} ions/cm² (Fig 4) and this dose was used for induction mutation of the *B. licheniformis*.

After that, the bombarded bacterium were screened and selected for antagonistic activity analysis. To focus on gene(s) and their functions involving in their antagonistic ability, the similarity of between the ion beam generated mutants and the wild type a dual culture test was used in which more than 100 colonies were selected at random from the bombarded bacterium. These bacteria initially had the same inhibition ability compared to the

control, but after being exposed to the ion beam at LD50 dose, one isolate of bacterium was found to have lost antifungal activity. However, none of the bacteria under vacuum without ion bombardment was obtained. Moreover, the HAT–RAPD fingerprint using random primer presented an absence of DNA bands in comparison between the mutant bacteria and wild type bacteria (Fig. 5).

The polymorphic fragment from HAT-RAPD fingerprint was subcloned into a pTZ57R/T plasmid and subsequently sequenced. This nucleotide sequence (*Trx1*) was blasted with genes involved genes in NCBI data. In this research, the gene was related to thioredoxin reductase (*trx*) gene. After that the full length of the *trx* was amplified by PCR using two regions primer selected from the *trx* gene published *B. licheniformis*. A fragment was released from another thioredoxin reductase organism species. When this nucleotide sequence was blasted against the NCBI database, it was found to be highly homologous to the thioredoxin reductase gene from multiple bacteria strains, such as *Bacillus licheniformis* ATCC 14580, *Bacillus licheniformis* DSM 13, *Exiguobacterium sibiricum* 255-15 with 96%, 96%, 75% identities, respectively (Table 1). Moreover the nucleotide sequence was translated to amino acid and its was found to be highly homologous to thioredoxin reductase amino acids from multiple *Bacillus* strains, such as *Bacillus licheniformis* ATCC 14580, *Bacillus* subtilis, *Bacillus pumilus* SAFR032 (Fig. 6).

For the function thioredoxin reductase gene, its importance in defense against stress, the thioredoxin system of bacteria, yeast, and mammals is involved in regulating DNA synthesis, gene transcription, enzyme synthesis, cell growth, and apoptosis[16]. Thioredoxin reductase, a flavoenzyme homodimer which binds flavin adenine dinucleotide and NADPH, reduces the oxidoreductase thioredoxin and is found in two forms throughout all five kingdoms. The high-molecular-weight isoform, which most likely evolved from glutathione reductase rather than the prokaryotic thioredoxin reductase [17], is present in mammals and some parasites, while the low-molecular-weight isoform is found in most bacteria, plants, and

fungi [18]. These two isoforms are thought to have independently evolved to having similar substrate specificity profiles. Though these isoforms have similar functions, they have very distinct protein structures.

In this paper, for investigate expression of *trx* gene (*Trx1*) related antagonistic activity, RT-PCR was used for gene analysis by specific primer. The result was shown *trx* gene from *B. licheniformis* (*Trx1*) was highest expression when co-cultivated with the bacteria and fungi disease (Fig. 7). However, the mechanism of this gene relates protein, enzyme or antagonistic activity will be more study.

5. Conclusions

In this study we cloned gene from B. licheniformis, using induction of low-energy ion beam by accelerating nitrogen ions at energy of 30 keV with a fluence range of 10^{16} ions/cm². In order to locate gene involving antagonistic mechanism of B. licheniformis to disease fungi, the polymorphism bands from fingerprint technique presented in the bacteria was subcloned and sequenced. Analysis of these PCR products was investigated in Gene Bank database and showed that gene related thioredoxin reductase gene. Moreover, the expression of the this gene (Trx1) was highest expression when the bacterium was co-cultivated with fungi disease.

Acknowledgments

We wish to thank The Naresuan University Phayao Research Fund, Thailand Research Fund (TRF) and National Research Council of Thailand (NRCT).

References

[1] T.Vilaithong, L.D. Yu, D. Suwannakachorn, S. Davydov, S. Thongtem, B. Yotsombat, S. Intarasiri Boonyawan, P. Vichaisirimongkol, Surf Coat Technol.83(1996) 322.

[2] Z.Yu, J. Deng, J. He, Y. Huo, Y. Wu, X. Wang, G. Lui, Nucl Instrum Methods

- Phys Res. 705 (1991) 59-60.
- [3] C. Shao, Z. Yu, Radiat Phys Chem. 44(6) (1994) 651.
- [4] H. Cui, L. Wu, Z. Yu, L. Qiu, J. He J. Anhui Agri. Uni. 21(3)(1994)303.
- [5] S. Mahadtanapuk, M. Sanguansermsri, L.D. Yu, S. Anuntalabhochai. Surf Coat Technol. 203 (2009) 2546–2549
- [6] J. A. Bailey, M.J. Jeger, International. Wallingford UK. (1992)38-120.
- [7] R.D O'Brien, S.E Lindow, Phytopathol. 79 (1989) 619-627.
- [8] R.J McLaughlin, C. L Wilson, S. Droby, R. Ben-Arie, E. Chalutz, Plant Dis. 76 (1992) 470-473.
- [9] K.G Mukerji, B.P Chamola, R.K Upadhyay, Phytochem. 54(2000) 445-446.
- [10] L. Korsten, P. Jeffries, International. Wallingford UK. (2000) 266-291.
- [11] A. Siala, T. R Gray, J Gen Microbial. 81 (1974)191-198.
- [12] L.D. Yu, T. Vilaithong, I. Brown (Eng. Eds.), Yu Zengliang (original Chinese author), Introduction to Ion Beam Biotechnology, Springer Science Business Media, Inc. New York, 2006, p. 189, 203.
- [13] S. Anuntalabhochai, R. Chandej, J. Chiangda, P. Apavatjrut, Acta Hortic. 575 (2000) 253.
- [14]. S. Mahadtanapuk, M. Sanguansermsri, R.W. Cutler, V. Sardsud, S. Anuntalabhochai, Am. J. Agric. Biol. Sci. 2 (2) (2007) 54.
- [15] J. F Ward, Int J Phy Chem. 3(1971)239.
- [16] A. Holmgren, Annu Rev Biochem 54 (1985) 71-237.
- [17] W. A Prinz, F. Aslund, A. Holmgren, J. Beckwith, J Biol Chem. 272(1997) 15661-15667.
- [18] H. J. Windle, A. Fox, D. Ni Eidhin, D. Kelleher, J Biol Chem. 275 (2000)5081-5089.

Table 1

The nucleotide sequence of thioredoxin reductase gene (Trx1) compare with the database of NCBI

Bacteria species	Identity (%)
Pasillus lielauifermis (this money)	100
Bacillus licheniformis (this paper)	100
Bacillus licheniformis ATCC 14580	96
Bacillus licheniformis DSM 13	96
Exiguobacterium sibiricum 255-15	75

Figure Captions

Fig. 1. Anthacnose of curcuma; (A) acervulus and (B) conidia of *Colletotrichum* sp., (C) diseased flower and (D) diseased flower control with *B. licheniformis*.

Fig. 2. A dual culture test; A: mutant of B. licheniformis, B: wild type of B. licheniformis.

Fig. 3. The bioengineering applicable heavy-ion-implantation facility at Chiang Mai University

Fig. 4. The median lethal dose (LD50).

Fig. 5. Amplification products of the bombarded bacterium; A: mutant bacteria was showed loosing antagonistic activity, B: bacteria was showed same ability inhibition, C: control right arrow indicates polymorphism that subcloned into pTZ57R/T plasmid.

Fig. 6. The amino alignment of *Trx1* gene from *B. licheniformis*.

Fig. 7. The expression gene analysis of *Trx1* gene in bacteria cells at different time of cocultivate with fungal; (I) bacteria was cocultivated with fungal at different time,(II) PT-PCR analysis; the bacteria was cocultivated with fungal at 5 days (A), at 7 days (B) and at 10 days (C), the bacteria was not cocultivated with fungal at 10 days (D).

Figure 1

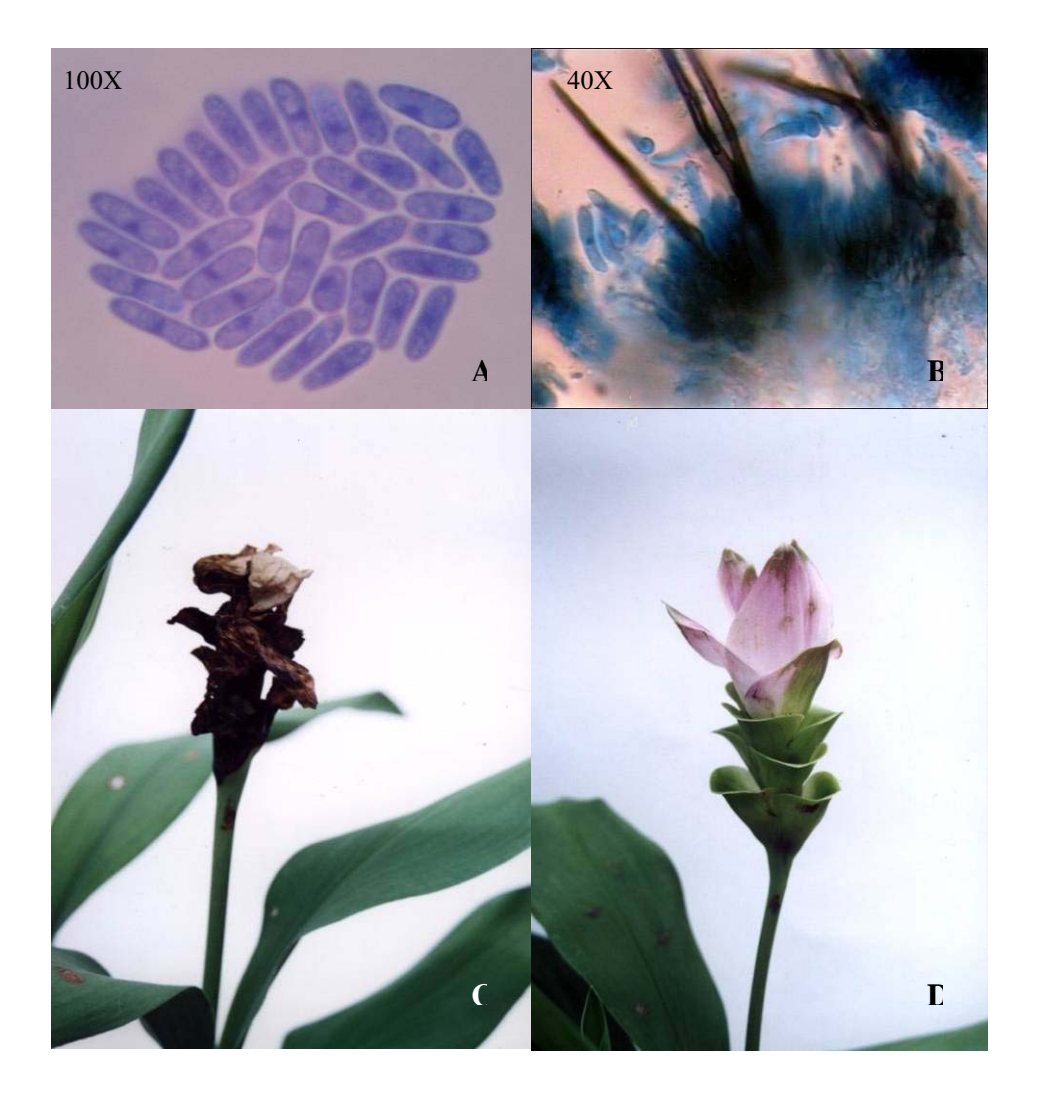


Figure 2

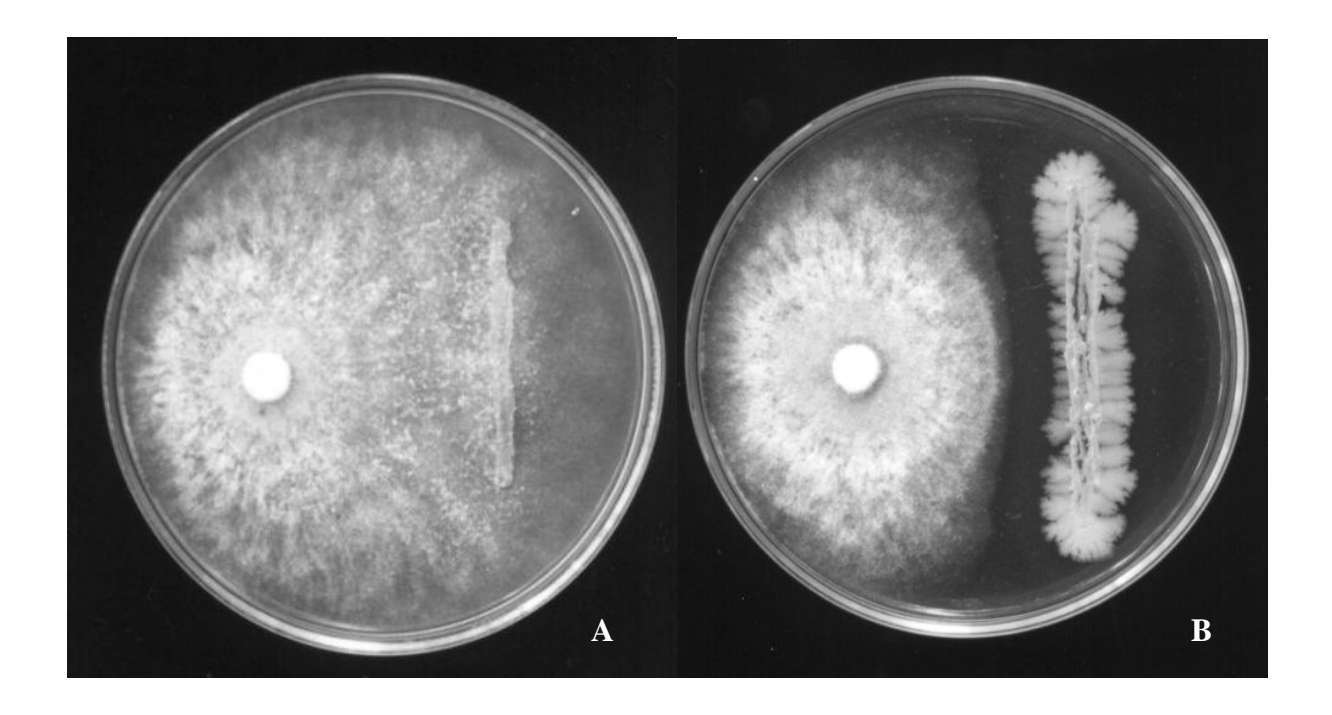


Figure 3

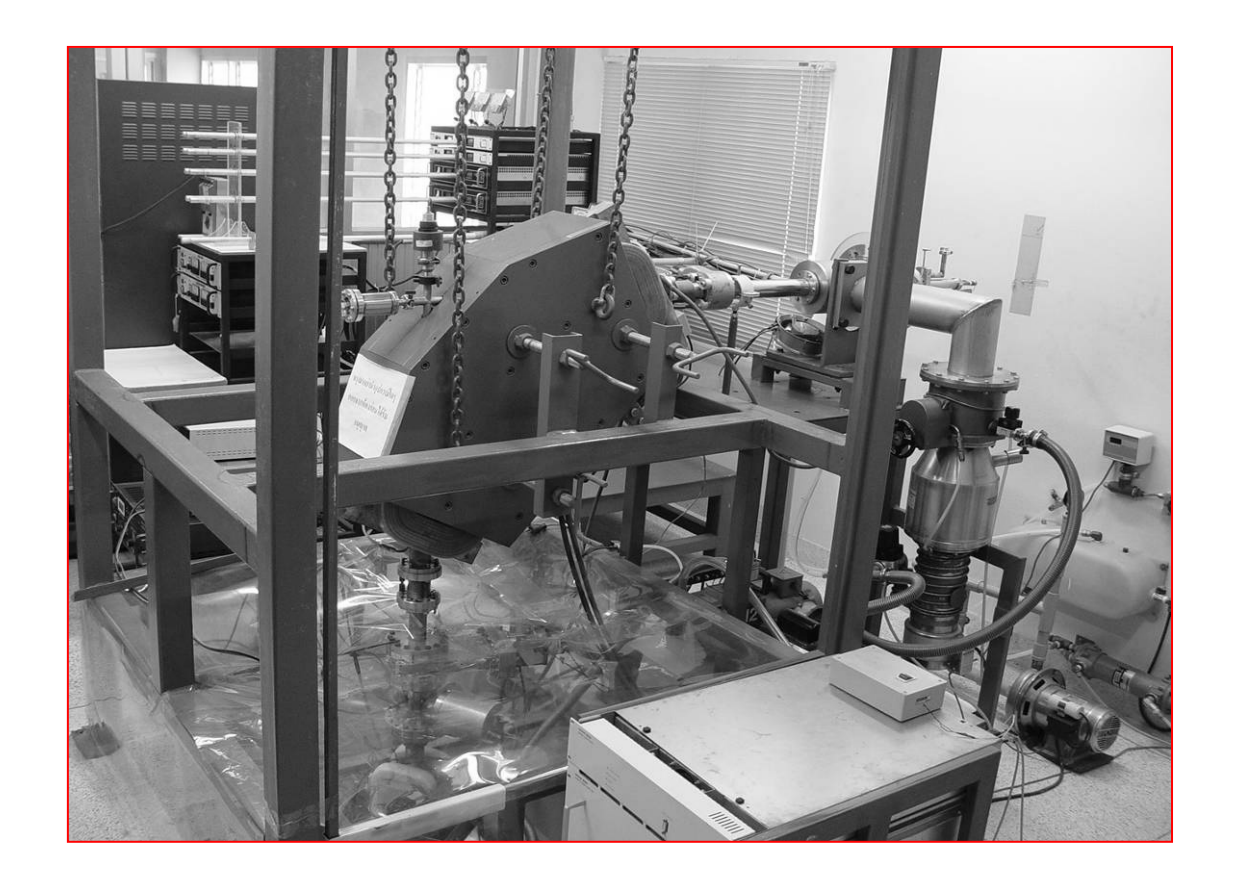


Figure 4

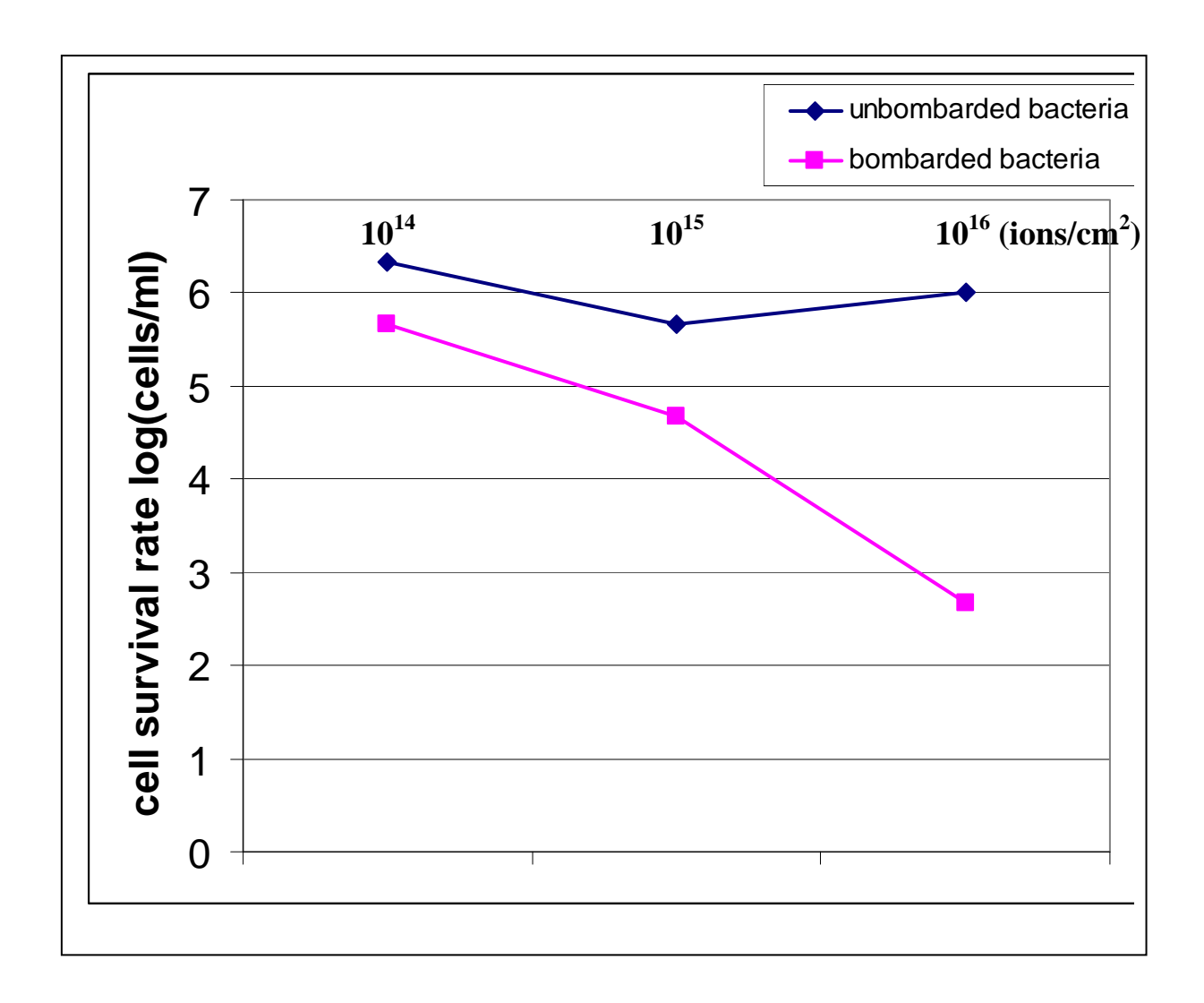


Figure 5

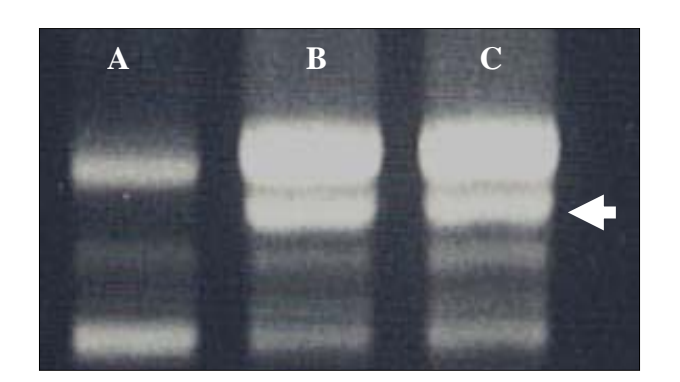


Figure 6

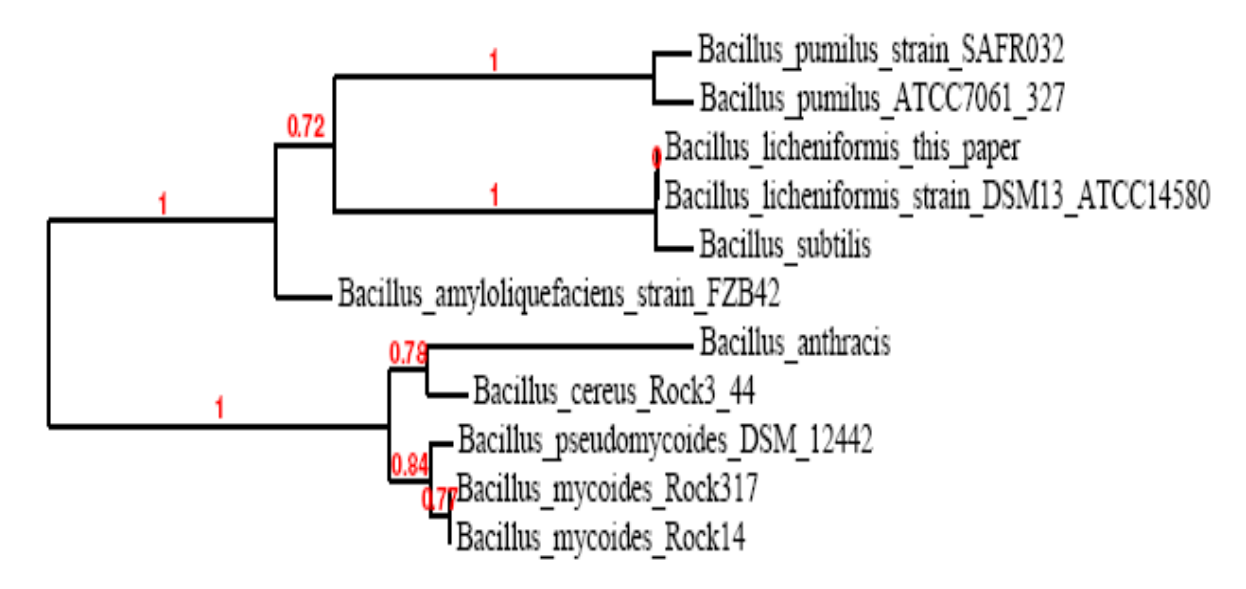
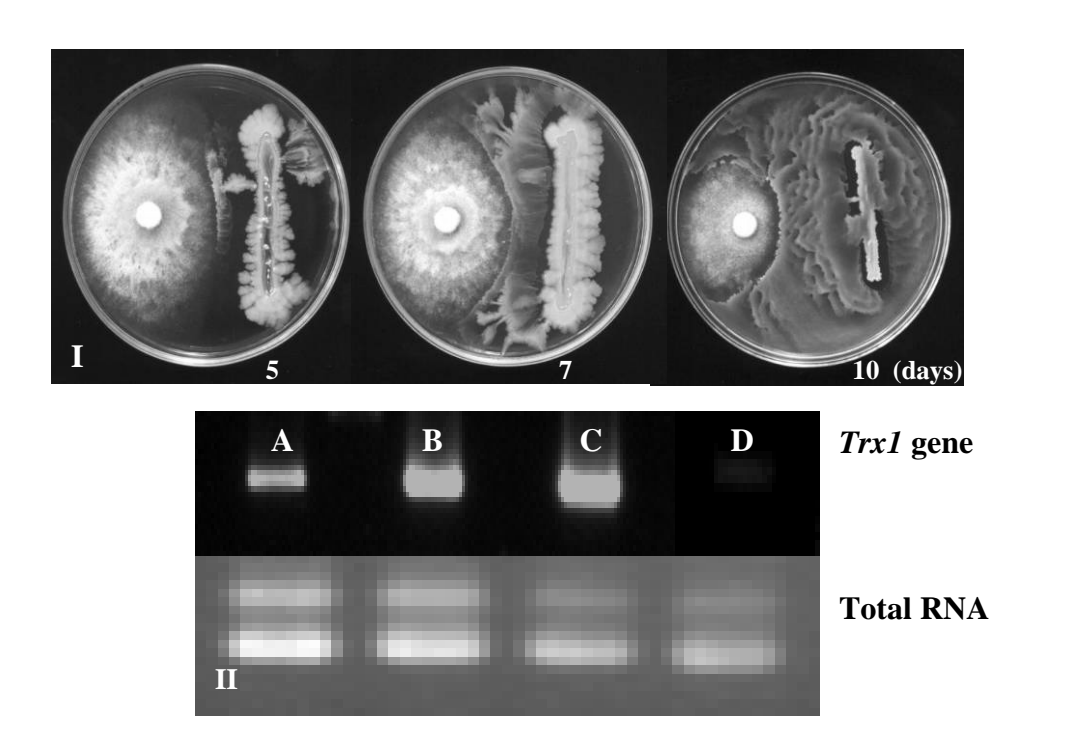


Figure 7



Cloning and Transformation of Gene Involving in Flower Senescence-Associaion from *Curcuma alismatifolia* Gagnep. by Application of Low-Energy Ion Beam

S. Mahadtanapuk⁽¹⁾, W. Teraarusiri⁽¹⁾, M. Sanguansermsri⁽²⁾, W. Nanakorn⁽²⁾, L. D. Yu⁽³⁾ and S. Anuntalabhochai⁽⁴⁾

Chiang Mai University, Chiang Mai 50200, Thailand

Corresponding Author: Somboon Anuntalabhochai (phone): 66 053 943346, (Fax):66 054 466 663 (e-mail):burinka@hotmail.com

Abstract

In this paper we present a novel method to induce gene transfer in plant using a low-energy ion beam. Aim of this work was to suppress an expression of ACC synthase gene in Siam tulip, *Curcuma alismatifolia* Gagnep. An cDNA fragment encoding ACC synthase from *C. alismatifolia* Gagnep. was isolated and its expression was analyzed. To determine the expression of p*Ca-ACSI*, the northern blot analysis and RT-PCR was used for gene analysis by specific primer. The result showed that the p*Ca-ACSI* gene was detected in bract of curcuma and the highest expression was observed at 2 days after flower was cut. The *Ca-ACSI* was subcloned pBI121 resulting in pBI121-*Ca-ACSI*, then transformed into model plant (*Torenia foumieri*) by application low-energy ion beam at an energy of 28–50 keV with a fluence range of 10¹⁴–10¹⁶ ions/cm². After this treatment, the transgenic plantlets were confirmed by PCR analysis and a histochemical GUS assay. Highly efficient of transformant tissue was showed as a method to plant transform with application low-energy ion beam bombardment.

Keywords

Ion beam bombardment, transformation, ACC synthase, cloning

⁽¹⁾ School of Agriculture Natural Resources and Environment, Naresuan University Phayao, Tumbol Maeka, Muang, Phayao, 56000, Thailand,

⁽²⁾ Naresuan University Phayao, Tumbol Maeka, Muang, Phayao, 56000, Thailand²,

⁽³⁾ Fast Neutron Research Facility, Department of Physics, Faculty of Science,

⁽⁴⁾Department of Biology, Faculty of Science, Chiang Mai University, Chiang Mai 50200, Thailand⁴

1. Introduction

Flower longevity is one of the most important characters of ornamental plants and extension of the longevity is a major target for improving the flower quality. Generally, the cause of short vase life is influenced by ethylene in many ornamental plants[1]. Ethylene, a gaseous major phytohormone, is one of the simplest organic molecular that exhibit biological The biochemistry of ethylene biosynthesis has been a subject of intensive study in plant hormone physiology [2]. In the ethylene synthesis pathway were the establishment of S-adenosylmethionine (SAdoMet) and ACC as the precursors of ethylene [3]. On the basis of the pathway, the first committed step of ethylene biosynthesis is the conversion of SAdoMet to ACC by ACC synthase (Sadenosyl-L-methionine methylthioadenosine-lyase, EC4.4.14) [4]. In addition ACC. ACC synthase (ACS) also produces 5-methylthioadenosine (MTA) in this reaction, which is then converted to methionine by using a modified methionine cycle [5]. Finally, ACC is oxidized by ACC oxidase (ACO) to form ethylene.

On the basis of this knowledge, the enzymes that catalyze these reactions were characterized and purified using biochemistry approaches. The first successes in molecular cloning of the 1-aminocyclopropane-1-carboxylic acid (ACC) synthase gene [6] and ACC oxidase (ACO) genes led to the demonstration that these enzymes belong to a multigene family [7]. Since then, ACC synthase has been isolated and its expression analyzed from many plants [8], such as winter squash, pear, apple, banana, and carnation. Further, the endogenous plant genes can be inhibited very effectively by antisense genes. This was shown Aida et al [9] who used an ACC oxidase antisense gene to inhibit ethylene production in the flower petals of transgenic torenia plants. These results indicate the general feasibility of down-regulating ethylene synthesis. It seems likely that, if the production of ethylene can be reduced further, it may be possible to delay senesces process in transgenic plants. In

addition, the introduction of ACC synthase gene, or ACC oxidase gene [10] by antisense technology caused reduction of ethylene production and a delay of flower senescence [11]. Therefore our hypothesis is that the suppression of the genes involving in ethylene biosynthesis that regulate flower senescence of curcuma might extend its flower longevity.

To understand the molecular functions of ACC synthase genes in Curcuma and to mean ethylene production knockout by recombinant technique, cloning and expression of ACC synthase genes are essential for anti-senesce or gene silencing technique that reduces ethylene production, ultimately enhancing the storage life and quality of the harvested products. Moreover, the new technique of transformation into plant tissue by application of low-energy ion bombardment has presented.

2. Experimental

2.1 Plant materials

Curcuma (*Curcuma alismalifolia* Gagnep.) were obtained from the Chiang Rai Horticultureal Research Center. The curcuma var. Chiang Mai Pink was grown under the greenhouse condition and used for RNA preparation.

2.2 RNA isolation, Cloning, and Sequencing

Total RNA from fresh Curcuma (*Curcuma alismalifolia* Gagnep.) flowers was extracted by using RNeasy® Mini Handbook (QIAGEN). The RNA was used as template for reverse transcriptase (RT-PCR), degenerate forward and reverse primers were designed from highly conserved domains of ACC synthase sequences such as TNPSNPLGTT (F1), PGWFRVCFAN (R1) and HIVYSLSKDL (R2) (forward primer1: 5'PAC IAA YCS ITC IAA YCC ICT IGG IAC, reverse primer1: 5'CG(CT) TT(AG) TG(ACGT) G(GT)(CT) TTG GT, reverse primer2: 5'PCC IAC ICK RAA ICC IGG for ACC synthase. The amplified cDNAs were ligated into pGEM T-easy plasmid and named pGEM-Teasy-*Ca-ACS*I. Plasmid vectors

that positive hybridized with ACC synthase gene were sequenced by BSU (Bio Service Unit), National Science and Technology Development Agency (NSTDA), Bangkok, Thailand. Plasmid DNA was prepared for sequencing using the Big-Dye Terminator Cycle Sequencing Kit (Perkin-Elmer) and following manufacturer's instructions. The sequences obtained were analyzed with the Genome Net (NCBI) database and the fragments for ACC synthase named *Ca-ACS* I.

2.3 Northern blot analysis

Total RNA isolated different organs (petal, bract, stem, and leave) and bracts after postharvest of cut flower were run on formaldehyde agarose gels (20 µg per lane). RNA was transferred to nylon membranes (Roche) with 20x SSC and the blots were baked by UV light. For probe preparation, a cDNA of ACC synthase named *Ca-ACS*I from pGEM-Teasy were digested with *Eco*RI and labeled with DIG High Prime DNA Labelling and Detection Starter Kit II (Roche) as probes. Hybridization and detection procedures were performed as described by manufacture. The prehybridization was performed for 3 hr at 68 °C in a solution containing 5x SSC, 50% formamides, 0.1% N-lauroylsarcosine, 0.02% SDS, and 2% blocking reagent (Roche). Hybridization and detection procedures were performed as described by manufacture (Amersham Pharmacia Biotech).

2.4 Plant Transformation

To prepare the plant tissue for transformation by ion beam bombardment, Leaf tissues of *Torenia foumieri* from tissues culture were cut with 0.5x0.5 cm. of size. Then the explants were transferred on a sterile adhesive tape which was attached to a Petri dish and then placed inside a sample holder. The holder was capable of sequentially exposing a number of samples to the ion beam, as well as housing the unbombarded control sample. Ion bombardment was carried out using the bioengineering applicable ion-implantation facility at

Chiang Mai University. Nitrogen ions were chosen for ion bombardment in the energy range of 28-50 keV with a fluence range of $10^{14}-10^{16}$ ions/cm². Inside the target chamber the temperature of the target was about 0 °C as both low ion flux and water cooling was used. The samples were maintained under these conditions for about 1.5-2 h, allowing for system pump-down and ion bombardment.

After implantation, the sample was immediately incubated at 25 °C in a shaker incubator with Murashige and Skoog medium (MS medium) containing 1 ug/ml of plasmid DNA for 30 min. Then the explants were cultured in vitro as described by Mahadtanapuk et al. [12] and transferred onto regeneration medium containing 100 mg/L kanamycin. The explants were subcultured every 2 weeks. After that transformants were detected according PCR and GUS assay were used to confirm the transformation. The histochemical GUS assay was conducted as described by Jefferson et al. [13].

3. Results and Discussion

For suppression of the genes involving in ethylene biosynthesis, the partial of ACC synthase was cloned by RT-PCR method. After sequencing, the cDNA of 645 bp contains an open reading frame encoding 215 amino acids. A homology search was performed using the BLAST program (NCBI). The analysis demonstrated that the amplified fragment encoded for part of the ACC synthase gene. When the sequence of the fragment was compared the ACC genes in databases by Phylogeny PhyML program, *Ca-ACS*I had a high sequence similarity (69-74%) to *Musa acuminata*, *Cymbidium sp. Vigna radiate*, *Citrus sinensis*, *Pelargonium hortorum*, Petunia and *Nicotiana tabacum* ACC synthase genes (Fig. 1). To determine the most significant ACS gene related to senescence in curcuma, northern analysis was performed with mRNA from different time points at postharvested curcuma. In Fig. 2., only signals for the *Ca-ACS*I gene were detected in the bracts of curcuma. The *Ca-ACS*I was expressed during postharvest in bracts at 2 days after cutting the flower. This result was related the

respiration and the ethylene production of open florets increased as they approached senescence. In bract of bloom curcuma results in an increase level of respiration and ethylene production from 2 to 4 day after harvesting and the prominent indication for the termination of vase life was the brown of the tip of coma bract or bract [14].

To manipulate these genetically-engineered plant tissue, the techniques in transformation or gene delivery are needed. Therefore, a model plant (*Torenia foumieri*) was used for gene transformation. Consequently, *Ca-ACSI* was subcloned in pBI121 resulting in pBI121-*Ca-ACSI*, and transformed into leaf tissues of *T. foumieri* by application of ion beam bombardment (Fig 3A). Six weeks after bombardment (Fig 3C,D), 12 and 14% explants of 50 shoots from *T. foumieri* transformed by pBI121 and pBI121-*Ca-ACS1* respectively, showed positive GUS gene. The transformation frequency was evaluated by histochemical GUS activity and PCR analysis (Table1). The PCR reaction revealed the presence of the GUS fragment with expected size of 500 bp in genomic DNA of each putative transgenic plant (Fig. 4). The prominent GUS activity was found in leaves and stems of the transformed plantlets with high expression in explants transformed with pBI121-*Ca-ACSI* (antisense) and pBI121 by using application low-energy ion beam at an energy of 30 keV with a fluence range of 10¹⁵ ions/cm² (Fig. 5).

In the knowledge of, the *Curcuma* is a monocotyledonous plant species. To introduce desirable traits by a gene transformation system, an efficient regeneration protocol is essential in *Curcuma*. The most important prerequisite for the method is the possibility to regenerate plants from callus tissues or explants, although comparative data, concerning tissue proposition and regeneration of *Curcuma* tissue, is very rare. In recent years, the *Agrobecerium*-mediated transformation for *Curcuma alismalifolia* Gagnep.has been reported by Supuk et al [12] and their transformation frequency was about 15%. In our transformation experiments, we report here the first transformation evidence of ACS gene from *C. alismalifolia* Gagnep. into *T. foumieri* by application of ion beam bombardment. This

establish, the transformation efficiency was calculated, based on the number of transgenic plants recovered by the number of the original intact shoots, the transformation frequency with pBI121 and pBI121-*Ca-ACS1* was approximately 2-14%. Moreover the antisense 1-aminocyclopropane-1-carboxylic acid (ACC) synthase gene isolated from *C. alismatifolia* was tried to introduce by this method, in an attempt to prolong vase life of the inflorescence after harvesting.

5. Conclusions

In this study we investigated the role of ACC synthase in curcuma by cloning cDNA and examining expression patterns of the genes. We have investigated the effects of wounding, organ difference, and posthavest of cut curcuma. The expression of curcuma ACC synthase gene (*Ca-ACSI*) was specifically in bracts and the high expression of the *Ca-ACSI* at 2 day after harvesting might be involved in vase life and the low ion beam bombardment at an energy of 30 keV with a fluence range of 10^{14} – 10^{16} ions/cm² can induct gene transformation in *Torenia foumieri*

Acknowledgments

We wish to thank The Naresuan University Phayao Research Fund, Thailand Research Fund (TRF) and National Research Council of Thailand (NRCT)

References

- [1] A. Borochov, W.R. Woodson, Sic Hortic. 11 (1989) 15-43.
- [2] X. Liang, S. Abel, J.A. Keller, N.F. Shen, A. Theologis, Proc Natl Acad Sci USA. 89(1992) 11046–11050.
- [3] S.F. Yang, N.E. Hoffman, Annu Rev Plant Physiol. 35 (1984) 155–189.
- [4] H. Kende, Annu Rev Plant Physiol. 44(1993) 283–307.
- [5] A.B. Bleecker, H. Kende, Annu Rev Cell Dev Biol. 16 (2000) 1–18.

- [6] T. Sato, A. Theologis, Proc Natl Acad Sci USA. 86 (1989) 6621–6625.
- [7] P. Spanu, D. Reinhardt, T. Boller, EMBO J. 10(1991) 2007–2013.
- [8] C.S. Barry, M.I. Llop-Tous, D. Grierson, Plant Physiol. 123(2000) 979–986.
- [9] R. Aida, T. Yoshida, K. Ichimura, R. Goto, M. Shibata, Plant Sci. 138 (1998) 91-101.
- [10] A.J. Hamilton, G.W. Lycett, D. Grierson, Nature. 346 (1990) 284-287.
- [11] K.W. Savin, S.C. Baudinette, M.W. Graham, M.Z. Michael, G.D. Nugent, C.Y. Lu, Sci Hortic. 30 (1995) 970-972.
- [12] S. Mahadtanapuk, N. Topoonyanont, T. Handa, M. Sanguansermsri, S. Anuntalabhochai, Plant Biotech. 23(2006) 233–237.
- [13] R.A. Jefferson, T.A. Kavanagh, M.W. Bevan, EMBO J. 6(1987) 3901–3907.
- [14] K. Bunya-Atichart, S. Ketsa, W.G. Doorn van, Postharvest Biol. 34(2004) 219–226.

Figure Captions

- Fig.1. The sequence of the fragment was compared the ACC genes in databases by Phylogeny PhyML program, *Ca-ACS*I had a high sequence similarity (69-74%) to *Musa acuminat*a, *Cymbidium sp. Vigna radiate*, *Citrus sinensis*, *Pelargonium hortorum*, Petunia and *Nicotiana tabacum* ACC synthase genes.
- Fig.2. Expression analysis of curcuma ACC synthase gene (*Ca-ACSI*) by Northern blotting on total RNA from different organ; L: Leaves, S: Stem, B: Bract, Pe: Petal and P: Bracts after postharvest of cut flower.
- Fig. 3. Plasmid DNA was transformed into leaf tissues of *Torenia foumieri* by application of ion beam bombardment; A: the preparation of the plant tissue for transformation by ion beam bombardment, B: the explants were cultured in vitro and transferred onto regeneration medium, C: the transformants at six weeks of age.

Fig. 4. PCR amplification; *Pst*I molecular size marker: 1, plasmid pBI121: 2, plant transform with plasmid pBI121: 3, plant transform with plasmid pBI121-*Ca-ACSI*: 4, non-transformed plant: 5. Arrow indicates the PCR products of expected size after GUS gene amplified (500 bp).

Fig. 5. Histochemical observation, shoots 6 weeks after transformation; non-transformed plant (A), plasmid pBI121(B), plasmid pBI121-*Ca-ACS1* (C).

Table 1. Transformation and selection ratio in transgenic plant.

Application low-energy ion beam	Percentage of explants showing		Frequency of transformed shoot	
at an energy of 30 keV with a	Gl	US spots (%)	showing positive PCR	
different fluence range	pBI121	pBI121-Ca-ACS1	pBI121	pBI121-Ca-ACS1
10 ¹⁴ ions/cm ²	2	4	8	8
10 ¹⁵ ions/cm ²	4	6	12	14
10 ¹⁶ ions/cm ²	0	4	6	12

Figure 1

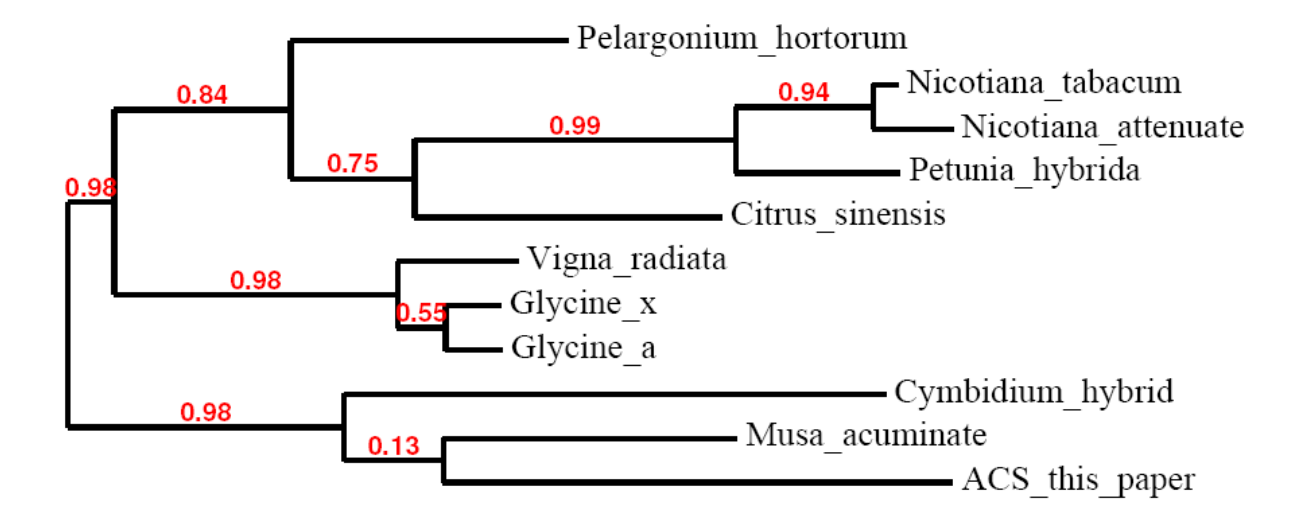


Figure 2.

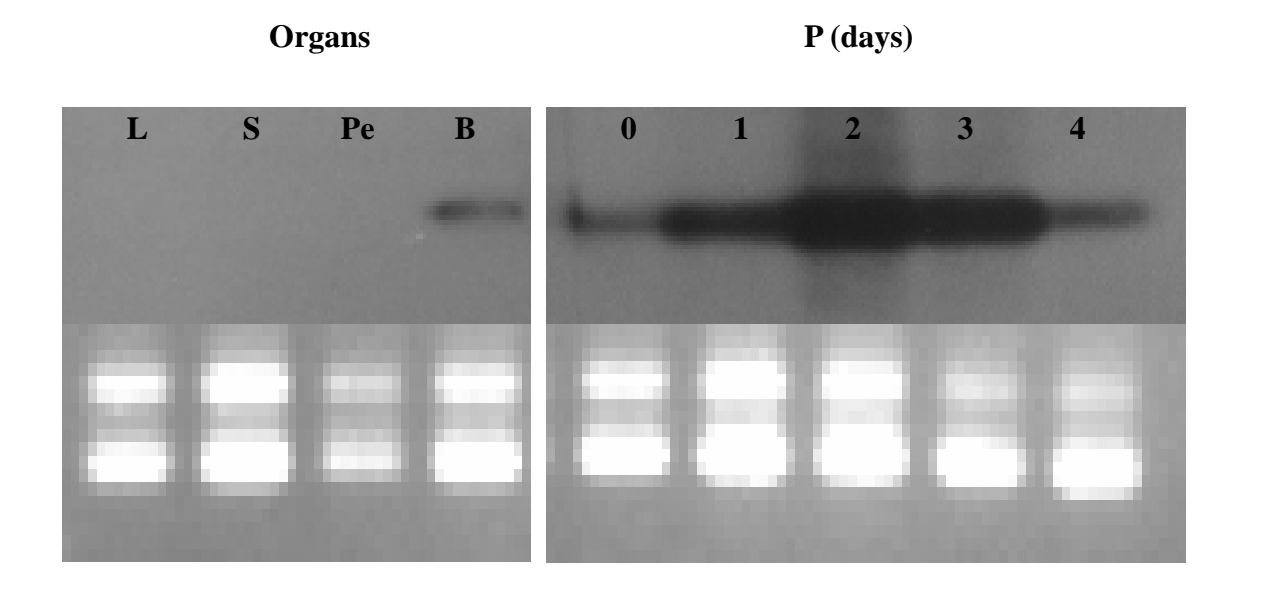


Figure 3.

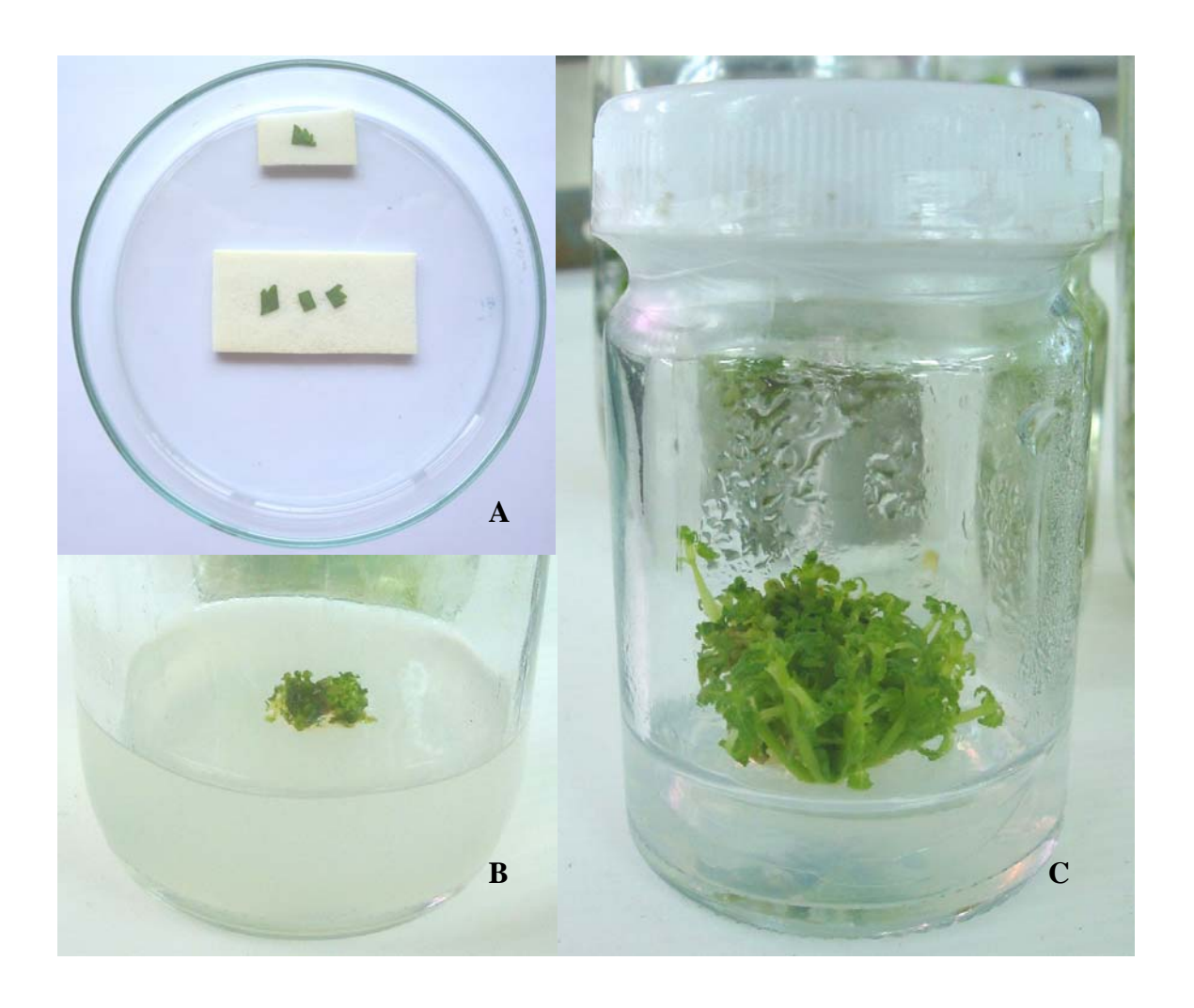


Figure 4.

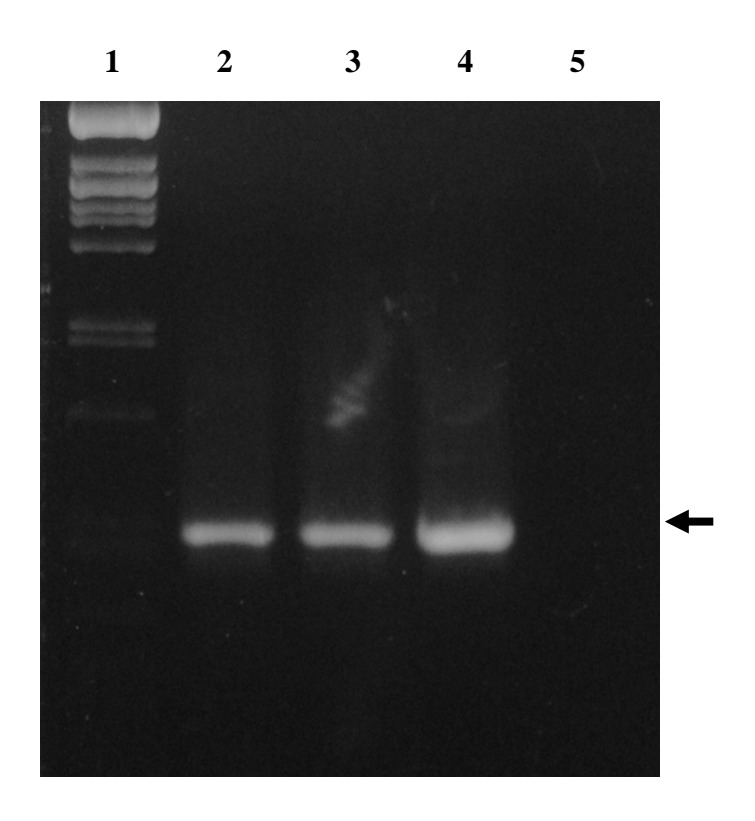
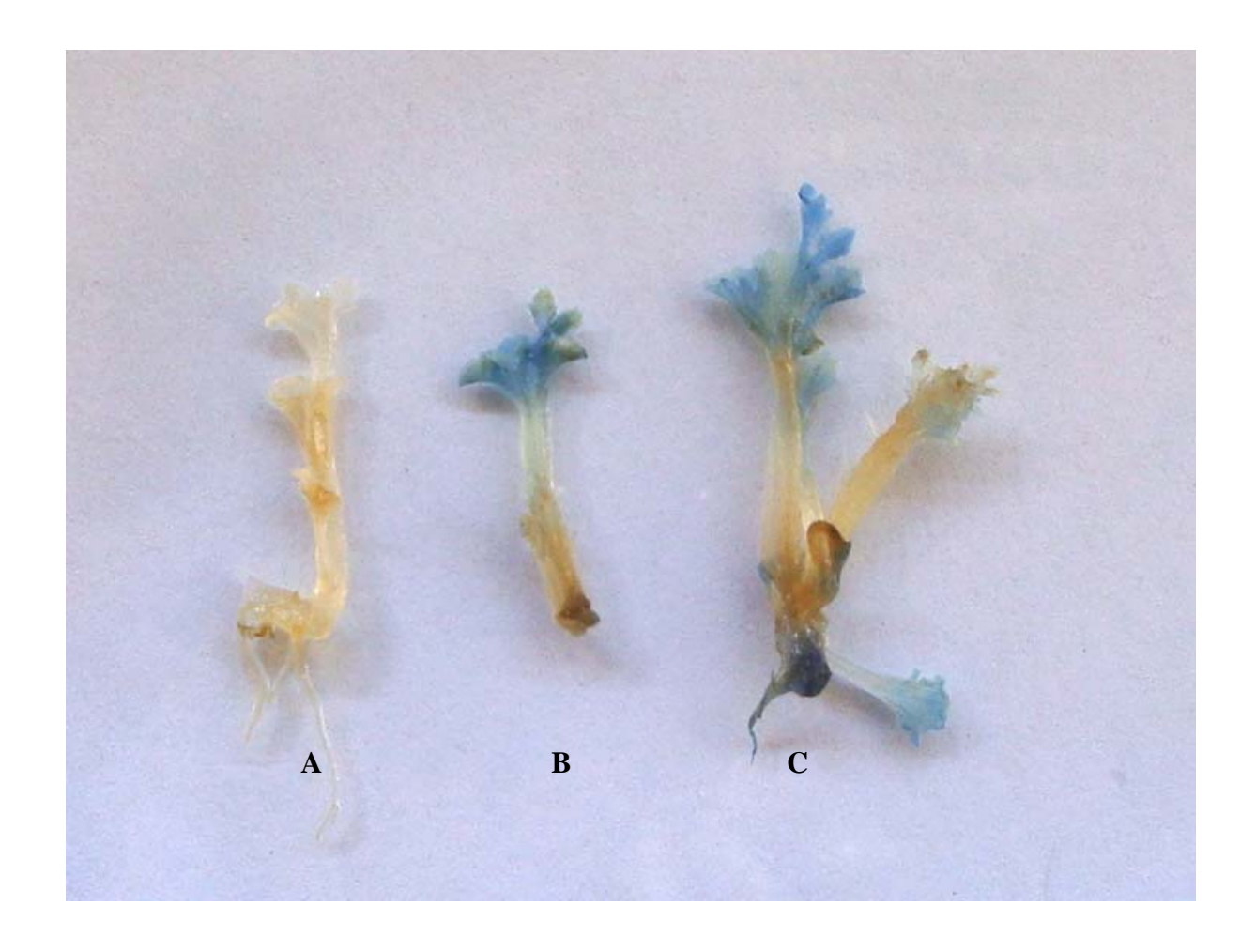


Figure 5.



Ion Beam Nanobiology at Chiang Mai University

- L.D. Yu^{a,b},* (Tel.: +66 53 943379, Fax: +66 53 222776, E-mail: yuld@fnrf.science.cmu.ac.th), V.S. Lee^c (Tel.: +66 53 943341 ext. 117, Fax: +66 53 892277, Email: yannajan@gmail.com), P. Nimmanpipug^c (Tel.: +66 53 943341, Fax: +66 53 892277, Email: npiyara@yahoo.com), K. Prakrajang^a (Tel.: +66 53 943379, Fax: +66 53 222776, Email: kittikun@fnrf.science.cmu.ac.th),
 - S. Sarapirom^a (Tel.: +66 53 943379, Fax: +66 53 222776, Email: missunaa@hotmail.com),
- S. Anuntalabhochai^d (Tel.: +66 53 943348, Fax: +66 53 892253, Email: soanu.1@gmail.com)
- ^a Plasma and Beam Physics Research Facility, Department of Physics and Materials Science, Faculty of Science, Chiang Mai University, Chiang Mai 50200, Thailand
 - ^b Thailand Center of Excellence in Physics, Commission on Higher Education, 328 Si Ayutthaya Road, Bangkok 10400, Thailand
 - ^c Computer Simulation and Modeling Laboratory, Department of Chemistry, Faculty of Science, Chiang Mai University, Chiang Mai 50200, Thailand
 - ^d Molecular Biology Laboratory, Department of Biology, Faculty of Science,
 Chiang Mai University, Chiang Mai 50200, Thailand

Abstract

When ion beam parameters are controlled properly, ion beam can irradiate materials in both

longitudinal and latitudinal nanoscales. When this type of ion beams irradiates biological objects

such as cells and DNA, it opens up a novel area, i.e. ion beam nanobiology. This paper reviews

recent progress achieved at Chiang Mai University in ion beam nanobiology research. The work

reported includes theoretical calculation of the nanoscaled low-energy ion range in DNA, study

on low-energy ion bombardment of naked DNA, molecular dynamics simulation of ultra-low-

energy ion interaction with DNA, observation of micro/nano-crater formation on the ion-

bombarded cell envelopes, and utilization of single-ion nanobeam for irradiation of cells.

Keywords: Ion beam, Nanobiology, DNA, Cell.

I. INTRODUCTION

Low-energy (the ion energy lower than 100 keV) ion implantation in materials is in principle

a nanoscale process, as in most conventional target materials the ion penetration range is around

100 nm or lower. This process has been well studied. However, when the target materials are

turned to be biological living materials, the process becomes more complex [1,2]. Particularly,

when the ion energy is sufficiently low (\leq keV), the ion implantation process in micro- and nano-

scale biological objects such as cells and DNA is of special novelty. When the ion fluence is

controlled to be sufficiently low, it is possible to obtain single ion delivery which is definitely at

a nanometer dimension. Thus, we come into a new area, i.e. ion beam nanobiology. We have

initiated research programs in this area at Chiang Mai University (CMU) for investigations of basic physics and biology involved in ion interaction with biological living materials. This paper reviews our preliminary work and recent progress.

II. LOW-ENERGY ION RANGE IN DNA

We have developed an approach for the calculation of ion range, using a simplified meanpseudo-atom model of the DNA target [3]. According to the model, a DNA molecule has a mean chemical composition of $H_{12}C_{10}N_4O_7P$ with a mean atomic number of 5.03 and a mean atomic weight of 9.74. For different forms of DNA, e.g. A-DNA, B-DNA and Z-DNA, the mass density ranges from about 0.6 to 1.1 g/cm³. Based on the ion stopping theory [4], for the case of low-energy ($E \le a$ few keV) ion implantation into DNA, the stopping S_n falls in the low reduced energy regime, which gives a cube-root energy dependence of the stopping ($E^{1/3}$)

$$S_n = AE^{1/3} \tag{1}$$

where

$$A = 4\pi a_{TF}^{4/3} (Z_1 Z_2 e^2)^{2/3} \left(\frac{M_1}{M_2}\right)^{1/3} \left[\frac{M_1 M_2}{(M_1 + M_2)^2}\right]^{2/3}.$$
 (2)

Here, a_{TF} is the Thomas-Fermi (TF) screening radius, Z_1 and Z_2 are the atomic numbers of the incident ion and the target material element, respectively, M_1 and M_2 are the atomic weights of the incident ion and the target material, respectively, and e is the electronic charge. Calculation formulae of the ion range in DNA are then obtained to unify the relevant calculations. Our calculation indicates that the low-energy ion range in DNA is in the nanoscale and sensitive to nanometer.

For example, the projected range of 4-keV Ar ion in the nature form B-DNA is 7.5 nm, 1-keV C ion about 5 nm and 60-eV H ion about 1.5 nm. Upper limits of the ion energy as a function of atomic number of the bombarding ion species are proposed for the low-energy case to hold. Comparison of the results of this approach with the results of some widely used computer simulation codes such as SRIM, PROFILE and PRAL and with results reported by other groups indicates that our approach provides convincing and dependable results.

III. LOW-ENERGY LOW-FLUENCE ION BOMBARDMENT OF NAKED DNA

A. Experiments

Samples of naked plasmid DNA pGFP (plasmid green fluorescent protein which fluoresces with green under ultraviolet light) were bombarded in vacuum (10⁻⁴ Pa) by nitrogen (N) and argon (Ar) ions coming from either ion beam [5] or RF-generated plasma [6] with energy ranging from 1.25 – 5 keV and fluence from 10¹¹ – 10¹³ ions/cm². The projected ranges of these ions in the low-pressure low-humidity form A-DNA were calculated with our developed approach normally less than 10 nm, e.g. about 6 nm for 1.25-keV N ions, 8 nm for 2.5-keV N ions, and 10 nm for 5 keV Ar ions. After ion bombardment, the DNA samples were treated with standard biological procedures for gel electrophoresis and gene transfer into bacteria *Eschericia coli* (*E. coli*).

B. Results and Discussion

Vacuum effect on DNA form change and subsequent mutation of the DNA-transferred bacteria was checked. The result shows that vacuum has some effect on DNA form change due

to an environment change. However, grown bacteria did not show color change and thus no mutation was induced by the vacuum exposure. This result indicates that without energetic ion bombardment DNA has no effective form change to induce mutation.

Pure plasma effect on DNA form change and subsequent mutation of the bacteria was checked either with grounding or without grounding of the sample holder. Under both conditions, the DNA samples were placed in the plasma but without using bias for minutes which were corresponding to an ion fluence of 10¹³ ions/cm². In the grounding case, the ions with only the thermal energy bombarded the DNA, while in the ungrounding case, the ions only "blew" the DNA with the thermal energy. From both conditions, no mutation of the bacteria was found. This result means that only with the ion energy of an order of eV, effective form change in DNA for bacterial mutation cannot be induced within the treatment time periods.

The effect from low-energy ion bombardment on DNA form change and subsequent induction of bacterial mutation was investigated. The quantified results on the DNA form change from the electrophoresis analysis of ion beam bombarded DNA are shown in Fig. 1. Upon the very low-energy low-fluence ion beam bombardment both relaxed and linear forms were produced and hence single strand break (SSB) and double strand break (DSB) occurred. As increasing the ion fluence, the amount of the original DNA supercoiled form decreased for the N-ion beam bombardment case but did not much change for the Ar-ion beam bombardment case; the amount of the relaxed form slightly increased for the N-ion beam case but did not change noticeably for the Ar-ion beam case; the amount of the linear form increased for the N-ion beam case more than for the Ar-ion beam case. The result of transfer of the ion-beam-bombarded DNA in *E. coli* showed green (non-mutant) and white (mutant) colonies produced, as shown in Fig. 2a. The appearance of white colonies that were the evidence of the GFP gene damaged and thus not

functioning confirmed that low-energy ion beam bombardment indeed induced bacterial mutation resulting from DNA damage. In the case of plasma immersion ion bombardment (PIIB) of DNA, DNA form change was also observed and the dominant change was the formation of the relaxed form but the linear form was negligible (Fig. 1b). This is due to a fairly large portion of low-energy ions in a pulse. Hence, when the same accelerating voltages were applied for both ion beam and plasma immersion ion implantations, in the latter case the number of the ions having standard energy was fairly less than in the former case, so that DNA could not be bombarded in the latter case as sufficiently as in the former case. However, with only relaxed form of DNA from PIIB, DNA misrepairing could still result in bacterial mutation as shown in Fig. 2b. In PIIB, N-ion bombardment induced DNA form change is seen more sensitive to ion fluence than Ar-ion bombardment.

C. Computer Simulation

Molecular dynamics simulation (MDS) was carried out to simulate ultra-low-energy ion bombardment of naked DNA in vacuum [7,8]. In the simulation, A-DNA was bombarded with carbon (C) or nitrogen (N) ions with energy of 0.1 eV to and 200 eV. According to our theoretical estimation of the nanoscaled ion range, with the energy mentioned the ions interact with a single DNA molecule.

In MDS of C-ion bombardment, the root mean square displacements (RMSD) of the backbone atoms of poly-AT were found remaining in small fluctuation after 1.0 ns of the equilibration, while those of poly-GC were stable after 1.5 ns of the equilibration. This indicates the poly-AT DNA double strands more inertia than the poly-GC backbones. The tendency of DNA strand splitting was inspected by measuring the distance between the backbone termini of

two strands, as shown in Table 1. It is seen that the poly-AT's T20-A21 backbone termini is the most sensitive to the ion irradiation as it exhibits the largest distance increase subjected to C-ion bombardment. As seen from Fig. 3, the base rings of poly-GC are quickly stabilized after about only 5 ps of ion bombardment, whereas those of poly-AT take the time more than ten times as poly-GC takes to stabilize. All of these results indicate that poly-AT is more unstable and more tend to be broken than poly-GC when subjected to ion attack.

(Table 1)

In N-ion bombardment, the radial distribution functions (RDF), the distances of maximum RDF, r_{max}, and the RDF integrals were studied after Monte Carlo simulation of N-ion bombardment of DNA, as shown in Table 2. The higher RDF integral indicates the higher absorption preference of the implanted ion. It is seen that the preference of N-ion interaction with the DNA atoms is in an order of OP, O, O', N, C and C'. The shortest r_{max} of OP indicates the strongest interaction with the incident ion as the distance represents the distance between the atom and the ion, obviously, the shorter the stronger the interaction force. The studied bond types included oxygen-phosphorus single bonds (O-P), oxygen-phosphorus aromatic bonds (O-P (ar)), carbon-carbon single bonds (C-C), carbon-nitrogen single bond (C-N), carbon-oxygen single bonds (C-O), carbon-carbon aromatic bonds (C-C (ar)), carbon-nitrogen aromatic bonds (C-N (ar)) and carbon-oxygen double bonds (C=O). The maximum, minimum and modal bond lengths in each bombardment were measured as summarized in Table 3. It is seen that the O-P bond is the weakest as it has the largest increase in the bond length after ion attack, and following the O-P bond are the C-C, C-C (aromatic) and C-N bonds, whereas the C=O bond is the strongest.

(Table 2 and Table 3)

The MDS findings demonstrate that low-energy ion beam induced DNA structural modification is not a random but preferential effect.

IV. ION BEAM CREATION OF NANOCRATERS ON THE CELL ENVELOPE

In study of physical mechanisms involved in ion beam induced DNA transfer [9], we tried to understand whether any pathways were created by ion beam bombardment in the cell envelope for exogenous macromolecules such as DNA to pass through. Ion beams with the same conditions used as for ion beam induction of DNA transfer, typically at energy of 20 – 30 keV and fluences of an order of 10^{15} ions/cm², were applied to bombard various cells such as plant onion skin and bacterial E. coli cells. Scanning electron microscopy (SEM) and atomic force microscopy (AFM) in situ or ex situ were used to observe the ion bombarded cell envelope surface. Craters with sizes of about 100 - a few 100 nm in diameter and a few hundred nanometers in depth were observed on the surface [10,11,12]. The formation of the micro/nanocraters was a general phenomenon induced during ion bombardment, no matter what ion species, under certain ion beam conditions such as ion beam energy and fluence range; the craters were inhomogeneously distributed, thus the crater formation was not a direct effect but probably an indirect consequence of ion bombardment; and the effect was not related to the material chemical composition and rapid water evaporation from the cell envelope, but related to the special microstructure of the cell envelope. We speculated that the craters might be pathways for exogenous DNA transfer into biological cells, but evidence was insufficient yet and to be further explored.

V. SINGLE ION IRRADIATION OF CELLS

Under a collaborative research program, we have had opportunities to carry out research using the single ion beam line at Ion Beam Centre, University of Surrey, UK [13] on cancer therapy study. Hamster cells, V79, which could rapidly grow to mimic human cancer cells, were irradiated by 2-MeV proton beam for a preliminary study. The V79 cells were placed in a Mylar metal dish which was then put on the sample stage of the end station. Protons were accelerated by the 2-MV tandetron accelerator, transported in a horizontal 10-m beam line, bent by a 90°-magnet to the vertical beam line, and delivered vertically up to the end station at the 4th floor. The proton beam was finally focused and steered using electromagnetic fields to enable single ions individually to target the well positioned cells with a spatial resolution of less than 10 nm. After the cells were irradiated with 20-60 protons per cell the metal dishes were put into an incubator. After several weeks of incubation, the irradiated cells were analyzed for their response in both physics and chemistry to the ultra-low-dose ion irradiation.

VI. CONCLUSION

Ion beam nanobiology deals with ion interaction with biological objects in either longitudinal or latitudinal nanoscale. When low-energy (keV or lower) ion beam irradiates biological targets such as DNA, the ion range in DNA was calculated by our theoretical approach to be in the order of nanometer. In such a short interaction range that is within a DNA molecule, keV ions are able to produce DNA form change, a kind of DNA damage, potentially to induce mutation of living organisms. The induction of the DNA damage is not random but preferential.

Nanoscaled single ion irradiation of cells provides a novel and powerful tool for investigation of cell response to ionizing radiation, eventually benefiting to cancer therapy study.

ACKNOWLEDGEMENTS

The work has been supported by Thailand Research Fund, National Research Council of Thailand and Thailand Center of Excellence in Physics.

REFERENCES

- 1. T. Vilaithong, L. D. Yu, P. Apavatjrut, B. Phanchaisri, S. Sangyuenyongpipat, S. Anuntalabhochai, I.G. Brown, Radiation Physics and Chemistry, 71/3-4, 927 (2004).
- 2. L. D. Yu, T. Vilaithong, I. Brown (Eng. Eds.), *Introduction to Ion Beam Biotechnology*. English edition, originally authored by Yu Zengliang in Chinese, Springer Science & Business Media, New York (2006).
- 3. L. D. Yu, T. Kamwanna, and I. G. Brown, Phys. Med. Biol., 54, 5009 (2009).
- 4. M. Nastasi, J. W. Mayer and J. K. Hirvonen, *Ion-Solid Interactions: Fundamentals and Applications*, Cambridge University Press, Cambridge (1996).
- 5. R. Norarat, N. Semsang, S. Anuntalabhochai, and L. D. Yu, Nucl. Instr. Meth. B 267, 1650 (2009).
- 6. S. Sarapirom, K. Sangwijit, S. Anuntalabhochai, L. D. Yu, orally presented to the 10th International Workshop on Plasma-Based Ion Implantation and Deposition, Sao Jose, Brazil, Sep. 7-11, 2009, to be published in Surf. Coat. Technol. (2010).

- 7. C. Ngaojampa, L. D. Yu, T. Vilaithong, P. Nimmanpipug and V. S. Lee, *The Proceedings of The 12th Annual Symposium on Computational Science and Engineering*, Thailand, NECTEC, 127 (2008).
- 8. C. Ngaojampa, P. Nimmanpipug, L. D. Yu, S. Anuntalabhochai, V. S. Lee, J. Molecular Graphics and Modeling (2009), in press.
- 9. S. Anuntalabhochai, R. Chandej, B. Phanchaisri, L. D. Yu, T. Vilaithong, I. G. Brown, Appl. Phys. Lett., 78(16), 2393 (2001).
- B. Phanchaisri, L. D. Yu, S. Anuntalabhochai, R. Chandej, P. Apavatjrut, T. Vilaithong, I.G. Brown, Surf. Coat. Technol., 158-159, 624 (2002).
- 11. S. Sangyuenyongpipat, L. D. Yu, T. Vilaithong and I. G. Brown, Nucl. Instr. Meth. B 242(1-2), 8 (2006).
- 12. S. Sangyuenyongpipat, L. D. Yu, I. G. Brown, C. Seprom and T. Vilaithong, Nucl. Instr. Meth. B 257, 136 (2007).
- 13. K. J. Kirkby, G. W. Grime, R. P. Webb, N. F. Kirkby, M. Folkard, K. Prise, and B. Vojnovic, Nucl. Instr. Meth. B 260, 97 (2007).

Table 1. Distance (angstrom, Å) between the backbone termini of two DNA strand after 150 ps MDS. In the case of 200-eV C-ion bombarding poly-GC, the ion passed through DNA after 150

ps simulation. The average distance change is the ratio of the difference between the mean distance of all non-zero energies and the distance of the zero energy over the latter.

	Ion energy (eV)				Average distance
Distance between	0	2	20	200	change (%)
Poly-AT A1-T40	11.7	12.6	13.0	11.1	4.56
Poly-AT T20-A21	12.0	17.4	17.6	16.3	42.5
Poly-GC G1-C40	16.0	19.1	18.1	1	16.3
Poly-GC C20-G21	15.2	15.2	16.4	-	3.95

Table 2. The N-ion bombardment simulation result of the mean values of the distance of maximum radial distribution functions, r_{max} , and the integral of radial distribution functions from 0.0 to 4.0 Å, $I_{4\text{Å}}$, of each atom type.

Atom type	r_{\max} (Å)	<i>I</i> _{4Å} (Å)
N	3.85	1.83
О	4.75	2.8
O'	4.45	2.6
OP	3.3	3.25
С	3.9	1.5
C'	4.0	1.43

Table 3. The bond lengths measured after certain time of N-ion bombardment simulation.

	Average	Modal bond length after ion irradiation (Å)			
Bond	equilibrium	1-N eV,	1 eV,	10 eV,	Mean
type	length (Å)	after 10 ps	after 10 ps	after 6 ps	increase (%)
O-P	1.582	1.618	1.702	1.698	5.73
O-P (ar)	1.486	1.498	1.498	1.481	0.43
C-C	1.518	1.560	1.570	1.544	2.64
C-N	1.490	1.489	1.543	1.515	1.72
С-О	1.433	1.445	1.432	1.459	0.86
C-C (ar)	1.387	1.426	1.408	1.399	1.73
C-N (ar)	1.351	1.388	1.381	1.336	1.28
С=О	1.230	1.220	1.221	1.218	-0.84

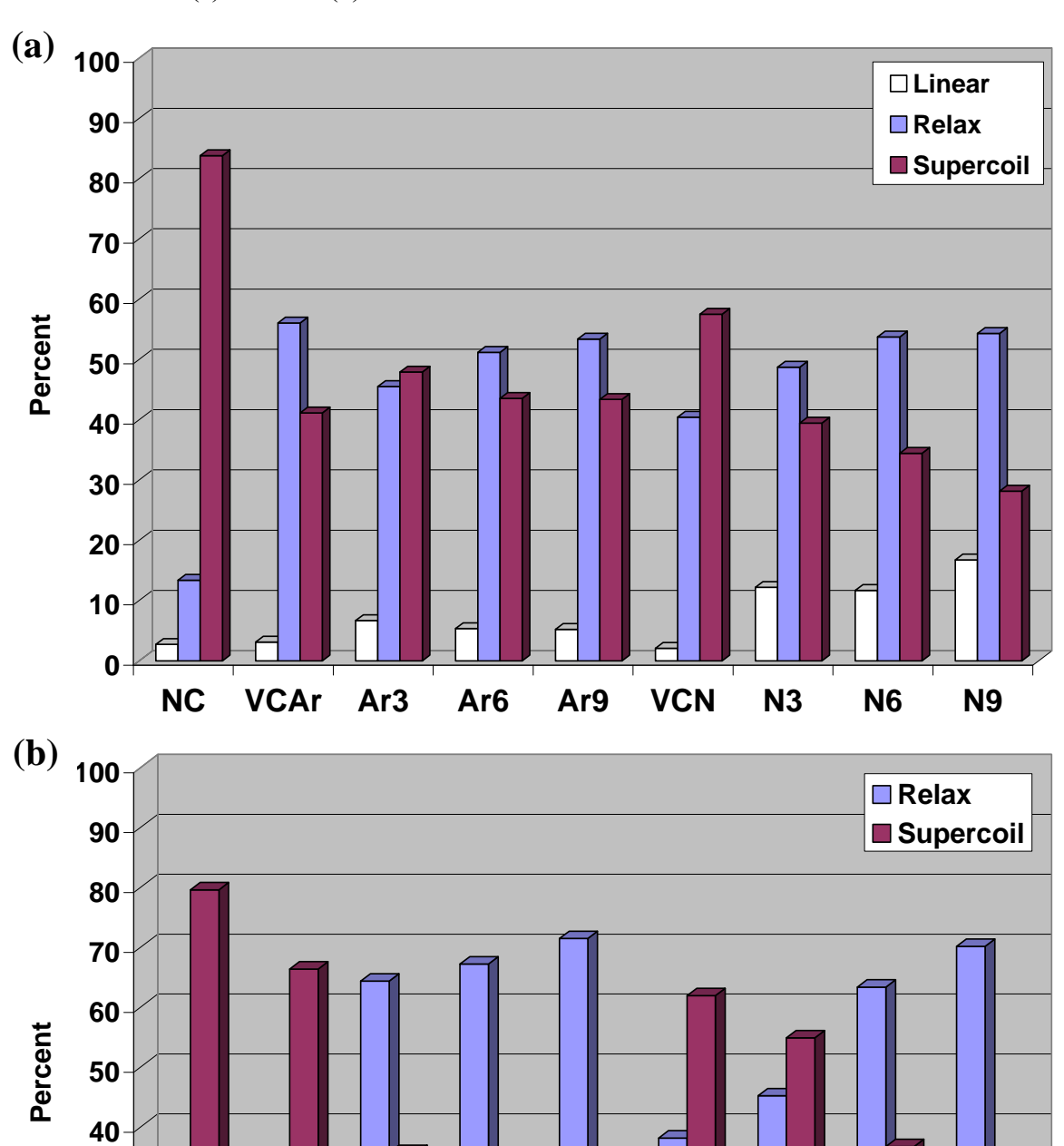
Figure captions

Fig. 1. Percentages of the DNA forms, quantified from the electrophoresis results, under different conditions: natural control (NC), vacuum control (VC) and after bombardment with ether nitrogen (N) or argon (Ar) ions from (a) ion beam and (b) plasma immersion ion implantation. The ion fluence is marked by (a) $3 - 3 \times 10^{13} \, \text{ions/cm}^2$, $6 \times 10^{13} \, \text{N-ions/cm}^2$, $9 \times 10^{13} \, \text{N-ions/cm}^2$; (b) $11 - 1 \times 10^{11} \, \text{ions/cm}^2$, $12 - 1 \times 10^{12} \, \text{ions/cm}^2$, $13 - 1 \times 10^{13} \, \text{ions/cm}^2$.

Fig. 2. UV observation of the plasmid DNA containing green fluorescence protein (pGFP) transferred into *E. coli*. White colony indicates pGFP damaged (not functioning), while green colony indicates no DNA damage. (a) After 2.5-keV N-ion beam bombardment to 6×10^{12} ions/cm²; the bacterial colonies in sections 1, 2, 4 and 5 show white. (b) After N-plasma immersion ion bombardment in the conditions of a bias of 2.5 kV and an ion fluence of 10^{13} ions/cm²; white colonies as indicated by the red circle are the mutant, compared with the unmutated green colonies as indicated by the blue circle. (c) Purified *E. coli* mutant from the red-circled mutant in (b) to show all of the subsequently cultured bacterial cells white, indicating the pure mutation without contamination.

Fig. 3. The MDS result of the RMSD of the non-hydrogen atoms in the base rings of (a) poly-AT and (b) poly-GC subjected to ultra-low-energy C-ion bombardment.

Fig. 4. SEM images of 25-keV Ar-ion beam bombarded onion skin cell envelopes with a fluence of 10¹⁵ ions/cm². (a) Control. (b) Bombarded.



VCAr Ar11 Ar12 Ar13

VCN

N11

N12

N13

30

20

10

0

NC

Figure 1 (L.D. Yu, Ion Beam Nanobiology)

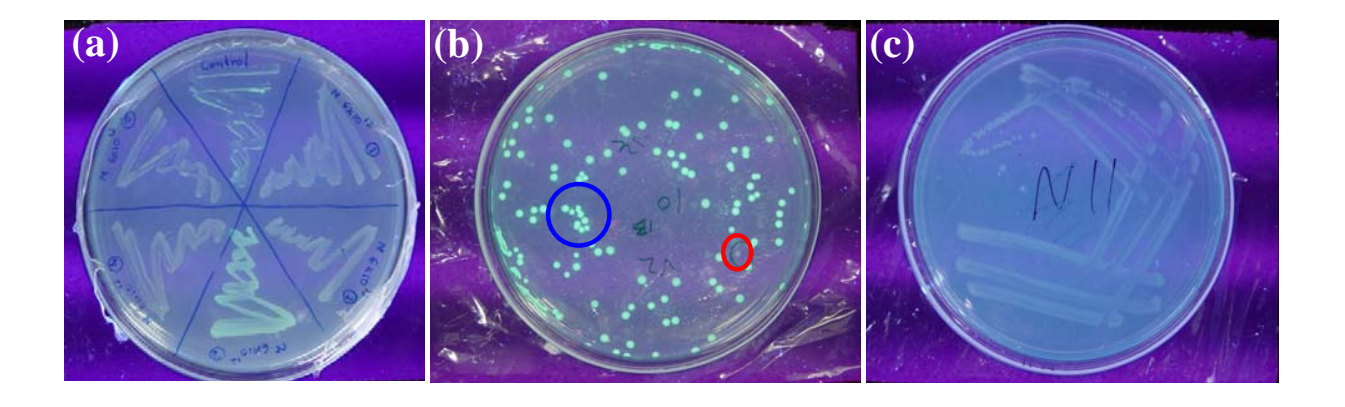


Figure 2 (L.D. Yu, Ion Beam Nanobiology)

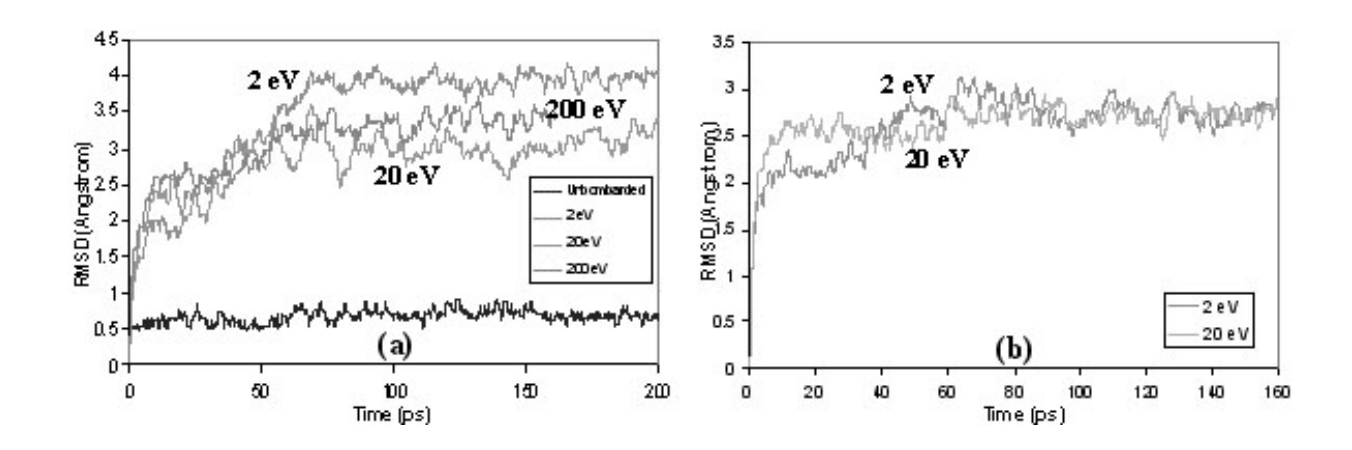


Figure 3 (L.D. Yu, Ion Beam Nanobiology)

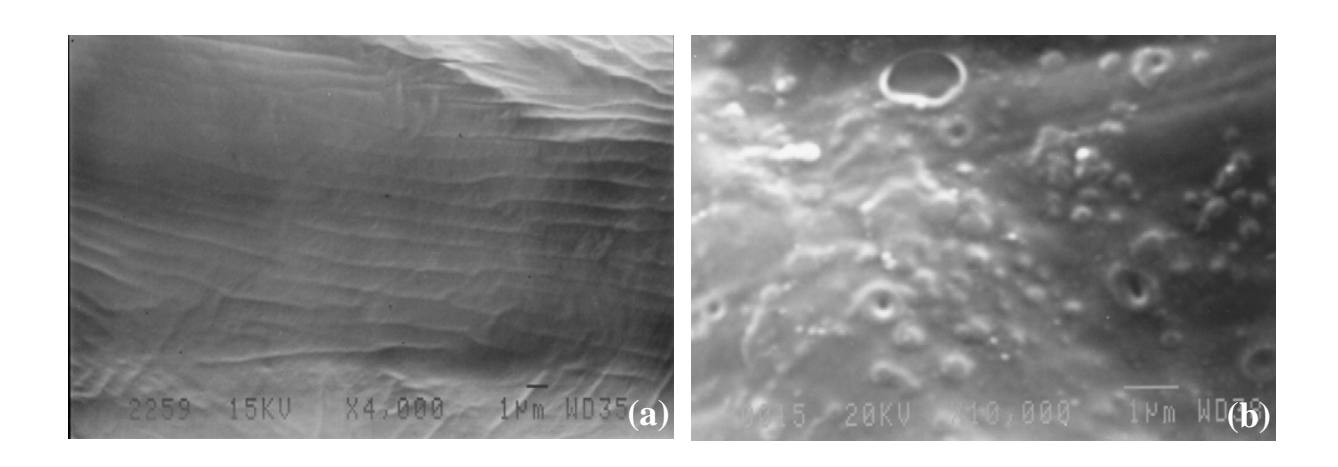


Figure 4 (L.D. Yu, Ion Beam Nanobiology)

Combined quantum-mechanics/molecular-mechanics (QM/MM) dynamics simulation of A-DNA double strands irradiated by ultra-low-energy carbon ions

C. Ngaojampa¹, P. Nimmanpipug^{1,3}, L.D. Yu^{2,3}*, S. Annuntalabhochai⁴ and V.S. Lee^{1,3}*

¹ Computer Simulation and Modeling Laboratory (CSML), Department of Chemistry and
Center for Innovation Chemistry, Faculty of Science, Chiang Mai University,
Chiang Mai 50200, Thailand

Plasma and Beam Physics Research Facility, Department of Physics and Materials Science,
 Faculty of Science, Chiang Mai University, Chiang Mai 50200, Thailand
 Thailand Center of Excellence in Physics, Commission on Higher Education,
 328 Si Ayutthaya Road, Bangkok 10400, Thailand
 Molecular Biology Laboratory, Department of Biology, Faculty of Science,
 Chiang Mai University, Chiang Mai 50200, Thailand

ABSTRACT

In order to promote understanding of fundamentals on ultra-low-energy ion interaction with DNA, the molecular dynamics simulations within the combined quantum mechanics/molecular mechanics (QM/MM) approach of poly-AT and poly-GC A-DNA double strands irradiated by ultra-low-energy (< 200 eV) carbon ion were carried out using AMBER 9 software package to investigate molecular implications of mutation bias in low-energy ion irradiated DNA. The simulations were focused on the responses of the DNA backbones and nitrogenous bases to the ion irradiation. The analyses of the root mean square

displacements (RMSD) of the backbones and non-hydrogen atoms of base rings of the

simulated DNA structure after ion irradiation revealed potential preference of DNA double

strand separation, which was dependent with the irradiating ion energy. The results show that

for the backbones, the large difference in the displacement between poly-GC and poly-AT in

the initial time period could be the reason for the backbone breakage; for the nitrogenous

base pairs, A-T is 30% more sensitive or vulnerable to ion irradiation than G-C,

demonstrating a preferential, instead of random, effect of ion-irradiation-induced mutation.

Keywords: Molecular dynamics, A-DNA, ultra-low-energy ion, ion irradiation, DNA double

strands.

PACS: 61.80.Jh, 87.10.Tf, 87.15.ap, 87.14.gk, 87.53.-j

*: Corresponding authors:

Email: yuld@fnrf.science.cmu.ac.th (Yu); vannajan@gmail.com (Lee)

2

1. Introduction

Along with recent rapid research developments in heavy ion therapy, ion beam biotechnology and life hazard study in space mission, a hot topic on low-energy ion irradiation of DNA is arising worldwide (e.g. [1,2]). While high-energy (> MeV) and medium-energy (an order of 10² keV) ion irradiation effects on DNA lesion have been long and widely studied and relevant knowledge has fairly sufficiently been acquired, studies on irradiation effect of ions with ultra low energy (< keV) on DNA yet lag quite behind the formers. The direct interaction between ions and DNA which is in the nuclear interaction dominance mainly occurs in the low energy region. Under low-energy ion irradiation, whether DNA can be damaged and what and how DNA structure is modified are of great interest. This study deals with the ion energy of eV to keV and focuses on the effect from the ion irradiation of isolated DNA on the DNA structural changes to reveal fundamentals in the ion interaction with DNA. The ion energy range we studied is similar to that of ultraviolet (UV) (about eV – 100 eV). UV radiation effect on DNA has been well studied. Although the energy of both quanta is in the same range, a UV photon has no mass while an ion has mass. Therefore, the physical effects of two are quite different.

A number of experiments were carried out using low-energy ions (< keV) to irradiate isolated or naked DNA in vacuum and obtained evidence of DNA strand breakages induced by the ion bombardment [3-6] and studies on ion irradiation induced DNA damage were previously summarized [7]. DNA strand breaks may occur at either the DNA backbones or the nitrogenous bases. Different mutagens such as chemical compounds and physical radiations cause dominant types of DNA damage differently. Compared with extensive studies and understandings of DNA damages caused by other physical radiations such as ultraviolet, x-ray, gamma ray, and high-energy ion or neutron irradiations, studies and

understandings on DNA damage from low-energy, especially ultra-low-energy, ion irradiation are not yet well developed. Preferential, instead of random, trend of the fragmentation of ion-impacted DNA has been known. The overall anionic base loss of DNA interacted with low-energy gas atoms was found to follow the trend $A^- >> G^- \approx T^- > C^-$ [8] (A = adenine, C = cytosine, G = guanine and T = thymine). It is normally thought that the GC base pair has three hydrogen bonds, whereas the AT base pair has only two, and as a consequence, the GC pair should be more stable. However, there were conflicting results showing that the DNA with higher GC contents yielded higher fragment ion abundance, indicating a higher instability [9].

The structural modifications of DNA may cause mutations, which can lead to new varieties of plants and animals but also to cancers of human tissues, and death of cells [2,10]. Therefore, understanding of intrinsic features of the DNA structural changes induced by lowenergy ion irradiation is of significances in both theories and applications. There must be important differences in relevant effects on DNA changes between high-energy and lowenergy ion beam irradiations. The former normally induces dominant ionization and excitation to produce significant secondary electron and photon emissions which can then cause severe damage in DNA. But, the latter process is normally dominated by elastic interaction between atoms to cause atomic displacements and thus DNA damage. It should be particularly noted that no matter what ion energy is applied for ion irradiation of biological materials, the majority of the ion energy loss and deposition occurs around the Bragg peak which locates immediately before the ions come to rest, namely, the ion energy deposition mainly occurs in the low energy region. Furthermore, low energy processes are important in high energy ion and electron irradiations because collision cascades generate low energy recoil atoms which may also interact with biological target materials to generate biological effects. Since it is technically difficult in determining the intrinsic features of ion-induced DNA changes, molecular modeling methods have become a very useful tool to assist in finding answers. Cooperating with research progress achieved in ion beam biotechnology at Chiang Mai University (e.g. [11-13]), we now involve molecular dynamics simulation (MDS) in the studies of low-energy ion interaction with DNA. In this study, MDS was selected for its capacity and ability to calculate structures and properties from such large, complex in interactions and dynamic structures of DNA. We focused our interest in both backbones and nitrogenous bases of the nucleotides for quantifying effects. Because if there are breaks of DNA strands they should primarily start to occur at either the two venues, behavior of the backbone and base responses to the low-energy ion irradiation will provide information on potential DNA breakage. In our study, carbon ions were applied not only for checking previously reported result but also due to the significance of the element in biology, life and medical therapy [5]. The implication for the mutation bias in the DNA irradiated by low-energy ion beam was expected in this study.

2. Methods

20 base pairs of alternating poly-AT and poly-GC double strands were constructed in twisted linear A-form of DNA helices using HyperChem 7.0 [14]. Fig. 1 shows the sequences and 3D structures. The reason of using A-DNA was that this DNA form is the form when DNA is in low pressure and low humidity environment which is corresponding to the experimental conditions of ion bombardment of naked DNA [3,5,6]. Sodium ions were then added to the structures to neutralize the overall charges of the A-DNA structures. The energies of the ion-neutralized structures were then minimized by steepest descent following by conjugate gradient algorithms. Then, the MD simulations were performed starting with pre-equilibrium heating for 200 pico seconds (ps) from 0 to 323 K (approximate temperature